1974

IMPERIAL COLLEGE OF SCIENCE AND TECHNOLOGY

DEPARTMENT OF AERONAUTICS

I.C. Aero Tech. Note 74 - Jan. 1974

MEASUREMENTS OF TURBULENT BOUNDARY LAYER GROWTH OVER A LONGITUDINALLY CURVED SURFACE

*R. N. MERONEY

*Assoc. Professor, FLUID DYNAMICS & DIFFUSION LABORATORY,
CIVIL ENGINEERING DEPARTMENT, COLORADO STATE UNIVERSITY,
Colorado, USA

*Work completed at Imperial College of Science and Technology during Academic Leave from Colorado State University and tenure of a Clean Air Act Fellowship, Environmental Protection Agency, 1972-73.

IMPERIAL COLLEGE OF SCIENCE AND TECHNOLOGY

DEPARTMENT OF AERONAUTICS

I.C. Aero Tech. Note 74 - Jan. 1974

MEASUREMENTS OF TURBULENT BOUNDARY LAYER GROWTH OVER A LONGITUDINALLY CURVED SURFACE

*R. N. MERONEY

*Assoc. Professor, FLUID DYNAMICS & DIFFUSION LABORATORY, CIVIL ENGINEERING DEPARTMENT, COLORADO STATE UNIVERSITY, Colorado, USA

*Work completed at Imperial College of Science and Technology during Academic Leave from Colorado State University and tenure of a Clean Air Act Fellowship, Environmental Protection Agency, 1972-73.

ABSTRACT

The result of an "additional rate of strain" on a turbulent parcel of fluid as it undergoes even mild streamline curvature can be very large. Yet until recently skin friction and heat transfer calculations have ignored this effect. Recent measurements over turbine cascades suggest curvature influences heat transfer by an order of magnitude. In addition there exists a strong analogy between the effects of centrifugal body forces and the buoyancy body force arising in density stratified flow in a gravity field.

This note reports the results of a set of measurements of boundary layer development over convex and concave surfaces and compares the results with various turbulence models utilized in computational programs. A moderate curvature wind tunnel test section was constructed ($\delta/R \approx .01$ to $.02$) to examine the influence of curvature on boundary layer structure.

The boundary layer rate of growth, compared to that of a boundary layer in the same pressure gradient on a flat surface, was decreased on the convex surface and increased on the concave surface by ten to twelve percent as a result of only an apparent one to two percent perturbation on the size of the source terms in the Reynolds stress equations. Measurements are available of longitudinal static wall pressure, vertical stagnation pressure and single and cross-wire anemometer voltages at a sequence of five downstream stations. Lateral traverses at six heights for two downstream stations were completed over the concave side. Analog and digital interpretation of anemometer signals provided data of $\overline{u}$, $\overline{v}$, $\overline{u'^2}$, $\overline{v'^2}$, $\overline{u'v'}$, $\overline{u'v'^2}$, $\overline{u'^2v'}$, $\overline{u'^3}$, and $\overline{v'^3}$.

TABLE OF CONTENTS

LIST OF PLATES

LIST OF FIGURES

LIST OF FIGURES (continued)

LIST OF SYMBOLS

English letters

d	Probe diameter
e'	Voltage fluctuation
E	Voltage
H	Shape factor δ^*/θ
n	Exponent in King's Anemometer Law
k	Curvature parameter, 1/R
p	Pressure
R	Radius of curvature
u'	Velocity fluctuation
u	Mean velocity
u^+	Dimensionless velocity u/u_τ
v'	Velocity fluctuation in vertical
w'	Velocity fluctuation in lateral
x, y, z	Coordinates
y^+	Dimensionless vertical co-ordinate $u_\tau y/\nu$

Greek Letters

β	Empirical constant in Bradshaw's curvature correction expression
δ^*	Displacement thickness
θ	Momentum thickness
κ	Von Karman's Constant
λ	Vortex lateral wavelength
ν	Kinematic viscosity

ν_τ	Turbulent eddy diffusivity
ρ	Density
ψ	Crosswise angle inclination

Subscripts and Superscripts

pw	potential value at wall
p	potential core value
ref	reference value
t	total pressure value
sw	static wall pressure value
0	zero velocity voltage

1. INTRODUCTION

The motivation for the present work stems from the observation that streamline curvature in the plane of the mean shear produces surprisingly large changes in the turbulence structure of shear layers. Such flows may be said with tongue in cheek to have a "sensuous or sexy" characteristic. "Sensuous" in the sense of a flow characteristic which arouses a disproportionate response - just as a slight change in a woman's curvature can arouse an exaggerated reaction in a man. These changes may be more important in magnitude than normal pressure gradients, property variations, or other explicit effects in the mean motion and the turbulence correlation equations for curved flows. Turbulence may be nearly eliminated in some regions of highly convex surfaces, whereas on highly concave surfaces quasi-steady longitudinal vortices may develop to dominate local transport.

The author is particularly interested in the penetrative convective instabilities and three dimensional motions resulting from the action of centrifugal buoyancy forces over concave surfaces. These instabilities are found to take the form of quasi-steady three dimensional vortices oriented in the streamwise direction. The occurrence of a closely analagous phenomenon in the atmosphere is fairly well documented (Kuettner, 1959; Kuo, 1963; Scorer, 1972). The large scale cloud streets frequently observed in satellite photographs are now accepted as direct evidence of the presence of longitudinal vortex instabilities in the earth's atmosphere. The presence of these rolls may well explain the inadequacies of K-theory-type approaches to predict uniformly momentum, heat, or vapor transport through the earth's boundary layer.

In the atmosphere these instabilities may be a combination of movements associated with surface heating, curvature, coriolis forces, and wind shear (Faller, 1965). Interest in this problem has led the present investigator to examine various aspects of the simplified linear and laminar problem (Rayt and Meroney, 1972; Kahawita and Meroney, 1972a, 1972b, 1972c), the effects of longitudinal vorticity on heat and mass transport (Meroney and Hsi, 1972), and the effects of curvature on a turbulent eddy diffusivity model (Anyiwo and Meroney, 1973). This report examines directly the influence of such secondary motions on the character of turbulence and transport in well developed turbulent boundary layers.

1.1 Review

An exceptionally competent review on "Effects of Streamline Curvature on Turbulent Flow" prepared by P. Bradshaw, 1973, now exists. Since this monograph reviews the work on boundary layer development over two dimensional curved surfaces from its first presentation in 1930 until the present only the pertinent conclusions need be presented here. Bradshaw indicates the following research needs

a) Data for boundary layers, and other (and geophysical) shear layers, with curvature effects typical of aeronautical practice rather than exaggerated effects studied in many previous experiments designed to investigate curvature effects.

b) Experiments on vortices and swirling flows that acknowledge the importance of curvature effects on turbulence.

c) Measurements of the triple velocity products that dominate turbulent transport of Reynolds stresses in the vertical direction.

The development of longitudinal vortices in the presence of a boundary layer deserves further comment. Although longitudinal rolls over concave surfaces (Goertler rolls) have been examined extensively in pseudo-laminar flows (Schultz-Grunow and Breuer, 1965) the measurements of the effects of such motions in a turbulent condition is limited. Tani (1969:1962) was the first to demonstrate the existence of longitudinal vortices in the turbulent boundary layer along a concave wall. Spangler and Wells (1964) generated artificial vortices in a turbulent boundary layer with vortex generators. Patel (1968) found such vortices on a concave wall in a 180° channel, and suggested that before studying the influence of concave curvature on a two-dimensional turbulent boundary layer, one should examine these vortices for their appearance and strength. Most recently, Soo and Mellor (1972) made $\overline{u}$, $\overline{u'^2}$, $\overline{v'^2}$, and $\overline{u'v}$ measurements in traverses through rolls developing over a concave surface.

Analytically the interaction of turbulent rolls and a shear flow is even more obscure. Sandmayr (1966) elaborated on an idea of Tani to calculate instability curves for a turbulent boundary layer with a variable eddy diffusivity. However the results cannot be compared directly with experimental data since transition occurs spatially in a boundary layer. Mori and Uchida (1966) have put such information to use in laminar flows to predict the nature of the perturbed parallel plate flow under unstable heating. R. A. Brown (1970) did solve a set of boundary layer equations in a similar manner for the vertical perturbation effects on the atmospheric shear layer. He assumed however that the eddy diffusivity was constant and nonvarying with height throughout the layer. Two dimensional calculation procedures such as those by Bradshaw (1969), Soo and Mellor (1972), or Launder (1970) may suffice to predict a laterally averaged effect of such rolls on a shear layer.

1.2 Remarks

One concludes that a full survey of the turbulent system in the presence of developing vortices has not been obtained. No spectra are available, no third order correlations. Wall shear measurements are limited. Since previous airfoil measurements were limited to velocity profiles and $\delta/R < .01$ and most channel boundary layer measurements exceed $\delta/R = .05$ or 0.1 this study has examined the moderate growth condition where $\delta/R \sim .01$ to .02. Turbulent measurements were made to establish flow history, eddy scales, and vortex spacing.

Numerically the value of Bradshaw's length scale modification for curved flows has been examined by use of the Bradshaw, Ferris, and Atwell (1967) program. Soo and Mellor's (1972) eddy diffusivity correction has been utilized in a modified program developed by Herring and Mellor (1968).

2. LABORATORY EQUIPMENT

2.1 Wind Tunnel and Test Section

The test section developed for this study was added to an existing centrifugal far blower tunnel present in the aeronautical laboratory at Imperial College of Science and Technology. (See Figure 2 and Plate 1). A 10,000 cfm centrifugal fan and a 12.5 kw motor force air through five screens into a plenum chamber. A nine to one contraction ratio reduces the flow field to a 5"x30" section with a turbulence level of about 0.1%. The boundary layers develop naturally over a 4'9" length before entering the curved section. Boundary layer thicknesses on top and bottom of the duct are both approximately one inch.

The curved test section is a 5"x30" extension section four feet long with a radius of curvature of 100" on the convex side. Static pressure taps are distributed over the section length on both the concave and convex sides. Five 3.5" diameter ports are available along the test section centerline. These ports provide access to the flow cross section. When a traversing device is mounted over the port openings vertical movement over the 5" tunnel width is possible and lateral movement over 3" is available. (See Figure 3 and Plate 2). A series of stagnation and surface tubes and single and cross wire anemometers were attached to the traversing gear (See Figure 3).

2.2 Measuring Equipment

Twenty-six static pressure holes were distributed over the upper (concave) and lower (convex) sides of the test section. These pressures were normalized by the total head presented by the reference velocity found at the entrance to the 5"x30" sections. Each surface tap was a ~.02" diameter hole through a brass or plastic insert. All taps were sanded smooth and checked for burrs or irregularities. Pressure measurements were made by an Airflow Mk 5 inclined manometer.

Two sets of stagnation and surface probes were prepared to measure pressure variation across the wind tunnel section. When possible measurements were made along section radii of curvature. The stagnation tubes were constructed from a set of telescoping hypodermic-size stainless steel tubing and soldered. The tip diameter was flattened to give an elliptic probe .025" high by .055" wide. Surface tubes were similarly formed; however, the tips were not flattened. Typical ID and OD diameters were .025" and .042" respectively. Distance of the probes from the wall were determined by a precalibrated traverse potentiometer. Wall location was determined for each measurement by means of a continuity circuit between the probe tip and a thin layer of conductive silver paint applied to the local wall surface.

The hot wire measurements were all based on the DISA range of equipment. The type 55D01 anemometers and signal conditioning equipment were used. All signals were linearized by the DISA 55D10 linearizer and DISA 55D25 auxiliary unit, mean signals were measured with the DISA 55D30 digital voltmeter. A DISA 55D26 sum and difference device was utilized to evaluate a set of the cross-wire output voltages. Anemometer output from the X-wire anemometer were recorded on separate channels of an Ampex FR1300 FM analog type recorder.

Subsequently analog tapes were digitized by means of a Digital Equipment Co., Ltd. system utilizing a DEC AD-08-B A-to-D converter, a PDP 8/L minicomputer and an Ampex TM-16 tape transport. The equipment and procedures utilized are described by Brandt and Bradshaw (1972). Digitized signals were evaluated by a program prepared by Dr. C. W. Von Atta and modified for use on the CDC 6400 system at Imperial College by Antonia and Bradshaw (1971).

3. MEASUREMENT TECHNIQUES AND DATA REDUCTION PROCEDURES

3.1 Mean Flow Quantities

A conventional pito-static probe is not appropriate for flow following curved streamlines because of the significant vertical static pressure gradient. Hence only stagnation tube measurements were made across the tunnel section. Fortunately given the radius of curvature of the flow one can determine the local static pressure from its value at the wall (Soo and Mellor, 1972) or one can integrate the stagnation pressure results outward from the wall (Wilcken, 1930). Both methods were used to calculate local longitudinal velocity; however the latter method seemed somewhat inconsistent, perhaps because of the accuracy required by the numerical integration. The expression utilized for the results displayed herein was

$$\frac{u}{u_{pw}} = \left(\frac{p_t - p_r}{p_r - p_{sw}} + e^{-2ky}\right)^{1/2} \tag{1}$$

where $u_{pw} = (2\ (p_r - p_{sw}))^{1/2}$

p_r = reference total pressure in potential core region

p_t = local total pressure

p_{sw} = static pressure at wall

k = 1/Radius of Curvature

This expression is obtained from the Bernoulli equation under the assumption $\frac{\partial p}{\partial y} = k\rho\ u^2$. Small terms which represent the difference between the static pressure calculated from the actual velocity and the potential velocity are dropped in this approximation. The major source of errors of a total head probe are the effect of turbulence, the effect of yawing, and the effect of wall. The errors due to the effects of turbulence are not well understood; various authors have suggested corrections ranging from positive to negutive valve for the same condition. However for turbulence less than 10%, the error in total pressure is probably less than 1% of the dynamic pressure. Total-head tubes are rather insensitive to yaw, misalignments of ± 15° are required to produce errors of the order of 1%. Corrections for the wall effect are made using the curve of Stanton, et al. (1920); however these should be significant only for the closest to the wall measurements.

Some care must be taken in defining the integral boundary layer parameters for a curved flow field. Since the potential velocity distribution increases linearly across the duct it is inappropriate to define a boundary layer thickness as 99% of some specific velocity value. Rather all velocities in the boundary layer should be compared with the potential velocity which would exist for an inviscid fluid; therefore to be consistent the momentum and displacement thicknesses are defined as

$$\theta = \int_0^\infty \frac{u(y)}{u_p(y)} \left(1 - \frac{u(y)}{u_p(y)}\right) dy \tag{2}$$

$$\delta^* = \int_0^\infty \left(1 - \frac{u(y)}{u_p(y)}\right) dy \tag{3}$$

and

$$H = \delta^*/\theta \tag{4}$$

Surface or Preston tube measurements were evaluated by arguing the pressure difference Δp between the stagnation tube resting on the surface and a nearby static-pressure tap should be only a function of shear stress, τ_w, the tube diameter, d, and the properties of the fluid, ρ and ν. We thus obtain

$$\frac{\Delta p \; d^2}{\rho \; \nu^2} = f_1\left(\frac{\tau_w \; d^2}{\rho \nu^2}\right) \quad \text{or}$$

rearranging

$$\frac{\tau_w}{\Delta p} = f_2 \left(\frac{\Delta p \; d^2}{\rho \nu^2}\right) .$$

A calibration chart prepared by F. Wong (Imperial College Aeronautic Notes for Undergraduates) from the measurements of V. C. Patel (1965) was used to interpret the measurements.

A second measurement of local skin friction was obtained by the classical "Clauser" chart technique. This technique assumes the presence of a universal logarithm velocity law near the wall. This law must be modified however to reflect the presence of mild curvature effects. An appropriate universal expression with mild curvature is (Bradshaw, 1973);

$$u = \frac{u_\tau}{\kappa} \left(\ell n \frac{u_\tau y}{\nu} + \kappa C\right) + \frac{2\beta}{\kappa} \int u \; dy \quad ,$$

or for $U \alpha y^{1/5}$ in the inner layer,

$$u \left(1 - 2 \cdot \frac{5}{6} \beta \frac{y}{R}\right) = \frac{u_\tau}{\kappa} \left(\ell n \frac{u_\tau y}{\nu} + kC\right) \quad .$$

Therefore one may plot

$$\frac{u}{u_{pw}} \left(1 - \frac{5}{3} \beta \frac{y}{R}\right) \quad \text{vs} \quad u_{pw} \; y/\nu$$

for various values of u_τ . (u_{pw} is potential velocity which would exist at wall for an inviscid flow). See Figure 10 and 21 for results over convex and concave surfaces. Soo and Mellor (1972) were pessimistic concerning the presence of a logarithm region over a concave surface. However the results found herein appear consistent.

Mean temperature of the flow field was monitored throughout the experiment by a themistor probe. This was especially critical because of the thermal drift which occurred daily in the laboratory. Runs where temperature drifted by more than 5°F were discarded.

3.2 Fluctuating Quantities

The hot wire anemometer was only used to determine fluctuating quantities in the process of these experiments. Every effort was made to eliminate the effects of temperature drift by taking a data set promptly and measuring primarily dimensionless quantities.

A single wire probe with the wire positioned normal to the flow was used to measure longitudinal velocity fluctuations. Several alternate methods of evaluating hot wire signals may be found in the literature. (Bradshaw, 1971; Sandborn, 1972a, 1972b). The following relation dependent on the definition of an "intercept" zero velocity voltage from the wire calibration was used.

$$\frac{\sqrt{\overline{u'^2}}}{u_{local}} = \frac{2}{n} \left(\frac{E^2}{E^2 - E_o^2} \right) \frac{\sqrt{\overline{e'^2}}}{E}$$

The constant n was set equal to 0.45 based on the consistent experience obtained with the version of DISA probe and holder utilized.

A conventional cross-wire anemometer probe was utilized to evaluate additional fluctuation correlations including $\overline{u'^2}$, $\overline{w^2}$, and $\overline{u'w'}$. Higher order correlations are available but are not recorded in this report.

The angle between the wires of each cross-wire probe was determined by mounting the probe in a free stream of constant velocity and measuring the anemometer output voltages for various yaw angles. The calibration is dependent on the cosine form of the anemometer response law

$$E^2 = E_o^2 + (B \cos^n\psi)\, u^n \; .$$

The data were plotted in the manner described by Bradshaw (1972, p. 123).

Voltage signals from the cross-wire anemometer were recorded directely on analog tape for subsequent reduction. Mean voltages were also recorded at this time to allow correction for signal reduction or variation in gain during processing. This data was analyzed both by analog and digital means. Since the voltage signals were linearized prior to recording on analog tape it is expected that the relation between instantaneous voltage and velocity will be

$$E = E_o + B^* \,(V \cos\psi)$$

When the instantaneous signals for each inclined wire are evaluated in the conventional manner the resulting expressions are

$$\frac{\overline{u'^2}}{u^2} = \left(\frac{\gamma_1}{\varepsilon_1}\right)^2 \overline{e_1^2} + \left(\frac{\varepsilon_1}{\varepsilon_2}\right)^2 \overline{e_2^2} + 2\left(\frac{\gamma_1\varepsilon_1}{\gamma_2\varepsilon_2}\right) \overline{e_1 e_2}$$

$$\frac{\overline{w'^2}}{u^2} = \left(\frac{\gamma_2}{\varepsilon_1}\right)^2 \overline{e_1^2} - \left(\frac{\varepsilon_2}{\varepsilon_2}\right)^2 \overline{e_2^2} - 2\left(\frac{\gamma_1\varepsilon_1}{\gamma_2\varepsilon_2}\right) \overline{e_1 e_2}$$

$$\frac{\overline{u'w'}}{u^2} = \left(\frac{\gamma_1}{\varepsilon_1}\right)^2 \left(\frac{\tan\psi_1 + \tan\psi_2}{2\tan\psi_1 \tan\psi_2}\right) \overline{e_1^2} - \left(\frac{\varepsilon_1}{\varepsilon_2}\right)^2 \left(\frac{\tan\psi_1 + \tan\psi_2}{2\tan\psi_1 \tan\psi_2}\right) \overline{e_2^2}$$

$$+ \left(\frac{\tan\psi_1 - \tan\psi_2}{2\tan\psi_1 \tan\psi_2}\right)\left(\frac{\overline{u'^2}}{u^2}\right)$$

where

$$\gamma_1 = \frac{\tan\psi_2}{(\tan\psi_1 + \tan\psi_2)(E_1 - E_{o_1})}$$

$$\gamma_2 = \frac{1}{(\tan\psi_1 + \tan\psi_2)(E_1 - E_{o_1})}$$

$$\varepsilon_1 = \frac{\tan\psi_1}{(\tan\psi_1 + \tan\psi_2)(E_2 - E_{o_2})}$$

$$\varepsilon_2 = \frac{1}{(\tan\psi_1 + \tan\psi_2)(E_2 - E_{o_2})}$$

Since the cross wire probe could not be positioned along a radius of curvature the approach flow did not normally bisect the crossed wires during a traverse. A number of alternative correction methods were tried, and the following method seemed most consistent. Let

$$\left.\begin{array}{l} E_1 - E_{01} \\ \\ E_2 - E_{02} \end{array}\right\} = \text{mean voltage output of inclined curves when positioned in potential core of channel}$$

$$\left.\begin{array}{l} E_{r1} - E_{01} \\ \\ E_{r2} - E_{02} \end{array}\right\} = \text{voltage output in normal uncurved flow when convection angle } \beta = 0°. \text{ (Obtained from calibration).}$$

$$\frac{\cos(\psi_2 + \beta)}{\cos(\psi_1 - \beta)} = \left(\frac{E_2 - E_{02}}{E_1 - E_{01}}\right)\left(\frac{E_{r1} - E_{01}}{E_{r2} - E_{02}}\right)\left(\frac{\cos\psi_2}{\cos\psi_1}\right)$$

where ψ_1 and ψ_2 are angles from the wire correlation calibration.

Then

$$(\tan \psi_1) \text{ corrected} = \tan(\psi_1 - \beta)$$

$$(\tan \psi_2) \text{ corrected} = \tan(\psi + \beta)$$

i.e.,

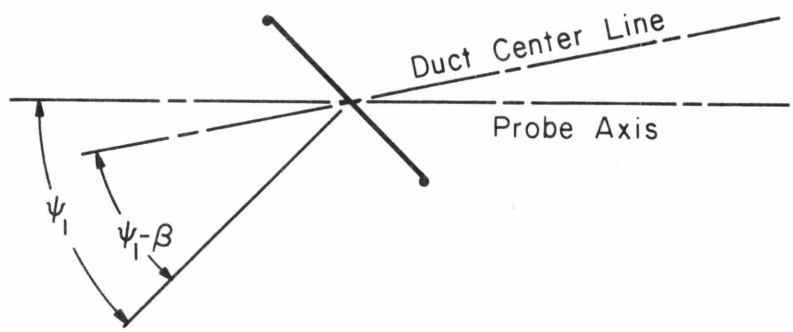

As an additional check on accuracy and in order to obtain higher order correlations the cross-wire signals were also analyzed digitally. In general the techniques described by Castro (1972) and Brandt and Bradshaw (1972) were followed. Analog tape records of E_1 and E_2 were transferred to digital tape by the A-D system previously described. Digital data were analyzed using Aeronautical Laboratory Program DIG2CHM, a version of CS4A described by Brandt and Bradshaw. Whether results are analog or digital are so noted on the figures.

4. RESULTS AND DISCUSSION

In the following, the discussion is divided into three sections. The first deals with efforts to check the "well behaved" nature of the flow - i.e., presence of separation or secondary flow. The second deals with the convex flow results and the third the concave results. The discussion takes the following format. The mean flow data are analyzed first followed by a discussion of the turbulence data. Tables 1-2 contain the results of the mean flow and turbulence measurements of the flow along a convex wall. Tables 3-4 reproduce the results of the concave wall experiment.

4.1 General Flow Field

Uniformity and straightness of flow in the curved section was checked by observing tufts attached to the wall of the tunnel. In addition smoke was released from a TEM model smoke probe. The flow remained attached and appeared visually uniform. A stethoscope was used to check for turbulence and the extent of the wall region at the duct outlet. The boundary layer was thicker on the top concave surface than on the bottom convex surface. The shear layer thickness appeared constant with no assymetry with respect to duct centerline. The potential core region appeared turbulence free. The large aspect ratio of the duct 1:6 apparently helped to avoid the large secondary wind veering typical of early experiments in rectangular ducts.

As a further check of the flow's symmetry two 1/4" diameter cylinders were placed normal to the flow, perpendicular to the duct wall surface and equal distance from the duct centerline (~ 4"). The wake produced by these cylinders were examined at the duct outlet.

There was no evidence that the wake profiles were deflected to either side over the length of the test section.

The pressure distribution the length of the entrance and wall sections are shown in Figure 5. The cross duct pressure distribution appears to adjust and balance for the curvature within two duct heights (~ 10"). This sudden pressure adjustment cannot be eliminated since it is inherently characteristic of a change from a straight to a curved flow field. Even so the total maximum pressure change amounts to less than 10 percent of the reference dynamic head. Since the curvature was relatively mild and the duct aspect ratio rather large no wall jets or flaps were employed to tailor the pressure distribution. It was felt that the effects of mild pressure variation are well understood and can be corrected for in any current numerical boundary layer calculation method.

4.2 Convex Surface Effects

The sequence of mean velocity profiles which grow over the convex side are shown in Figure 6. Note the low rate of boundary layer growth which is almost half that which would be expected for the corresponding straight section. The profile gradients become less intense near the wall and the power law parameter increases from 1/7 toward 1/2. Since the skin friction is not measured independent of the velocity profile, the skin friction quoted depends on the validity of the modified Clauser plot or the Preston tube to determine C_f for curved flow. The measured velocity profiles were plotted in Clausser plot form in Figure 10. All profiles show an extensive straight line region which begin to deviate at the same point ($yu_\tau/\nu \approx 200$) where a flat plate profile begins to deviate from the Law of the Wall. Thus it can be said that a modified Law of the Wall, which is given by

$$u^+(1 - \frac{5}{3} \beta \frac{y}{R}) = \frac{1}{\kappa} \ln y^+ + C$$

exists for flow along convex surfaces.

For flows over convex surfaces, the centrifugal force on a fluid element must be balanced by an inward pressure gradient. If a particle is moving too fast (or slow) for its location the centrifugal force component is large (or small), and the particle moves outward (or inward). Hence in a turbulent flow the vertical motions over a convex surface are hindered resulting in a decrease in the interchange of momentum and energy.

Consider Figure 11a which displays the variation of skin friction, C_f; momentum thickness, θ; and a shape factor, H, over the span of the convex wall. A curvature perturbation of $\delta/R \simeq .01$, which might be expected to cause only a one percent change in the Reynolds' stress equations, has resulted in approximately a ten percent decrease in skin friction, a decreased rate of momentum thickness growth and a slight increase in shape factor. Also included in Figure 11a are lines depicting behavior as predicted by the hyperbolic boundary layer program of Ferris and Bradshaw (1968), modified for a curvature correction as described by Bradshaw (1969). For a constant β of 7.0 the results display fairly good agreement with the experimental data.

Figure 11b compares the same experimental data with the eddy-diffusivity relation results of Soo and Mellor (1972). They proposed

$$-\overline{uv'} = \frac{\partial u}{\partial y}(1-S)^2 \quad 1 - 4.05\,\frac{(1+S)}{(1-S)}\,2 \quad ^{3/2}$$

where $S \equiv (u/R)/(\partial u/\partial y)$ and ν_T is the empirical eddy viscosity value used in plane flow. The linearized version of the correction factor corresponds to an F factor with $\beta = 4.0$. Therefore Soo and Mellor's relation predicted fairly close but somewhat smaller results to that of Bradshaw.

The decrease in mixing activity is also evident from the turbulence measurements, Figures 7 to 9. It can be seen that there are significant decreases in the turbulent intensities across the boundary layer.

The change in the $\overline{u'v'}$ profile from that corresponding to flat plate flow is especially interesting. Most of the suppression occurs in the outer region of the boundary layer. Extrapolated values of the shear near the wall closely approximate the results from the Preston tube or the Clauser plot. The flow perceives a favorable pressure gradient initially as it readjusts to curved flow lines; subsequently the convex curvature prevents the turbulence intensity from increasing. Examination of the intensities, $\overline{u'}$ and $\overline{v'}$, and the shear, $\overline{u'v'}$, suggests the flow has almost reached a new equilibrium state where profiles become similar.

4.3 Concave Surface Effects

The distinguishing characteristic of flow over the concave surface is the presence of significant lateral variation in all flow properties. A survey of stagnation pressure at two heights (1.0 and 0.5 inch) above the surface over a sixteen inch lateral fetch is shown in Figure 17. The pressure variations can be explained by assuming the existence of a system of longitudinal vortices similar to the Taylor-Gortler type vortices inside the boundary layer. The positions of the high points (crests) on the trace can be taken to correspond to the position between two vortices whose flow direction is toward the wall, and the position of the low points (trough) could be taken as a position between the vortices where the flow directions are away from the wall. Thus the wave-like behavior. The boundary layer thickness at this position was of the order of 2 to 2 1/2 inches. The apparent wavelength between rolls was approximately 2.42 inches. These rolls and their positions were very stable. Traverses made at two different times some days apart reproduced the same structure. It is probable that the exact roll positions are tied in some manner to irregularities in upstream screens, boundaries, or turbulence transition location.

The growth of the mean velocity distribution along the concave surface and down the centerline of the duct is shown in Figure 12. The lateral variation of such profiles in the presence of longitudinal rolls is displayed by Figure 21. Boundary layer thickness varies by 25 percent over the wavelength of such a roll. Momentum thickness varies from 50 to 100 percent over a roll width. Local skin friction appears to vary by 20 percent. (See Figures 22 and 23). All of this arises from only a magnitude of $\delta/R \cong 0.02$.

The test span variation of C_f, θ, and H are shown in Figure 24. Again one sees the influence of curvature; however this time centrifugal effects act to enhance mixing and increase momentum transport in the average. A two dimensional analysis will obviously be unable to predict the nature of the three-dimensional influence of longitudinal rolls. Nonetheless the predictive results of the method of Bradshaw are displayed as before. An average 10 to 12% increase in skin friction, a decrease in shape factor, and an increase in momentum thickness are suggested. The experimental variation in C_f and H are not nearly as great as the variation in θ .

In order to interpret the hot wire anemometer results one must assume that the lateral velocities developed by the roll do not significantly change the signal measured. With this rather serious limitation in mind one can examine Figures 13 to 20.

Profiles of $\overline{u}'/u$ are shown in Figure 13. The rapid penetration of turbulent energy into the potential core region together with a significant spanwise variation is apparent. Figure 14 displays a similar behavior for $\overline{v}'/u_{pw}$; however the character of $\overline{u'v'}/u_{pw}{}^2$ is perhaps most interesting. In a flat plate boundary layer the "constant flux" region extends outward to 0.15 δ. For this concave boundary layer case the results suggest a nearly constant shear extending to 0.3 - 0.45 δ. Spanwise variation of the various correlations are found in Figures 17 through 20.

5. CONCLUSIONS

As a result of this investigation a body of data was developed on boundary layer flow over moderately curved convex and concave surfaces. The following conclusions may be drawn from examination of the results and comparison with recent analytical models.

Turbulent Boundary Layers along Convex Surfaces:

i) The Law of the Wall holds in a modified form along convex surfaces.

ii) Initial and subsequent decreases in the intensities of turbulence are due partly to favorable pressure gradient and partly to curvature. The curved streamlines interact with the boundary layer to inhibit vertical mixing.

iii) The shear stress decreases steeply outside the near wall region and approaches zero well inside the typical boundary layer (about 0.88 for $\delta/R \simeq .01$).

iv) A length scale correction of the sort proposed by Bradshaw suffices to predict the effect of moderate convex curvature in skin friction, shape factor, and momentum thickness.

v) A small change in curvature ($\delta/R \simeq .01$) arouses a large (10%) change in integral properties of the flow field.

Turbulent Boundary Layers along Concave Surfaces:

i) The Law of the Wall appears to hold in a modified form along concave surfaces.

ii) Concave curvature may induce parallel sets of longitudinal rolls in the turbulent boundary layer. These rolls appear to extend the height of the boundary layer and characteristically show a wave length of the order of the boundary layer thickness.

iii) As a result of increased mixing promoted by the concave curvature there is a substantial increase in the turbulent energy all across the boundary layer.

iv) The various turbulence correlations and mean velocities are distributed laterally in a wave-like manner indicating the presence of a vortex system.

v) The shear correlation coefficient appears to remain large for an extended distance from the wall before it begins to diminish.

REFERENCES

Anyiwo, J. C. and Meroney, R. N., "Effective Viscosity Model for Turbulent Wall Boundary Layers", to be published Aeronautical Quarterly, 1973.

Bradshaw, P. R., "The Analogy Between Streamline Curvature and Buoyancy in Turbulent Shear Flow," J. Fluid Mech., Vol. 36, p. 177, 1969.

Bradshaw, P. R., "An Introduction to Turbulence and Its Measurement," Pergamon Press, Oxford 1972.

Bradshaw, P. R., "Effects of Streamline Curvature on Turbulent Flow," AGARD ograph No. 169, 1973.

Bradshaw, P. R., "Advances in Turbulent Shear Flow," Notes for von Karman Institute for Fluid Dynamics Short Course, March 19-23, 1973.

Bradshaw, P., D. H. Ferris, and NPA Twell, "Calculation of Boundary Layer Development Using the Turbulent Energy Equation. NPL Aero Report 1182 (1966) and J. Fluid Mechanics, Vol. 28, pp. 593 ff (1967).

Brandt, A. and P. Bradshaw, "Apparatus and Programs for Digital Analysis of Fluctuating Quantities in Turbulent Flow," Dept. of NPL Aero Report 1269, National Physical Lab., Teddington, U.K., March 1968.

Brown, R. A. "A Secondary Flow Model for the Planetary Boundary Layer", J. of Atm. Sci., Vol. 27, pp. 743-757, August 1970.

Castro, I. P., "Digital and Analog Reduction of Basic Hot Wire Data," Dept. of Aeronautics, Imperial College of Science and Technology, London Notes., January, 1972.

Faller, A. J., "Large Eddies in the Atmospheric Boundary Layer and Their Possible Role in the Formation of Cloud Rows", J. of Atmospheric Sciences, Vol. 22, pp. 176-184.

Ferris, D. H. and P. R. Bradshaw, "A Computer Program for the Calculation of Boundary Layer Development Using the Turbulent Energy Equation." NPL Aero Report 1269, National Physical Lab., Teddington, U.K., March 1968.

Herring, H. J. and G. L. Mellor "A Method of Calculating Compressible Turbulent Boundary Layers," NABA CR-1144, 1968.

Kahawita, R. A. and Meroney, R. N., "Penetrative Convective Instabilities in Parallel Flows", Submitted to Physics of Fluids, 1972.

Kahawita, R. A. and Meroney, R. N., "Convective Instabilities in Parallel, Quasi-Parallel, and Stationary Flows", CERL Report 1972 (in press).

Kahawita, R. A. and Meroney, R. N., "The Vortex Mode of Instability in Natural Convection Along Inclined Plates", submitted to JFM, 1972.

Kuettner, J., "The Band Structure of the Atmosphere", Tellus, Vol. 11, No. 3, p. 267, 1959.

Kuo, H. L., "Perturbations of Plane Couette Flow in Stratified Fluid and Origin of Cloud Streets", Physics of Fluids, Vol. 6, No. 2, p. 195, 1963.

Meroney, R. N. and Hsi, G., "Vortex Enhancement of Parallel Plate Heat and Mass Transport", submitted to IJHMT, 1972.

Mori, Y. and Uchida, Y., "Forced Convective Heat Transfer Between Horizontal Flat Plates", IJHMT, Vol. 9, p. 803-817, 1966.

Patel, V. C., "Calibration of the Preston Tube and Its Limitations on its Use In Pressure Gradients", J. Fluid Mechanics, Vol. 23, pp. 185-208, 1965.

Patel, V. C., "Measurements of Secondary Flow in the Boundary Layers of a 180° Channel", ARC-30428, 1968.

Rastogi, A. K. and J. H. Whitelaw, "A Procedure for Predicting the Influence of Longitudinal Curvature on Boundary Layer Flows," Imperial College of Science and Technology, Rept. of Mech. Engr. Tech. Report BL/TN/A37, 1970.

Rayt, M. J. and Meroney, R. N., "Longitudinal Rolls in Layers of Water", AIAA J. (1972) to be published.

Sandborn, V. A., "Class Notes for Experimental Methods in Fluid Mechanics," Colorado State University, CER71-72 VAS-40, 1972.

Sandborn, V. A., "Resistance Temperature Transducers", Metrology Press, Ft. Collins, Colorado, 1972.

Sandmayr, G.,"Uber das Auftreten von Langswirbeln in turbulenten Grenzschichten an konkaven Wanden", Deutsch Luftund Raumfahrt, DLR FB66-41, 1966.

Scorer, R. "Clouds of the World", David and Charles Ltd., 1972.

Soo, R. M. and G. L. Mellor, "An Experimental Investigation of Turbulent Boundary Layers Along Curved Surfaces," NASA CR-1940, 1972.

Spangler, J. G. and Wells Jr. C. S., "Effects of Spiral Longitudinal Vortices on Trubulent Boundary Layer Friction", NASA CR-145, Dec. 1964.

Stanton, T. E., Marshall, D. and C. N. Bryant, "On the Conditions at the Boundary of a Fluid in Turbulent Motion", Proc. Pap. Soc. London, Series A, No. 97, 1920.

Tani, I., "Boundary Layer Transition", Annual Review of Fluid Mechanics, Vol. 1, pp. 169, 1969.

Wilcken, H., Effect of Curved Surfaces on Turbulent Boundary Layers. NASA TT F-11421, 1967 (translation of Eng. Arch., Vol. 1, p. 357, 1930).

TABLE

TABLE 1. PRESSURE AND VELOCITY PROFILES

Convex Surface

x = -3.0

y (inch)	P_t-P_{sw} (inches H_2O)	P_s-P_{sw} (inches H_2O)	U_p/U_{pw}	$U_{(S\&M)}/U_{pw}$	$U_{(W)}/U_{pw}$
.04600	.81300	.00000	1.00000	.59991	.59991
.06600	.91300	.00000	1.00000	.63574	.63574
.08600	.98700	.00000	1.00000	.66100	.66100
.10600	1.04900	.00000	1.00000	.68144	.68144
.12600	1.11300	.00000	1.00000	.70192	.70192
.14600	1.15900	.00000	1.00000	.71628	.71628
.16600	1.22900	.00000	1.00000	.73759	.73759
.17600	1.25300	.00000	1.00000	.74476	.74476
.22600	1.36300	.00000	1.00000	.77676	.77676
.27600	1.45300	.00001	1.00000	.80200	.80200
.32600	1.55700	.00001	1.00000	.83020	.83020
.37600	1.65300	.00001	1.00000	.85541	.85542
.42600	1.73300	.00001	1.00000	.87587	.87587
.47600	1.81100	.00001	1.00000	.89536	.89536
.52600	1.90300	.00001	.99999	.91782	.91782
.62600	2.01900	.00002	.99999	.94538	.94538
.72600	2.13900	.00002	.99999	.97307	.97307
.82600	2.21700	.00003	.99999	.99065	.99065
.92600	2.25300	.00003	.99999	.99866	.99866
1.02600	2.25900	.00004	.99999	.99999	.99999
1.27600	2.25900	.00005	.99999	.99999	.99999
1.52600	2.25900	.00006	.99998	.99998	.99999

U_{pw} = 99.63805

$\Theta_{(S\&M)}$ = .09786 $\Theta_{(W)}$ = .09786 $\delta^*_{(S\&M)}$ = .13495 $\delta^*_{(W)}$ = .13495

x = 3.0

y (inch)	P_t-P_{sw} (inches H_2O)	P_s-P_{sw} (inches H_2O)	U_p/U_{pw}	$U_{(S\&M)}/U_{pw}$	$U_{(W)}/U_{pw}$
.02600	.81400	.00022	.99973	.59073	.59111
.04600	.93600	.00059	.99952	.63318	.63375
.06600	1.00400	.00100	.99931	.65551	.65625
.08600	1.04700	.00143	.99910	.66913	.67003
.10600	1.11700	.00188	.99888	.69092	.69195
.12600	1.17700	.00237	.99867	.70903	.71018
.14600	1.21900	.00287	.99846	.72134	.72261
.16600	1.29100	.00339	.99825	.74218	.74354
.17600	1.31900	.00367	.99815	.75009	.75151
.22600	1.41300	.00510	.99762	.77586	.77750
.27600	1.50300	.00662	.99710	.79972	.80156
.32600	1.58900	.00824	.99657	.82184	.82385
.37600	1.68300	.00994	.99605	.84542	.84756
.42600	1.75900	.01174	.99553	.86390	.86615
.47600	1.83300	.01360	.99500	.88151	.88385
.52600	1.92500	.01556	.99448	.90306	.90546
.62600	2.04500	.01967	.99343	.93004	.93253
.72600	2.15900	.02402	.99239	.95490	.95744
.82600	2.24900	.02857	.99134	.97386	.97641
.92600	2.29900	.03325	.99030	.98377	.98633
1.02600	2.31900	.03799	.98926	.98709	.98964
1.27600	2.32900	.04984	.98666	.98666	.98924
1.52600	2.32900	.06163	.98417	.98407	.98668
1.77600	2.32900	.07333	.98148	.98148	.98413
2.02600	2.32900	.08494	.97890	.97890	.98159
2.27600	2.32900	.09646	.97633	.97633	.97907
2.52600	2.32900	.10789	.97376	.97376	.97656

U_{pw} = 101.17003

$\Theta_{(S\&M)}$ = .10240 $\Theta_{(W)}$ = .09659 $\delta($$_{(S\&M)}$ = .13726 $\delta^*_{(W)}$ = .13106

Convex Surface (Continued)

x = 15.0

y (inch)	$P_t - P_{sw}$ (inches H_2O)	$P_s - P_{sw}$ (inches H_2O)	U_p/U_{pw}	$U_{(S\&M)}/U_{pw}$	$U_{(W)}/U_{pw}$
.02600	.67100	.00018	.99973	.53694	.53737
.03600	.72700	.00033	.99962	.55875	.55930
.04600	.74300	.00049	.99952	.56469	.56536
.05600	.78100	.00065	.99941	.57881	.57959
.06600	.81900	.00081	.99931	.59260	.59347
.07600	.85100	.00099	.99920	.60394	.60491
.08600	.88700	.00117	.99910	.61646	.61752
.09600	.91100	.00136	.99899	.62462	.62576
.10600	.93700	.00155	.99888	.63335	.63458
.11600	.96500	.00175	.99878	.64263	.64394
.12600	.99100	.00196	.99867	.65112	.65250
.14600	1.05100	.00239	.99846	.67035	.67187
.16600	1.12100	.00284	.99825	.69215	.69379
.18600	1.16300	.00332	.99804	.70480	.70655
.20600	1.21100	.00382	.99783	.71901	.72088
.22600	1.25100	.00433	.99762	.73060	.73257
.27600	1.34700	.00569	.99710	.75767	.75987
.32600	1.44100	.00715	.99657	.78325	.78565
.37600	1.55100	.00871	.99605	.81227	.81481
.42600	1.62900	.01037	.99553	.83206	.83474
.47600	1.70100	.01210	.99500	.84987	.85266
.52600	1.79300	.01391	.99448	.87226	.87513
.62600	1.90700	.01775	.99343	.89879	.90182
.72600	2.03100	.02183	.99239	.92689	.93000
.82600	2.09300	.02608	.99134	.94008	.94327
.92600	2.21700	.03052	.99030	.96699	.97017
1.02600	2.27700	.03513	.98926	.97920	.98238
1.27600	2.32300	.04688	.98686	.98666	.98986
1.52600	2.32300	.05866	.98407	.98407	.98729
1.77600	2.32300	.07034	.98148	.98148	.98474
2.02600	2.32300	.08193	.97890	.97890	.98221

U_{pw} = 101.17248

$\Theta_{(S\&M)}$ = .12562 $\Theta_{(W)}$ = .12038 $\delta^*_{(S\&M)}$ = .17421 $\delta^*_{(W)}$ = .16833

x = 27.0

.02600	.72100	.00020	.99973	.54432	.54475
.03600	.78700	.00036	.99962	.56855	.56908
.04600	.82700	.00053	.99952	.58267	.58331
.05600	.86700	.00070	.99941	.59646	.59720
.06600	.90100	.00089	.99931	.60790	.60874
.07600	.93300	.00108	.99920	.61847	.61941
.08600	.96700	.00128	.99910	.62952	.63054
.09600	.99300	.00149	.99899	.63780	.63890
.10600	1.02300	.00170	.99888	.64725	.64843
.11600	1.04900	.00192	.99878	.65531	.65656
.12600	1.07500	.00214	.99867	.66326	.66460
.14600	1.12300	.00260	.99846	.67769	.67916
.16600	1.19300	.00309	.99825	.69833	.69991
.18600	1.23600	.00360	.99804	.71059	.71230
.20600	1.27900	.00412	.99783	.72265	.72447
.22600	1.32100	.00467	.99762	.73423	.73615
.27600	1.41100	.00609	.99710	.75836	.76052
.32600	1.50900	.00762	.99657	.78384	.78620
.37600	1.60700	.00924	.99605	.80852	.81104
.42600	1.68700	.01096	.99553	.82801	.83067
.47600	1.76300	.01276	.99500	.84607	.84886
.52600	1.85300	.01463	.99448	.86709	.86997
.62600	1.97300	.01860	.99343	.89397	.89700
.72600	2.09300	.02281	.99239	.92006	.92319
.82600	2.19700	.02724	.99134	.94194	.94513
.92600	2.28500	.03185	.99030	.95900	.96312

Convex Surface (Continued)

x = 27.0

y (inch)	P_t-P_{sw} (inches H_2O)	P_s-P_{sw} (inches H_2O)	U_p/U_{pw}	$U_{(S\&M)}/U_{pw}$	$U_{(W)}/U_{pw}$
1.02600	2.35300	.03661	.98926	.97332	.97654
1.27600	2.42900	.04882	.98666	.98666	.98994
1.52600	2.42900	.06114	.98407	.98407	.98734
1.77600	2.42900	.07335	.98148	.98148	.98478
2.02600	2.42900	.08548	.97890	.97890	.98225

U_{pw} = 103.45502

$\Theta_{(S\&M)}$ = .12822 $\Theta_{(W)}$ = .12296 $\delta^*_{(S\&M)}$ = .17559 $\delta^*_{(W)}$ = .16967

x = 39.0

.02600	.68300	.00019	.99973	.52164	.52209
.04600	.78100	.00049	.99952	.55750	.55819
.06600	.85100	.00084	.99931	.58166	.58257
.08600	.92500	.00121	.99910	.60618	.60727
.10600	.98700	.00161	.99888	.62593	.62719
.12600	1.04300	.00204	.99867	.64321	.64463
.14600	1.10700	.00249	.99846	.66246	.66402
.16600	1.18100	.00297	.99825	.68408	.68576
.17600	1.19500	.00322	.99815	.68800	.68975
.22600	1.30100	.00453	.99762	.71737	.71941
.27600	1.39900	.00594	.99710	.74343	.74573
.32600	1.50100	.00745	.99657	.76965	.77216
.37600	1.60500	.00907	.99605	.79551	.79818
.42600	1.68500	.01079	.99553	.81469	.81753
.47600	1.76100	.01258	.99500	.83248	.83545
.52600	1.85500	.01446	.99448	.85411	.85717
.62600	1.98100	.01844	.99343	.88189	.88513
.72600	2.11100	.02267	.99239	.90970	.91305
.82600	2.22900	.02715	.99134	.93412	.93754
.92600	2.32500	.03184	.99030	.95333	.95678
1.02600	2.40100	.03669	.98926	.96805	.97151
1.27600	2.49500	.04920	.98666	.98463	.98811
1.52600	2.50500	.06188	.98407	.98407	.98757
1.77600	2.50500	.07448	.98148	.98148	.98502
2.02600	2.50500	.08699	.97890	.97890	.98248
2.27600	2.50500	.09940	.97633	.97633	.97996
2.52600	2.50500	.11172	.97376	.97376	.97745

U_{pw} = 105.06103

$\Theta_{(S\&M)}$ = .13683 $\Theta_{(W)}$ = .12940 $\delta^*_{(S\&M)}$ = .19016 $\delta^*_{(W)}$ = .18196

TABLE I PRESSURE AND VELOCITY PROFILES

Concave Surface

x = -3.0

y (inch)	P_t-P_{sw} (inches H_2O)	P_s-P_w (inches H_2O)	U_p/U_{pw}	$U_{(S\&M)}$	$U_{(W)}/U_{pw}$
.02600	.68600	.00000	1.00000	.55765	.55765
.04600	.77600	.00000	1.00000	.59310	.59310
.06600	.86100	.00000	1.00000	.62474	.62474
.08600	.96000	.00000	1.00000	.65968	.65968
.10600	1.04600	.00000	1.00000	.68859	.68859
.12600	1.11000	.00000	1.00000	.70935	.70935
.14600	1.17800	.00000	1.00000	.73075	.73075
.16600	1.24800	.00000	1.00000	.75215	.75215
.17600	1.28000	.00000	1.00000	.76173	.76173
.22600	1.39200	.00000	1.00000	.79436	.79436
.27600	1.48600	.00001	1.00000	.82074	.82074
.32600	1.58600	.00001	1.00000	.84790	.84791
.37600	1.68600	.00001	1.00000	.87423	.87423
.42600	1.76200	.00001	1.00000	.89371	.89371
.47600	1.85000	.00001	1.00000	.91576	.91576
.52600	1.93800	.00001	.99999	.93728	.93729
.62600	2.05200	.00002	.99999	.96446	.96446
.72600	2.14600	.00002	.99999	.98630	.98630
.82600	2.18600	.00003	.99999	.99545	.99545
.92600	2.20400	.00003	.99999	.99954	.99954
1.02600	2.20600	.00004	.99999	.99999	.99999
1.27600	2.20600	.00005	.99999	.99999	.99999
1.52600	2.20600	.00006	.99998	.99998	.99999
1.77600	2.20600	.00007	.99998	.99998	.99998
2.02600	2.20600	.00008	.99998	.99998	.99998
2.27600	2.20600	.00009	.99998	.99998	.99998
2.52600	2.20600	.00010	.99997	.99997	.99998

U_{pw} = 98.46228

$\Theta_{(S\&M)}$ = .08866 $\Theta_{(W)}$ = .08865 $\delta^*_{(S\&M)}$ = .12280 $\delta^*_{(W)}$ = .12279

x = 6.0, z = 0.0

y (inch)	P_t-P_{sw} (inches H_2O)	P_s-P_w (inches H_2O)	U_p/U_{pw}	$U_{(S\&M)}$	$U_{(W)}/U_{pw}$
.01500	.44000	-.00007	1.00015	.46727	.46698
.02500	.63200	-.00017	1.00025	.56007	.55970
.03500	.69400	-.00031	1.00035	.58703	.58656
.04500	.74600	-.00045	1.00045	.60875	.60819
.05500	.78400	-.00060	1.00055	.62418	.62354
.07500	.84400	-.00093	1.00075	.64787	.64707
.09500	.89200	-.00128	1.00095	.66628	.66532
.11500	.93600	-.00164	1.00115	.68274	.68165
.13500	.97200	-.00203	1.00135	.69597	.69474
.15500	1.02800	-.00243	1.00155	.71591	.71458
.17500	1.05600	-.00285	1.00175	.72581	.72436
.19500	1.08800	-.00328	1.00195	.73692	.73537
.21500	1.12000	-.00372	1.00215	.74787	.74622
.26500	1.19200	-.00488	1.00265	.77201	.77013
.31500	1.26000	-.00612	1.00315	.79417	.79209
.36500	1.34600	-.00743	1.00366	.82117	.81895
.41500	1.41400	-.00883	1.00416	.84204	.83968
.46500	1.47800	-.01029	1.00466	.86125	.85878
.61500	1.66000	-.01506	1.00617	.91377	.91108
.81500	1.86200	-.02223	1.00818	.96909	.96629
1.01500	1.98200	-.03009	1.01020	1.00133	.99854
1.26500	2.01600	-.04038	1.01273	1.01224	1.00947
1.51500	2.01800	-.05084	1.01527	1.01527	1.01252
1.76500	2.01800	-.06138	1.01781	1.01781	1.01510
2.01500	2.01800	-.07201	1.02035	1.02035	1.01769
2.26500	2.01800	-.08271	1.02291	1.02291	1.02029
2.51500	2.01800	-.09350	1.02547	1.02547	1.02290

U_{pw} = 94.29711

$\Theta_{(S\&M)}$ = .11885 $\Theta_{(W)}$ = .12451 $\delta^*_{(S\&M)}$ = .16201 $\delta^*_{(W)}$ = .16822

Concave Surface

x = 18.0, z = 0.0

y (inch)	P_t-P_{sw} (inches H_2O)	P_s-P_w (inches H_2O)	U_p/U_{pw}	$U_{(S\&M)}$	$U_{(W)}/U_{pw}$
.01500	.39600	-.00006	1.00015	.44823	.44793
.02500	.61200	-.00016	1.00025	.55725	.55688
.03500	.68000	-.00029	1.00035	.58752	.58705
.04500	.72800	-.00043	1.00045	.60803	.60746
.05500	.76600	-.00058	1.00055	.62382	.62317
.07500	.83400	-.00090	1.00075	.65115	.65034
.09500	.88800	-.00125	1.00095	.67212	.67118
.11500	.92600	-.00161	1.00115	.68659	.68550
.13500	.95800	-.00199	1.00135	.69858	.69736
.15500	1.00400	-.00238	1.00155	.71534	.71402
.17500	1.02400	-.00279	1.00175	.72267	.72122
.19500	1.05400	-.00321	1.00195	.73338	.73182
.21500	1.07400	-.00363	1.00215	.74053	.73886
.26500	1.12200	-.00474	1.00265	.75743	.75551
.31500	1.17600	-.00590	1.00315	.77593	.77378
.36500	1.23000	-.00711	1.00366	.79399	.79165
.41500	1.28000	-.00838	1.00416	.81041	.80788
.46500	1.33200	-.00970	1.00466	.82711	.82443
.61500	1.46000	-.01394	1.00617	.86717	.86411
.81500	1.65000	-.02028	1.00818	.92320	.91986
1.01500	1.80600	-.02735	1.01020	.96716	.96372
1.26500	1.94000	-.03699	1.01273	1.00419	1.00076
1.51500	1.97400	-.04712	1.01527	1.01527	1.01187
1.76500	1.97400	-.05742	1.01781	1.01781	1.01444
2.01500	1.97400	-.06780	1.02035	1.02035	1.01703
2.26500	1.97400	-.07826	1.02291	1.02291	1.01963
2.51500	1.97400	-.08880	1.02547	1.02547	1.02224

U_{pw} = 93.26343

$\Theta_{(S\&M)}$ = .14730 $\Theta_{(W)}$ = .15395 $\delta^*_{(S\&M)}$ = .19733 $\delta^*_{(W)}$ = .20478

x = 18, z = 0.4

y (inch)	P_t-P_{sw} (inches H_2O)	P_s-P_w (inches H_2O)	U_p/U_{pw}	$U_{(S\&M)}$	$U_{(W)}/U_{pw}$
.01500	.39800	-.00006	1.00015	.44981	.44951
.02500	.60200	-.00016	1.00025	.55325	.55287
.03500	.67600	-.00029	1.00035	.58639	.58591
.04500	.73200	-.00043	1.00045	.61031	.60975
.05500	.76400	-.00058	1.00055	.62363	.62299
.07500	.83200	-.00090	1.00075	.65103	.65022
.09500	.87800	-.00124	1.00095	.66902	.66807
.11500	.91600	-.00160	1.00115	.68358	.68249
.13500	.95000	-.00197	1.00135	.69637	.69515
.15500	1.00000	-.00237	1.00155	.71465	.71331
.17500	1.02400	-.00277	1.00175	.72340	.72194
.19500	1.04600	-.00319	1.00195	.73135	.72978
.21500	1.08000	-.00362	1.00215	.74333	.74166
.26500	1.12600	-.00473	1.00265	.75953	.75761
.31500	1.17600	-.00589	1.00315	.77671	.77456
.36500	1.24000	-.00710	1.00366	.79798	.79564
.41500	1.28400	-.00838	1.00416	.81247	.80996
.46500	1.32800	-.00970	1.00466	.82671	.82404
.61500	1.47000	-.01396	1.00617	.87096	.86792
.81500	1.65600	-.02032	1.00818	.92577	.92246
1.01500	1.82000	-.02743	1.01020	.97178	.96839
1.26500	1.94000	-.03710	1.01273	1.00518	1.00180
1.51500	1.96800	-.04723	1.01527	1.01477	1.01141
1.76500	1.97000	-.05750	1.01781	1.01781	1.01449
2.01500	1.97000	-.06786	1.02035	1.02035	1.01708
2.26500	1.97000	-.07830	1.02291	1.02291	1.01968
2.51500	1.97000	-.08882	1.02547	1.02547	1.02229

U_{pw} = 93.16889

$\Theta_{(S\&M)}$ = .14514 $\Theta_{(W)}$ = .15172 $\delta^*_{(S\&M)}$ = .19473 $\delta^*_{(W)}$ = .20209

Concave Surface

$x = 18, \quad z = 0.8$

.01500	.41200	-.00006	1.00015	.45718	.45689
.02500	.59800	-.00016	1.00025	.55085	.55047
.03500	.67600	-.00029	1.00035	.58579	.58532
.04500	.72200	-.00043	1.00045	.60552	.60496
.05500	.76800	-.00058	1.00055	.62463	.62398
.07500	.82600	-.00090	1.00075	.64803	.64722
.09500	.87200	-.00124	1.00095	.66607	.66511
.11500	.92200	-.00160	1.00115	.68511	.68402
.13500	.96000	-.00198	1.00135	.69930	.69809
.15500	1.00200	-.00237	1.00155	.71464	.71330
.17500	1.03000	-.00278	1.00175	.72477	.72332
.19500	1.06000	-.00320	1.00195	.73545	.73389
.21500	1.08600	-.00363	1.00215	.74462	.74296
.26500	1.14000	-.00475	1.00265	.76343	.76152
.31500	1.19200	-.00592	1.00315	.78113	.77901
.36500	1.24800	-.00716	1.00366	.79972	.79740
.41500	1.29400	-.00844	1.00416	.81477	.81228
.46500	1.34000	-.00977	1.00466	.82956	.82691
.61500	1.48600	-.01407	1.00617	.87474	.87173
.81500	1.67600	-.02051	1.00818	.93031	.92705
1.01500	1.83800	-.02770	1.01020	.97551	.97218
1.26500	1.95200	-.03745	1.01273	1.00721	1.00390
1.51500	1.97400	-.04761	1.01527	1.01527	1.01199
1.76500	1.97400	-.05792	1.01781	1.01781	1.01456
2.01500	1.97400	-.06830	1.02035	1.02035	1.01715
2.26500	1.97400	-.07876	1.02291	1.02291	1.01975
2.51500	1.97400	-.08930	1.02547	1.02547	1.02237

$U_{pw} = 93.26343$

$\Theta_{(S\&M)} = .14196 \quad \Theta_{(W)} = .14843 \quad \delta^*_{(S\&M)} = .19061 \quad \delta^*_{(W)} = .19783$

$x = 18; \quad z = 1.2$

y (inch)	$P_t - P_{sw}$ (inches H_2O)	$P_s - P_w$ (inches H_2O)	U_p/U_{pw}	$U_{(S\&M)}$	$U_{(W)}/U_{pw}$
.01500	.45000	-.00007	1.00015	.47923	.47895
.02500	.66000	-.00018	1.00025	.58042	.58007
.03500	.74800	-.00032	1.00035	.61802	.61758
.04500	.80000	-.00047	1.00045	.63926	.63874
.05500	.85000	-.00064	1.00055	.65904	.65845
.07500	.92400	-.00099	1.00075	.68735	.68663
.09500	.97400	-.00138	1.00095	.70593	.70508
.11500	1.01000	-.00177	1.00115	.71909	.71811
.13500	1.08000	-.00219	1.00135	.74375	.74268
.15500	1.11000	-.00263	1.00155	.75422	.75305
.17500	1.13400	-.00308	1.00175	.76255	.76128
.19500	1.16400	-.00354	1.00195	.77277	.77141
.21500	1.17800	-.00402	1.00215	.77764	.77618
.26500	1.23600	-.00523	1.00265	.79705	.79538
.31500	1.27400	-.00649	1.00315	.80973	.80787
.36500	1.35400	-.00782	1.00366	.83513	.83313
.41500	1.40000	-.00921	1.00416	.84964	.84750
.46500	1.44000	-.01065	1.00466	.86214	.85987
.61500	1.58200	-.01524	1.00617	.90482	.90227
.81500	1.75000	-.02203	1.00818	.95309	.95036
1.01500	1.87400	-.02945	1.01020	.98775	.98497
1.26500	1.95200	-.03930	1.01273	1.01021	1.00744
1.51500	1.96200	-.04945	1.01527	1.01527	1.01252
1.76500	1.96200	-.05970	1.01781	1.01781	1.01510
2.01500	1.96200	-.07003	1.02035	1.02035	1.01769
2.26500	1.96200	-.08044	1.02291	1.02291	1.02029
2.51500	1.96200	-.09092	1.02547	1.02547	1.02291

$U_{pw} = 92.97952$

$\Theta_{(S\&M)} = .12130 \quad \Theta_{(W)} = .12685 \quad \delta^*_{(S\&M)} = .15905 \quad \delta^*_{(W)} = .16512$

Concave Surface

x = 18, z = 1.6

.01500	.47600	-.00007	1.00015	.49387	.49360
.02500	.68400	-.00019	1.00025	.59207	.59173
.03500	.76800	-.00033	1.00035	.62749	.62706
.04500	.82400	-.00049	1.00045	.65008	.64958
.05500	.86800	-.00066	1.00055	.66732	.66675
.07500	.94000	-.00102	1.00075	.69467	.69397
.09500	.99600	-.00141	1.00095	.71528	.71446
.11500	1.04400	-.00182	1.00115	.73252	.73159
.13500	1.08800	-.00225	1.00135	.74800	.74697
.15500	1.14000	-.00270	1.00155	.76585	.76472
.17500	1.17000	-.00316	1.00175	.77607	.77485
.19500	1.19200	-.00363	1.00195	.78354	.78223
.21500	1.23200	-.00412	1.00215	.79675	.79537
.26500	1.28600	-.00539	1.00265	.81453	.81295
.31500	1.34400	-.00671	1.00315	.83315	.83142
.36500	1.41000	-.00810	1.00366	.85377	.85191
.41500	1.46400	-.00955	1.00416	.87038	.86840
.46500	1.51800	-.01106	1.00466	.88669	.88461
.61500	1.66400	-.01590	1.00617	.92950	.92721
.81500	1.82400	-.02301	1.00818	.97463	.97224
1.01500	1.92000	-.03067	1.01020	1.00155	.99915
1.26500	1.95000	-.04064	1.01273	1.01172	1.00933
1.51500	1.95400	-.05077	1.01527	1.01527	1.01291
1.76500	1.95400	-.06098	1.01781	1.01781	1.01548
2.01500	1.95400	-.07128	1.02035	1.02035	1.01808
2.26500	1.95400	-.08165	1.02291	1.02291	1.02068
2.51500	1.95400	-.09211	1.02547	1.02547	1.02330

U_{pw} = 92.78977

$\Theta_{(S\&M)}$ = .10494 $\Theta_{(W)}$ = .10984 $\delta^*_{(S\&M)}$ = .13780 $\delta^*_{(W)}$ = .14309

x = 18; z = 2.0

y (inch)	P_t-P_{sw} (inches H_2O)	P_t-P_w (inches H_2O)	U_p/U_{pw}	$U_{(S\&M)}$	$U_{(W)}/U_{pw}$
.01500	.47400	-.00007	1.00015	.49333	.49307
.02500	.65400	-.00018	1.00025	.57956	.57921
.03500	.74600	-.00032	1.00035	.61908	.61865
.04500	.80600	-.00048	1.00045	.64361	.64310
.05500	.84800	-.00064	1.00055	.66028	.65970
.07500	.91200	-.00100	1.00075	.68498	.68425
.09500	.96400	-.00137	1.00095	.70446	.70361
.11500	1.01900	-.00177	1.00115	.72448	.72351
.13500	1.06000	-.00219	1.00135	.73912	.73805
.15500	1.11200	-.00262	1.00155	.75721	.75604
.17500	1.14000	-.00308	1.00175	.76689	.76563
.19500	1.16400	-.00354	1.00195	.77513	.77378
.21500	1.19400	-.00401	1.00215	.78525	.78382
.26500	1.24800	-.00524	1.00265	.80331	.80168
.31500	1.31600	-.00653	1.00315	.82534	.82354
.36500	1.38000	-.00789	1.00366	.84559	.84365
.41500	1.43400	-.00931	1.00416	.86239	.86033
.46500	1.48400	-.01079	1.00466	.87771	.87553
.61500	1.63400	-.01553	1.00617	.92213	.91974
.81500	1.80800	-.02254	1.00818	.97140	.96889
1.01500	1.91400	-.03016	1.01020	1.00102	.99850
1.26500	1.94600	-.04010	1.01273	1.01172	1.00921
1.51500	1.95000	-.05021	1.01527	1.01527	1.01279
1.76500	1.95000	-.06040	1.01781	1.01781	1.01537
2.01500	1.95000	-.07067	1.02035	1.02035	1.01796
2.26500	1.95000	-.08102	1.02291	1.02291	1.02056
2.51500	1.95000	-.09145	1.02547	1.02547	1.02318

U_{pw} = 92.69475

$\Theta_{(S\&M)}$ = .10950 $\Theta_{(W)}$ = .11462 $\delta^*_{(S\&M)}$ = .14455 $\delta^*_{(W)}$ = .15011

Concave Surface

x = 18; z = 2.4

.01500	.46400	-.00007	1.00015	.48149	.48122
.02500	.67400	-.00018	1.00025	.58037	.58002
.03500	.76800	-.00033	1.00035	.61962	.61919
.04500	.83000	-.00049	1.00045	.64426	.64375
.05500	.87400	-.00066	1.00055	.66123	.66065
.07500	.94400	-.00102	1.00075	.68743	.68671
.09500	.99400	-.00141	1.00095	.70563	.70478
.11500	1.04400	-.00182	1.00115	.72337	.72240
.13500	1.08400	-.00225	1.00135	.73731	.73623
.15500	1.13600	-.00269	1.00155	.75496	.75380
.17500	1.16600	-.00315	1.00175	.76508	.76381
.19500	1.19000	-.00363	1.00195	.77312	.77177
.21500	1.22200	-.00411	1.00215	.78364	.78220
.26500	1.26400	-.00536	1.00265	.79753	.79587
.31500	1.33200	-.00667	1.00315	.81914	.81731
.36500	1.39400	-.00805	1.00366	.83841	.83644
.41500	1.44400	-.00948	1.00416	.85375	.85164
.46500	1.49800	-.01097	1.00466	.86997	.86774
.61500	1.65000	-.01576	1.00617	.91418	.91171
.81500	1.82800	-.02284	1.00818	.96364	.96103
1.01500	1.95000	-.03057	1.01020	.99678	.99414
1.26500	1.99800	-.04074	1.01273	1.01125	1.00863
1.51500	2.00200	-.05111	1.01527	1.01477	1.01218
1.76500	2.00400	-.06158	1.01781	1.01781	1.01525
2.01500	2.00400	-.07213	1.02035	1.02035	1.01784
2.26500	2.00400	-.08277	1.02291	1.02291	1.02044
2.51500	2.00400	-.09348	1.02547	1.02547	1.02306

U_{pw} = 93.96945

$\Theta_{(S\&M)}$ = .11476 $\Theta_{(W)}$ = .12008 $\delta^*_{(S\&M)}$ = .15114 $\delta^*_{(W)}$ = .15693

x = 30; z = 0.0

y (inch)	P_t-P_{sw} (inches H_2O)	P_t-P_w (inches H_2O)	U_p/U_{pw}	$U_{(S\&M)}$	$U_{(W)}/U_{pw}$
.01500	.52200	-.00008	1.00015	.49628	.49602
.02500	.72200	-.00020	1.00025	.58373	.58339
.03500	.79600	-.00035	1.00035	.61304	.61261
.04500	.85200	-.00052	1.00045	.63436	.63384
.05500	.89400	-.00069	1.00055	.64992	.64933
.07500	.97000	-.00107	1.00075	.67721	.67648
.09500	1.03000	-.00147	1.00095	.69806	.69720
.11500	1.07200	-.00189	1.00115	.71238	.71139
.13500	1.10000	-.00233	1.00135	.72186	.72075
.15500	1.14200	-.00278	1.00155	.73571	.73449
.17500	1.16600	-.00324	1.00175	.74363	.74230
.19500	1.19800	-.00371	1.00195	.75397	.75254
.21500	1.21200	-.00420	1.00215	.75860	.75706
.26500	1.25800	-.00544	1.00265	.77340	.77162
.31500	1.30000	-.00673	1.00315	.78673	.78473
.36500	1.34800	-.00807	1.00366	.80161	.79941
.41500	1.38800	-.00945	1.00416	.81390	.81151
.46500	1.41800	-.01087	1.00466	.82315	.82058
.61500	1.53600	-.01536	1.00617	.85803	.85504
.81500	1.69400	-.02194	1.00818	.90263	.89925
1.01500	1.83600	-.02917	1.01020	.94113	.93753
1.26500	1.99200	-.03902	1.01273	.98202	.97833
1.51500	2.09600	-.04961	1.01527	1.00921	1.00555
1.76500	2.11800	-.06060	1.01781	1.01688	1.01325
2.01500	2.12200	-.07175	1.02035	1.02035	1.01676
2.26500	2.12200	-.08298	1.02291	1.02291	1.01937
2.51500	2.12200	-.09431	1.02547	1.02547	1.02198

U_{pw} = 96.69544

$\Theta_{(S\&M)}$ = .16138 $\Theta_{(W)}$ = .16826 $\delta^*_{(S\&M)}$ = .20845 $\delta^*_{(W)}$ = .21623

Concave Surface

x = 42; z = 0.0

.01500	.63800	-.00010	1.00015	.55041	.55018
.02500	.72200	-.00023	1.00025	.58567	.58533
.03500	.78000	-.00038	1.00035	.60887	.60844
.04500	.82400	-.00054	1.00045	.62593	.62542
.05500	.86400	-.00071	1.00055	.64107	.64047
.07500	.92800	-.00107	1.00075	.66463	.66388
.09500	.98000	-.00145	1.00095	.68323	.68234
.11500	1.02000	-.00185	1.00115	.69726	.69624
.13500	1.05600	-.00227	1.00135	.70968	.70854
.15500	1.10000	-.00270	1.00155	.72452	.72326
.17500	1.13200	-.00315	1.00175	.73519	.73382
.19500	1.15200	-.00361	1.00195	.74189	.74041
.21500	1.17200	-.00408	1.00215	.74852	.74693
.26500	1.22000	-.00528	1.00265	.76424	.76240
.31500	1.26000	-.00653	1.00315	.77720	.77513
.36500	1.29600	-.00782	1.00366	.78875	.78645
.41500	1.33000	-.00915	1.00416	.79954	.79704
.46500	1.36600	-.01051	1.00466	.81077	.80808
.61500	1.45400	-.01480	1.00617	.83793	.83473
.81500	1.58000	-.02099	1.00818	.87519	.87148
1.01500	1.70400	-.02771	1.01020	.91042	.90636
1.26500	1.85400	-.03687	1.01273	.95138	.94710
1.51500	1.98600	-.04682	1.01527	.98635	.98201
1.76500	2.07000	-.05739	1.01781	1.00891	1.00459
2.01500	2.10400	-.06835	1.02035	1.01942	1.01515
2.26500	2.10600	-.07948	1.02291	1.02244	1.01821
2.51500	2.10800	-.09071	1.02547	1.02547	1.02129

U_{pw} = 96.37694

$\Theta_{(S\&M)}$ = .19139 $\Theta_{(W)}$ = .19907 $\delta^*_{(S\&M)}$ = .2446 $\delta^*_{(W)}$ = .25337

x = 42; z = 0.4

y (inch)	$P_t - P_{sw}$ (inches H_2O)	$P_t - P_w$ (inches H_2O)	U_p/U_{pw}	$U_{(S\&M)}$	$U_{(W)}/U_{pw}$
.01500	.65000	-.00010	1.00015	.55583	.55560
.02500	.78000	-.00024	1.00025	.60899	.60867
.03500	.85200	-.00040	1.00035	.63660	.63620
.04500	.89600	-.00058	1.00045	.65296	.65248
.05500	.94000	-.00076	1.00055	.66891	.66836
.07500	1.01000	-.00115	1.00075	.69360	.69291
.09500	1.07200	-.00157	1.00095	.71479	.71398
.11500	1.12000	-.00201	1.00115	.73083	.72991
.13500	1.16200	-.00247	1.00135	.74462	.74359
.15500	1.21000	-.00294	1.00155	.76004	.75891
.17500	1.23600	-.00344	1.00175	.76838	.76715
.19500	1.25000	-.00394	1.00195	.77295	.77163
.21500	1.27200	-.00444	1.00215	.77993	.77852
.26500	1.33000	-.00575	1.00265	.79802	.79640
.31500	1.36600	-.00711	1.00315	.80929	.80746
.36500	1.39000	-.00850	1.00366	.81691	.81490
.41500	1.42000	-.00992	1.00416	.82620	.82400
.46500	1.45000	-.01137	1.00466	.83538	.83301
.61500	1.51400	-.01588	1.00617	.85515	.85231
.81500	1.62200	-.02228	1.00818	.88691	.88361
1.01500	1.74000	-.02917	1.01020	.92017	.91655
1.26500	1.88000	-.03849	1.01273	.95829	.95444
1.51500	2.00400	-.04856	1.01527	.99113	.98723
1.76500	2.08000	-.05921	1.01781	1.01172	1.00785
2.01500	2.10200	-.07020	1.02035	1.01942	1.01560
2.26500	2.10600	-.08134	1.02291	1.02291	1.01913
2.51500	2.10600	-.09257	1.02547	1.02547	1.02174

U_{pw} = 96.33120

$\Theta_{(S\&M)}$ = .17438 $\Theta_{(W)}$ = .18137 $\delta^*_{(S\&M)}$ = .21785 $\delta^*_{(W)}$ = .22581

Concave Surface

x = 42; z = 0.8

y (inch)	P_t-P_{sw} (inches H_2O)	P_t-P_w (inches H_2O)	U_p/U_{pw}	$U_{(S\&M)}$	$U_{(W)}/U_{pw}$
.01500	.62400	-.00009	1.00015	.54669	.54645
.02500	.83400	-.00024	1.00025	.63209	.63179
.03500	.91400	-.00041	1.00035	.66183	.66145
.04500	.96400	-.00060	1.00045	.67981	.67936
.05500	1.02600	-.00080	1.00055	.70143	.70092
.07500	1.10400	-.00123	1.00075	.72783	.72720
.09500	1.17000	-.00168	1.00095	.74947	.74874
.11500	1.22600	-.00216	1.00115	.76740	.76658
.13500	1.27200	-.00267	1.00135	.78187	.78095
.15500	1.32400	-.00319	1.00155	.79787	.79688
.17500	1.36400	-.00373	1.00175	.81002	.80896
.19500	1.38800	-.00428	1.00195	.81733	.81619
.21500	1.41400	-.00484	1.00215	.82515	.82394
.26500	1.46400	-.00629	1.00265	.84011	.83874
.31500	1.50000	-.00778	1.00315	.85090	.84937
.36500	1.53400	-.00932	1.00366	.86099	.85932
.41500	1.56400	-.01088	1.00416	.86986	.86806
.46500	1.58400	-.01247	1.00466	.87592	.87399
.61500	1.64400	-.01739	1.00617	.89386	.89158
.81500	1.73800	-.02428	1.00818	.92088	.91826
1.01500	1.81800	-.03157	1.01020	.94359	.94072
1.26500	1.94400	-.04127	1.01273	.97763	.97462
1.51500	2.03000	-.05158	1.01527	1.00103	.99798
1.76500	2.07800	-.06231	1.01781	1.01498	1.01196
2.01500	2.08800	-.07327	1.02035	1.01989	1.01691
2.26500	2.09000	-.08435	1.02291	1.02291	1.01998
2.51500	2.09000	-.09551	1.02547	1.02547	1.02260

U_{pw} = 95.96458

$\Theta_{(S\&M)}$ = .13941 $\Theta_{(W)}$ = .14511 $\delta^*_{(S\&M)}$ = .17051 $\delta^*_{(W)}$ = .17679

x = 42; z = 1.2

y (inch)	P_t-P_{sw} (inches H_2O)	P_t-P_w (inches H_2O)	U_p/U_{pw}	$U_{(S\&M)}$	$U_{(W)}/U_{pw}$
.01500	.62000	-.00009	1.00015	.54467	.54444
.02500	.87200	-.00024	1.00025	.64601	.64571
.03500	.95600	-.00043	1.00035	.67652	.67615
.04500	1.02200	-.00062	1.00045	.69959	.69916
.05500	1.05600	-.00083	1.00055	.71125	.71076
.07500	1.15200	-.00127	1.00075	.74308	.74248
.09500	1.22000	-.00175	1.00095	.76490	.76421
.11500	1.28200	-.00225	1.00115	.78429	.78351
.13500	1.32600	-.00277	1.00135	.79784	.79698
.15500	1.38600	-.00332	1.00155	.81586	.81493
.17500	1.42200	-.00388	1.00175	.82658	.82558
.19500	1.45600	-.00446	1.00195	.83660	.83553
.21500	1.48600	-.00505	1.00215	.84536	.84424
.26500	1.54200	-.00658	1.00265	.86163	.86037
.31500	1.58000	-.00815	1.00315	.87268	.87129
.36500	1.62600	-.00977	1.00366	.88576	.88426
.41500	1.65600	-.01142	1.00416	.89438	.89278
.46500	1.69600	-.01312	1.00466	.90557	.90387
.61500	1.77000	-.01839	1.00617	.92653	.92459
.81500	1.86200	-.02580	1.00818	.95210	.94994
1.01500	1.94000	-.03359	1.01020	.97358	.97129
1.26500	2.02000	-.04380	1.01273	.99559	.99324
1.51500	2.07200	-.05443	1.01527	1.01055	1.00819
1.76500	2.09000	-.06531	1.01781	1.01734	1.01502
2.01500	2.09200	-.07633	1.02035	1.02035	1.01808
2.26500	2.09200	-.08743	1.02291	1.02291	1.02068
2.51500	2.09200	-.09863	1.02547	1.02547	1.02330

U_{pw} = 96.01048

$\Theta_{(S\&M)}$ = .10861 $\Theta_{(W)}$ = .11326 $\delta^*_{(S\&M)}$ = .13328 $\delta^*_{(W)}$ = .13829

Concave Surface

x = 42; z = 1.6

.01500	.64800	-.00010	1.00015	.55789	.55766
.02500	.86200	-.00025	1.00025	.64353	.64323
.03500	.94800	-.00043	1.00035	.67498	.67461
.04500	1.00600	-.00062	1.00045	.69543	.69500
.05500	1.05200	-.00083	1.00055	.71127	.71077
.07500	1.14600	-.00127	1.00075	.74257	.74197
.09500	1.21600	-.00174	1.00095	.76511	.76442
.11500	1.27800	-.00224	1.00115	.78457	.78379
.13500	1.31600	-.00277	1.00135	.79636	.79549
.15500	1.38000	-.00331	1.00155	.81565	.81472
.17500	1.41600	-.00387	1.00175	.82642	.82542
.19500	1.44600	-.00444	1.00195	.83532	.83426
.21500	1.46600	-.00503	1.00215	.84129	.84016
.26500	1.52600	-.00653	1.00265	.85881	.85754
.31500	1.57000	-.00809	1.00315	.87160	.87020
.36500	1.62200	-.00970	1.00366	.88636	.88485
.41500	1.66000	-.01136	1.00416	.89715	.89554
.46500	1.69600	-.01306	1.00466	.90728	.90559
.61500	1.79200	-.01837	1.00617	.93395	.93204
.81500	1.88200	-.02586	1.00818	.95891	.95681
1.01500	1.97600	-.03376	1.01020	.98422	.98203
1.26500	2.04200	-.04412	1.01273	1.00273	1.00051
1.51500	2.07600	-.05481	1.01527	1.01337	1.01117
1.76500	2.08200	-.06569	1.01781	1.01734	1.01517
2.01500	2.08400	-.07667	1.02035	1.02035	1.01823
2.26500	2.08400	-.08773	1.02291	1.02291	1.02083
2.51500	2.08400	-.09889	1.02547	1.02547	1.02345

U_{pw} = 95.82673

$\Theta_{(S\&M)}$ = .10173 $\Theta_{(W)}$ = .10618 $\delta^*_{(S\&M)}$ = .12569 $\delta^*_{(W)}$ = .13047

x = 42; = 2.0

y (inch)	P_t-P_{sw} (inches H_2O)	P_t-P_w (inches H_2O)	U_p/U_{pw}	$U_{(S\&M)}$	$U_{(W)}/U_{pw}$
.01500	.64000	-.00010	1.00015	.55444	.55421
.02500	.84800	-.00024	1.00025	.63829	.63799
.03500	.93200	-.00042	1.00035	.66927	.66889
.04500	.97600	-.00061	1.00045	.68500	.68456
.05500	1.03800	-.00082	1.00055	.70653	.70603
.07500	1.11800	-.00125	1.00075	.73346	.73285
.09500	1.18200	-.00171	1.00095	.75437	.75366
.11500	1.23400	-.00219	1.00115	.77099	.77018
.13500	1.28600	-.00270	1.00135	.78727	.78637
.15500	1.35600	-.00323	1.00155	.80856	.80760
.17500	1.38200	-.00378	1.00175	.81649	.81545
.19500	1.40600	-.00434	1.00195	.82375	.82265
.21500	1.43400	-.00491	1.00215	.83211	.83094
.26500	1.48600	-.00638	1.00265	.84756	.84623
.31500	1.53600	-.00790	1.00315	.86219	.86072
.36500	1.57600	-.00947	1.00366	.87382	.87223
.41500	1.61200	-.01108	1.00416	.88422	.88251
.46500	1.64800	-.01273	1.00466	.89450	.89269
.61500	1.74200	-.01789	1.00617	.92101	.91895
.81500	1.85000	-.02521	1.00818	.95087	.94859
1.01500	1.93800	-.03298	1.01020	.97491	.97250
1.26500	2.03200	-.04321	1.01273	1.00034	.99789
1.51500	2.06600	-.05384	1.01527	1.01100	1.00856
1.76500	2.08000	-.06468	1.01781	1.01686	1.01445
2.01500	2.08200	-.07564	1.02035	1.01988	1.01752
2.26500	2.08400	-.08670	1.02291	1.02291	1.02059
2.51500	2.08400	-.09785	1.02547	1.02547	1.02321

U_{pw} = 95.82673

$\Theta_{(S\&M)}$ = .11224 $\Theta_{(W)}$ = .11709 $\delta^*_{(S\&M)}$ = .13868 $\delta^*_{(W)}$ = .14392

Concave Surface

x = 42; z = 2.4

.01500	.59600	-.00009	1.00015	.52606	.52581
.02500	.83200	-.00023	1.00025	.62161	.62130
.03500	.91800	-.00041	1.00035	.65306	.65267
.04500	.98200	-.00060	1.00045	.67555	.67509
.05500	1.03600	-.00080	1.00055	.69399	.69346
.07500	1.13000	-.00123	1.00075	.72500	.72436
.09500	1.18800	-.00170	1.00095	.74359	.74284
.11500	1.24600	-.00219	1.00115	.76172	.76088
.13500	1.28600	-.00269	1.00135	.77407	.77313
.15500	1.34600	-.00322	1.00155	.79209	.79107
.17500	1.38200	-.00377	1.00175	.80281	.80172
.19500	1.41200	-.00433	1.00195	.81168	.81051
.21500	1.43600	-.00490	1.00215	.81875	.81751
.26500	1.47600	-.00637	1.00265	.83061	.82919
.31500	1.52600	-.00788	1.00315	.84505	.84347
.36500	1.57600	-.00945	1.00366	.85925	.85753
.41500	1.60000	-.01105	1.00416	.86628	.86443
.46500	1.63800	-.01269	1.00466	.87697	.87500
.61500	1.72600	-.01781	1.00617	.90163	.89934
.81500	1.83000	-.02506	1.00818	.93018	.92759
1.01500	1.93400	-.03277	1.01020	.95788	.95511
1.26500	2.05200	-.04304	1.01273	.98863	.98576
1.51500	2.11690	-.05386	1.01527	1.00629	1.00342
1.76500	2.15000	-.06501	1.01781	1.01644	1.01359
2.01500	2.15600	-.07634	1.02035	1.02035	1.01755
2.26500	2.15600	-.08777	1.02291	1.02291	1.02015
2.51500	2.15600	-.09930	1.02547	1.02547	1.02277

U_{pw} = 97.46803

$\Theta_{(S\&M)}$ = .13103 $\Theta_{(W)}$ = .13656 $\delta^*_{(S\&M)}$ = .16234 $\delta^*_{(W)}$ = .16840

TABLE 2

LONGITUDINAL TURBULENCE INTENSITY

Convex Surface

	x = -3.0 inches		x = +3.0 inches		x = 15.0 inches
y (inches)	$\overline{u'}/U$	y	$\overline{u'}/U$	y	$\overline{u'}/U$
.12500	.10880	.12500	.10049	.12500	.10227
.13500	.11163	.13500	.09804	.13500	.10090
.14500	.11139	.14500	.09580	.14500	.09809
.15500	.10824	.15500	.09393	.15500	.09697
.16500	.10698	.16500	.09200	.16500	.09475
.18500	.10248	.18500	.08876	.18500	.09195
.20500	.09898	.20500	.08424	.20500	.08769
.22500	.09455	.22500	.08112	.22500	.08650
.24500	.09000	.24500	.07868	.24500	.08276
.26500	.08407	.26500	.07497	.26500	.07928
.28500	.08099	.28500	.07293	.28500	.07639
.30500	.07695	.30500	.06999	.30500	.07410
.32500	.07503	.32500	.06773	.32500	.07176
.37500	.06840	.37500	.06283	.37500	.06565
.42500	.06283	.42500	.05881	.42500	.06064
.47500	.05732	.47500	.05306	.47500	.05450
.52500	.05165	.52500	.05002	.52500	.04967
.57500	.04606	.57500	.04500	.57500	.04598
.72500	.02853	.72500	.03065	.72500	.03394
.92500	.00894	.92500	.01539	.92500	.01466
1.12500	0	1.12500	0	1.12500	.00677
1.37500	0	1.37500	0	1.37500	0
1.62500	0	1.62500	0	1.62500	0
1.87500	0	1.87500	0	1.87500	0
2.12500	0	2.12500	0	2.12500	0
2.37500	0	2.37500	0	2.37500	0
2.62500	0	2.62500	0	2.62500	0

	x = 27.0 inches		x = 39.0 inches
.12500	.10085	.12500	.10371
.13500	.10003	.13500	.10316
.14500	.09697	.14500	.10144
.15500	.09477	.15500	.09753
.16500	.09310	.16500	.09558
.18500	.09004	.18500	.09222
.20500	.08799	.20500	.08917
.22500	.08459	.22500	.08608
.24500	.08179	.24500	.08303
.26500	.07830	.26500	.07959
.28500	.07608	.28500	.07737
.30500	.07447	.30500	.07447
.32500	.07220	.32500	.07350
.37500	.06726	.37500	.06814
.42500	.06206	.42500	.06368
.47500	.05615	.47500	.05734
.52500	.05194	.52500	.05323
.57500	.04845	.57500	.04955
.72500	.03651	.72500	.03795
.92500	.19386	.92500	.02237
1.12500	.01156	1.12500	.01697
1.37500	0	1.37500	0
1.62500	0	1.62500	0
1.87500	0	1.87500	0
2.12500	0	2.12500	0
2.37500	0	2.37500	0
2.62500	0	2.62500	0

Concave Surface

y (inches)	x = -3: $\overline{u'}/U$	y	x = 6.0; z = 0.0: $\overline{u'}/U$	y	x = 18; z = 0.0: $\overline{u'}/U$
.10000	.10572	.10000	.10142	.10000	.11598
.11000	.10623	.11000	.09934	.11000	.11386
.12000	.10448	.12000	.09845	.12000	.11139
.13000	.10169	.13000	.09611	.13000	.11053
.14000	.09942	.14000	.09522	.14000	.10933
.16000	.09561	.16000	.09202	.16000	.10695
.18000	.09124	.18000	.08974	.18000	.10400
.20000	.08822	.20000	.08809	.20000	.10230
.22000	.08593	.22000	.08550	.22000	.10044
.24000	.08068	.24000	.08243	.24000	.09709
.26000	.07695	.26000	.07961	.26000	.09474
.28000	.07536	.28000	.07779	.28000	.09344
.30000	.07249	.30000	.07466	.30000	.09249
.35000	.06752	.35000	.06554	.35000	.08769
.40000	.06084	.40000	.05639	.40000	.08465
.45000	.05524	.45000	.04463	.45000	.07973
.50000	.04923	.50000	.03518	.50000	.07542
.55000	.04360	.55000	.02841	.55000	.07301
.70000	.02172	.70000	.01549	.70000	.06129
.90000	.00647	.90000	.00539	.90000	.04649
1.10000	0	1.10000	.00324	1.10000	.02699
1.35000	0	1.35000	.00279	1.35000	.00913
1.60000	0	1.60000	0	1.60000	.00173
1.85000	0	1.85000	0	1.85000	.00077
2.10000	0	2.10000	0	2.10000	0
2.35000	0	2.35000	0	2.35000	0
2.60000	0	2.60000	0	2.60000	0

y	x = 18; z = 0.4	y	x = 18, z = 0.8	y	x = 18, z = 12
.10000	.11155	.10000	.10613	.10000	.10215
.11000	.10942	.11000	.10485	.11000	.10029
.12000	.10916	.12000	.10309	.12000	.09899
.13000	.10694	.13000	.10217	.13000	.09759
.14000	.10483	.14000	.10078	.14000	.09592
.16000	.10191	.16000	.09886	.16000	.09332
.18000	.10019	.18000	.09694	.18000	.09066
.20000	.09813	.20000	.09414	.20000	.08875
.22000	.09644	.22000	.09171	.22000	.08575
.24000	.09422	.24000	.08993	.24000	.08344
.26000	.09228	.26000	.08868	.26000	.08199
.28000	.09053	.28000	.08557	.28000	.07958
.30000	.08852	.30000	.08444	.30000	.07755
.35000	.08379	.35000	.08025	.35000	.07351
.40000	.07953	.40000	.07611	.40000	.06953
.45000	.07651	.45000	.07254	.45000	.06612
.50000	.07268	.50000	.06886	.50000	.06275
.55000	.06889	.55000	.06640	.55000	.05977
.70000	.05859	.70000	.05558	.70000	.04881
.90000	.04329	.90000	.03955	.90000	.03276
1.10000	.02338	1.10000	.01536	1.10000	.00770
1.35000	.00879	1.35000	.00500	1.35000	.00307
1.60000	.00132	1.60000	.00085	1.60000	.00041
1.85000	.00054	1.85000	.00035	1.85000	.00015
2.10000	0	2.10000	0	2.10000	0
2.35000	0	2.35000	0	2.35000	0
2.60000	0	2.60000	0	2.60000	0

Concave Surface (Continued)

x = 18, z = 1.6

y (inches)	$\overline{u'}/U$
.10000	.09869
.11000	.09683
.12000	.09533
.13000	.09374
.14000	.09290
.16000	.09040
.18000	.08773
.20000	.08470
.22000	.08262
.24000	.07981
.26000	.07734
.28000	.07494
.30000	.07327
.35000	.06981
.40000	.06636
.45000	.06153
.50000	.05726
.55000	.05497
.70000	.04120
.90000	.02052
1.10000	.00104
1.35000	.00129
1.60000	.00026
1.85000	.00005
2.10000	0
2.35000	0
2.60000	0

x=18, z = 2.0

y	u'/U
.10000	.09839
.11000	.09707
.12000	.09488
.13000	.09309
.14000	.09215
.16000	.08962
.18000	.08748
.20000	.08598
.22000	.08305
.24000	.07965
.26000	.07812
.28000	.07660
.30000	.07564
.35000	.07209
.40000	.06732
.45000	.06296
.50000	.05955
.55000	.05618
.70000	.04244
.90000	.01929
1.10000	.00052
1.35000	0
1.60000	0
1.85000	0
2.10000	0
2.35000	0
2.60000	0

x=18, z = 2.4

y	$\overline{u'}/U$
.10000	.09801
.11000	.09740
.12000	.09519
.13000	.09443
.14000	.09300
.16000	.08988
.18000	.08734
.20000	.08557
.22000	.08369
.24000	.08038
.26000	.07851
.28000	.07734
.30000	.07581
.35000	.07203
.40000	.06793
.45000	.06425
.50000	.06042
.55000	.06599
.70000	.04565
.90000	.02660
1.10000	.00071
1.35000	0
1.60000	0
1.85000	0
2.10000	0
2.35000	0
2.60000	0

x = 30.0, z= 0.0

.10000	.11923
.11000	.12462
.12000	.11470
.13000	.11262
.14000	.11090
.16000	.10819
.18000	.10441
.20000	.10238
.22000	.09923
.24000	.09552
.26000	.09406
.28000	.09243
.30000	.09072
.35000	.08683
.40000	.08235
.45000	.07785
.50000	.07411
.55000	.07120
.70000	.06166
.90000	.04935
1.10000	.03256
1.35000	.00778
1.60000	.00728
1.85000	.00451
2.10000	.00364
2.35000	0
2.60000	0

x = 42; z = 0.0

.10000	.12599
.11000	.12478
.12000	.12153
.13000	.11992
.14000	.11853
.16000	.11574
.18000	.11161
.20000	.10867
.22000	.10749
.24000	.10339
.26000	.10175
.28000	.09999
.30000	.09822
.35000	.09429
.40000	.08953
.45000	.08542
.50000	.08324
.55000	.08011
.70000	.07483
.90000	.06792
1.10000	.05920
1.35000	.04606
1.60000	0.2855
1.85000	.01152
2.10000	.00374
2.35000	.00165
2.60000	0

x = 42, z = 0.4

.10000	.12093
.11000	.11934
.12000	.11775
.13000	.11580
.14000	.11423
.16000	.11114
.18000	.10840
.20000	.10673
.22000	.10277
.24000	.10006
.26000	.09732
.28000	.09597
.30000	.09289
.35000	.08851
.40000	.08492
.45000	.08088
.50000	.07856
.55000	.07606
.70000	.07109
.90000	.06435
1.10000	.05687
1.35000	.04261
1.60000	.02396
1.85000	.00985
2.10000	.00293
2.35000	.00159
2.60000	0

Concave Surface (Continued)

x = 42, z = 0.8

y (inches)	$\overline{u'}/U$
.10000	.11407
.11000	.11078
.12000	.10968
.13000	.10779
.14000	.10702
.16000	.10393
.18000	.10116
.20000	.09823
.22000	.09507
.24000	.09194
.26000	.09099
.28000	.08825
.30000	.08477
.35000	.08195
.40000	.07888
.45000	.07452
.50000	.07165
.55000	.06957
.70000	.06454
.90000	.05812
1.10000	.04877
1.35000	.03456
1.60000	.01331
1.85000	.00719
2.10000	.00229
2.35000	.00107
2.60000	0

x = 42, z = 1.2

y	u'/U
.10000	.10949
.11000	.10721
.12000	.10624
.13000	.10365
.14000	.10212
.16000	.09919
.18000	.09516
.20000	.09250
.22000	.08817
.24000	.08526
.26000	.08264
.28000	.08088
.30000	.07952
.35000	.07537
.40000	.07106
.45000	.06657
.50000	.06473
.55000	.06159
.70000	.05611
.90000	.04760
1.10000	.03576
1.35000	.02053
1.60000	.00536
1.85000	.00399
2.10000	.00160
2.35000	.00091
2.60000	0

x = 42, z = 1.6

y	$\overline{u'}/U$
.10000	.10949
.11000	.10775
.12000	.10489
.13000	.10431
.14000	.10129
.16000	.09854
.18000	.09575
.20000	.09279
.22000	.08909
.24000	.08553
.26000	.08264
.28000	.08151
.30000	.07957
.35000	.07602
.40000	.07087
.45000	.06788
.50000	.06474
.55000	.06159
.70000	.05392
.90000	.04076
1.10000	.02854
1.35000	.00934
1.60000	.00179
1.85000	0
2.10000	0
2.35000	0
2.60000	0

x = 42, z = 2.0

.10000	.11055
.11000	.10785
.12000	.10556
.13000	.10426
.14000	.10271
.16000	.09852
.18000	.09705
.20000	.09452
.22000	.09099
.24000	.08785
.26000	.08435
.28000	.08315
.30000	.08164
.35000	.07780
.40000	.07287
.45000	.07018
.50000	.06681
.55000	.06438
.70000	.05718
.90000	.04451
1.10000	.03161
1.35000	.01077
1.60000	.00198
1.85000	0
2.10000	0
2.35000	0
2.60000	0

x = 42, z = 2.4

.10000	.11101
.11000	.10867
.12000	.10640
.13000	.10449
.14000	.10233
.16000	.09927
.18000	.09759
.20000	.09399
.22000	.09040
.24000	.08791
.26000	.08542
.28000	.08407
.30000	.08324
.35000	.07859
.40000	.07492
.45000	.07143
.50000	.06876
.55000	.06707
.70000	.06104
.90000	.05200
1.10000	.03978
1.35000	.02544
1.60000	.00489
1.85000	.00452
2.10000	.00152
2.35000	.00087
2.60000	0

PLATES AND FIGURES

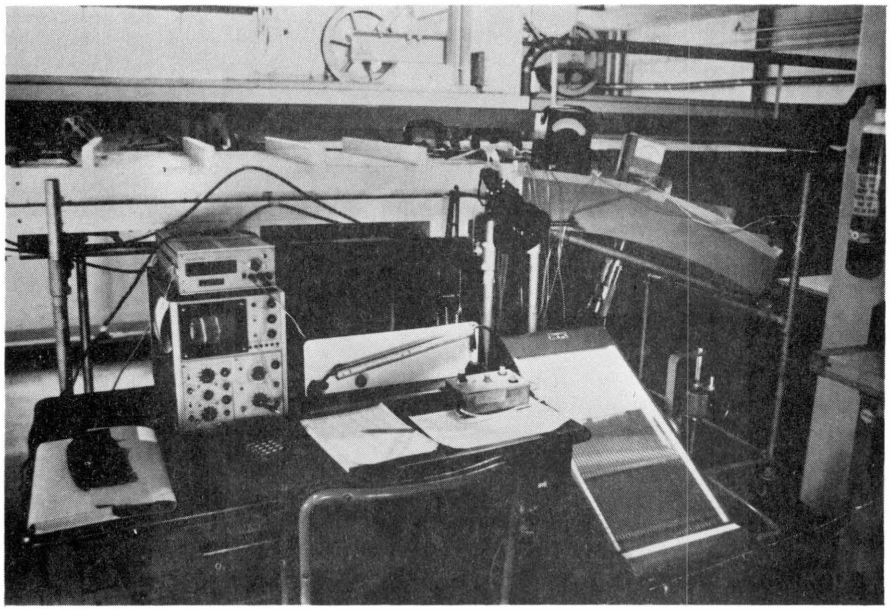

Plate 1: Blower tunnel

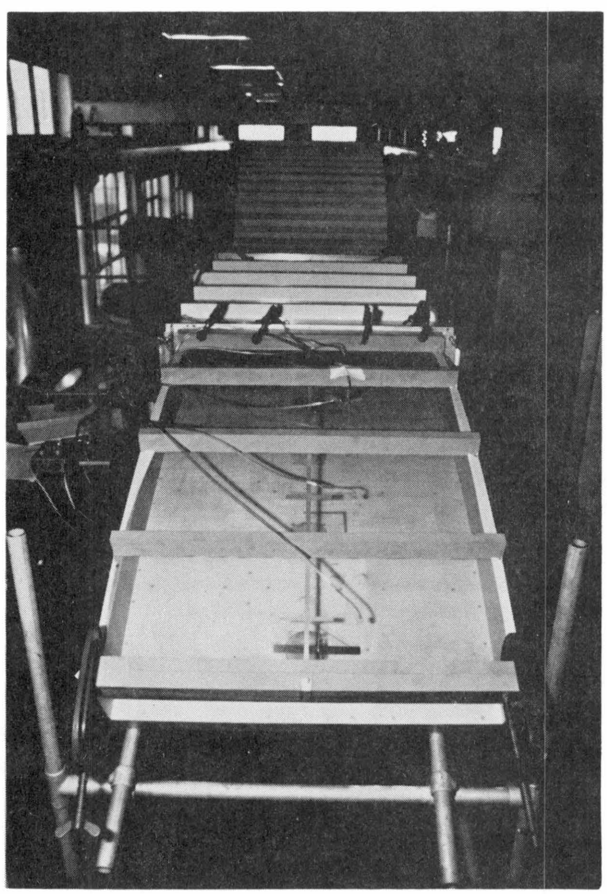

Plate 2: Curved test section

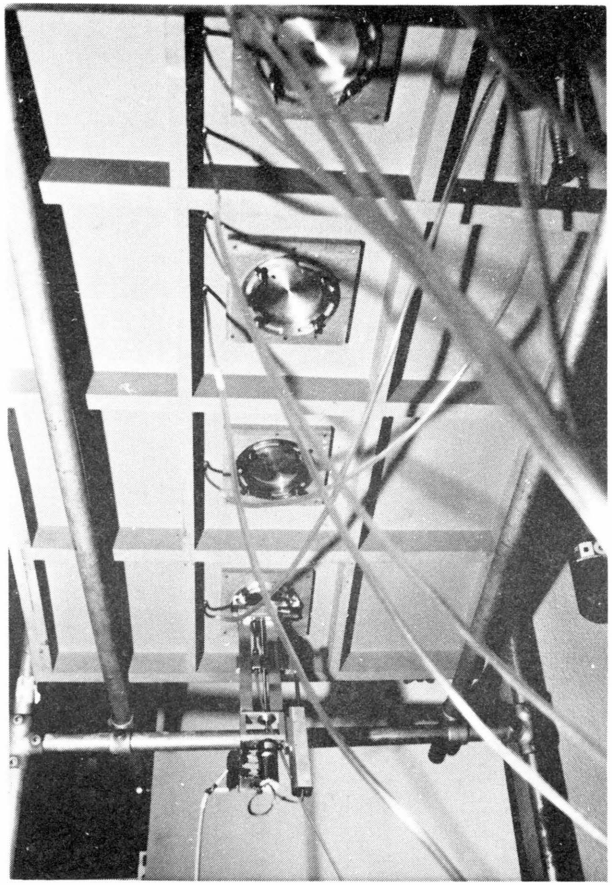

Plate 3: Test section convex side: ports and traversing gear

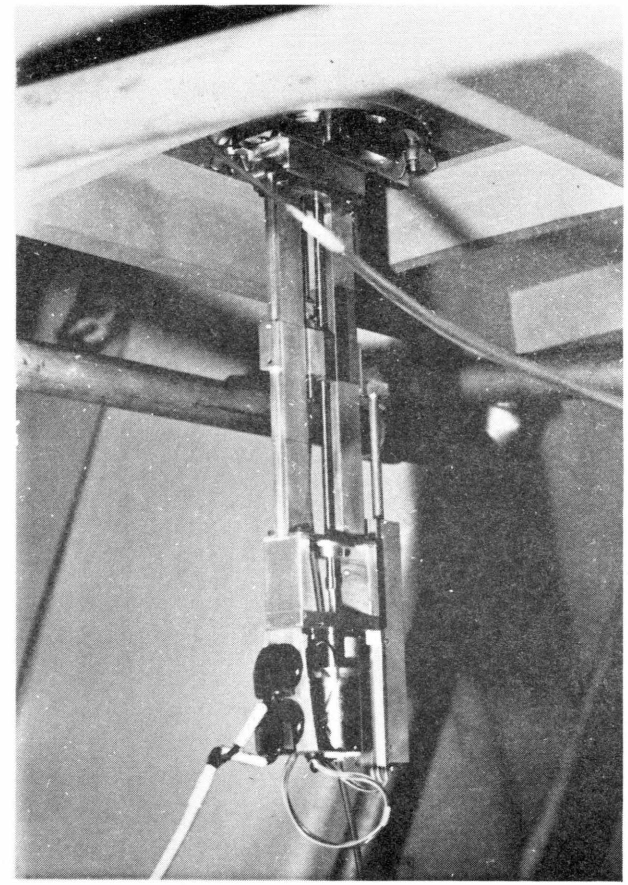

Plate 4: Traverse mounted in access port

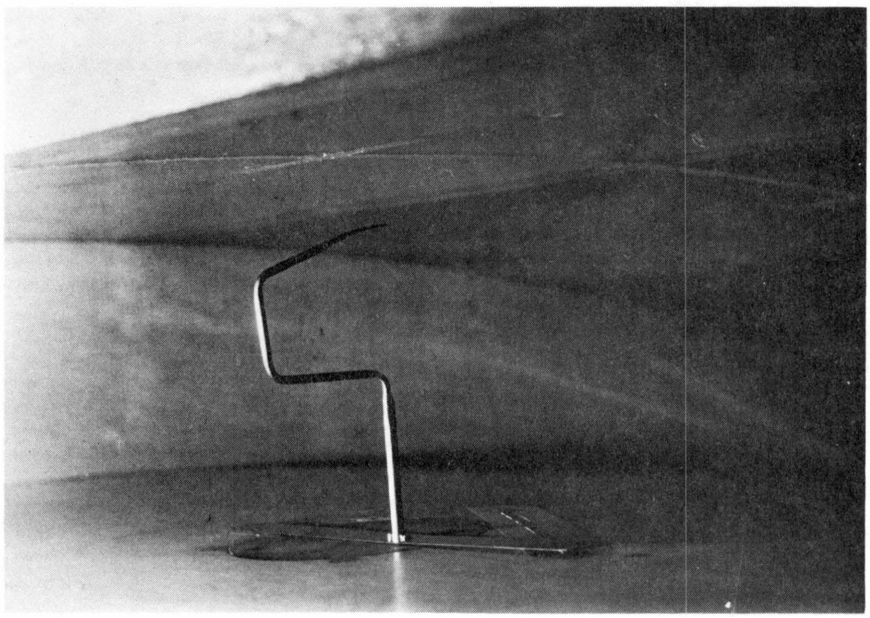

Plate 5: Stagnation tube installed to make traverse from concave wall

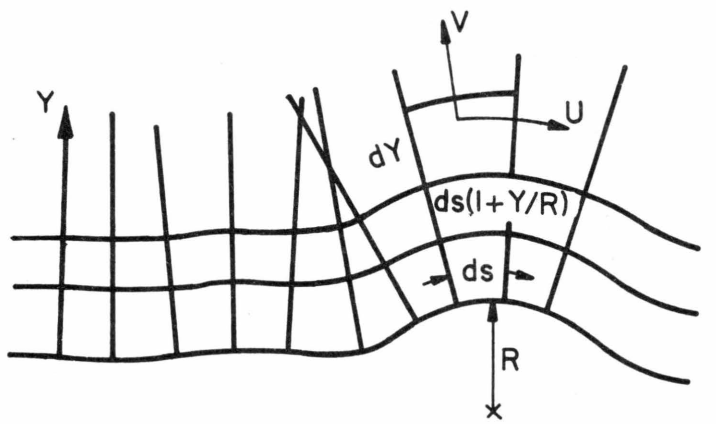

Orthogonal Curvilinear Coordinate System

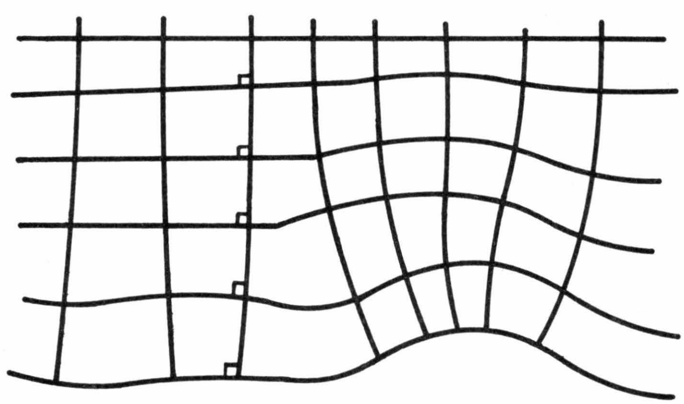

Doubly-curvilinear Orthogonal Coordinate System

Figure 1: Coordinate systems

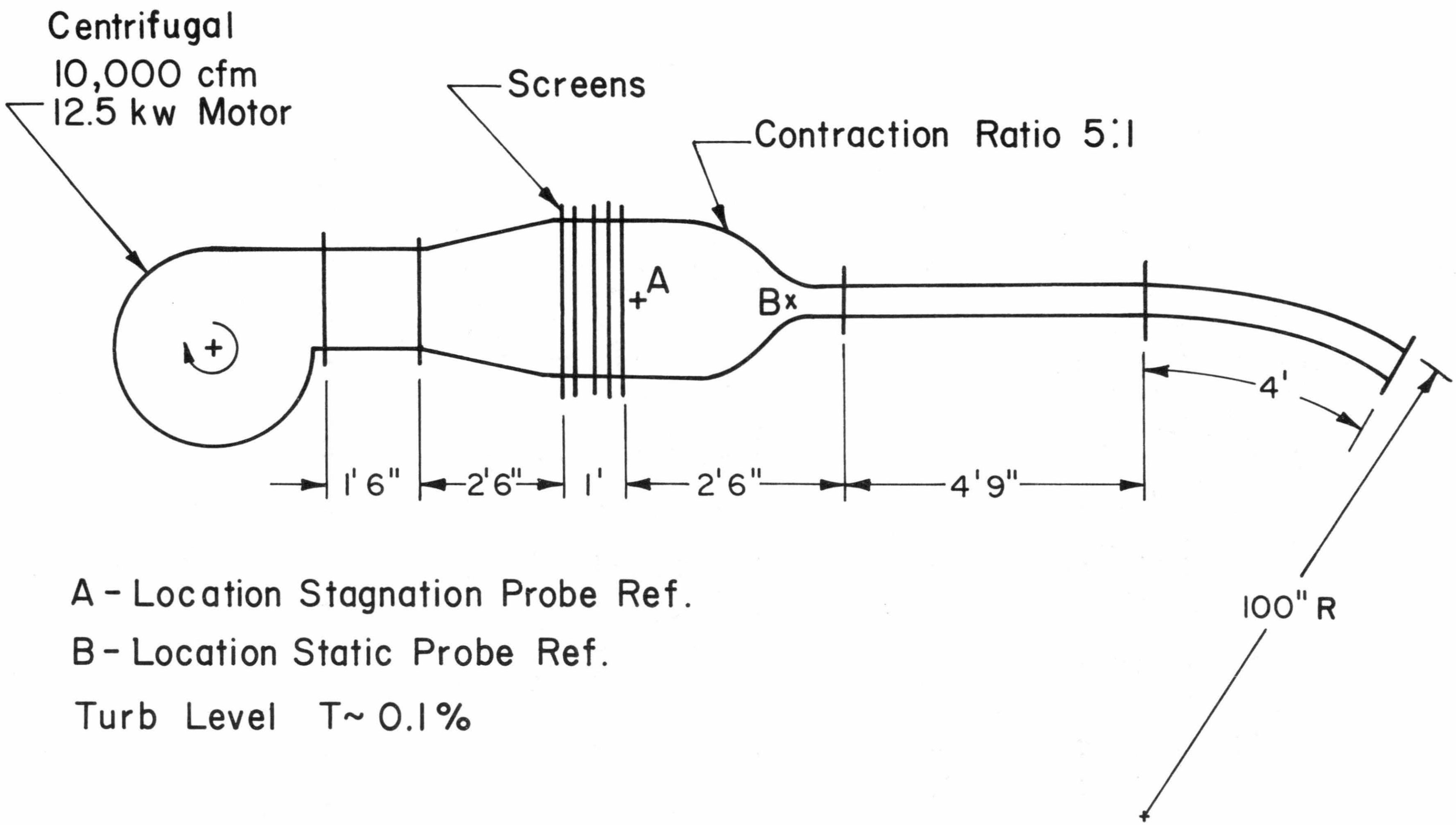

Figure 2: Imperial College blower tunnel

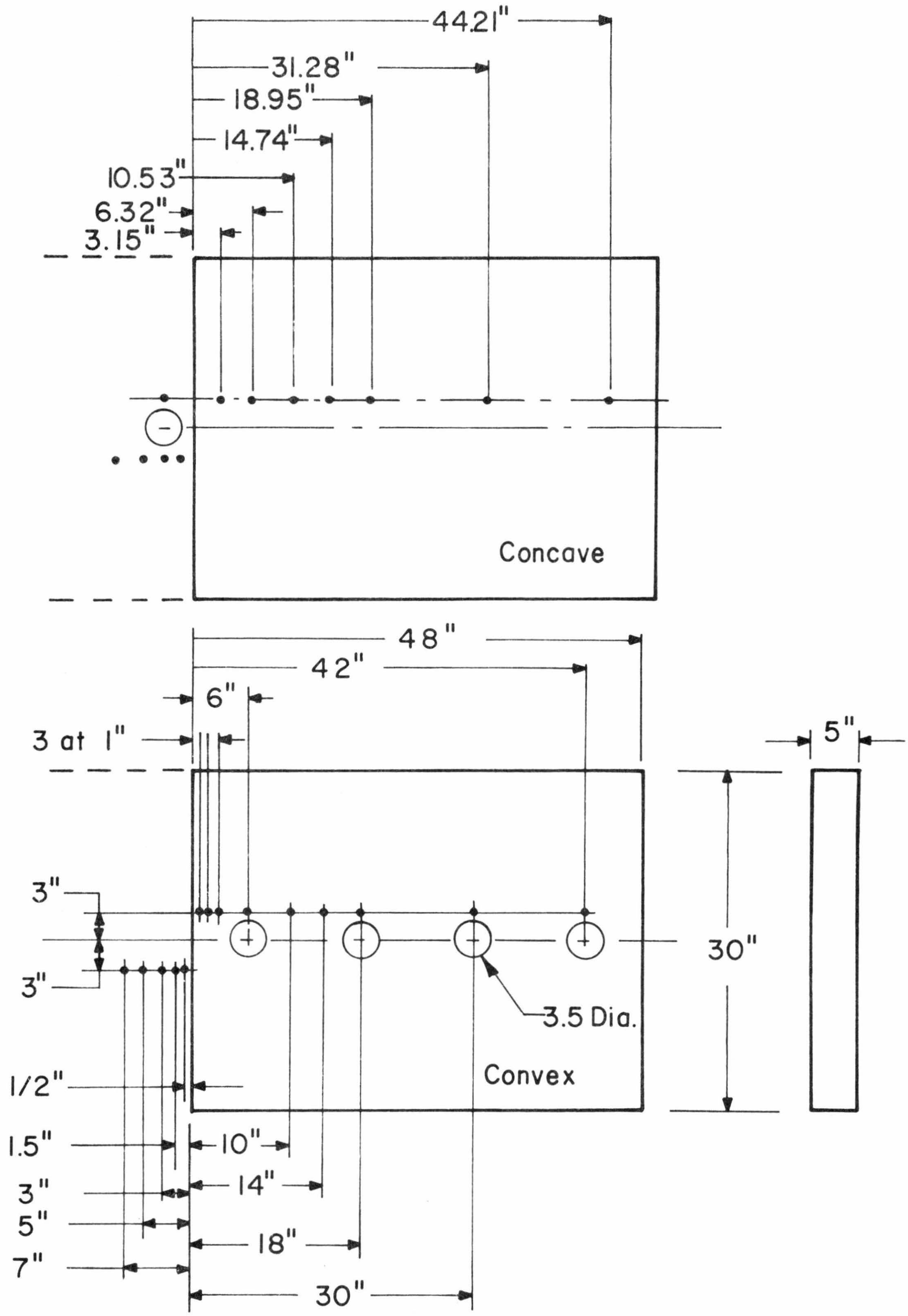

Figure 3: Test section dimensions, pressure tap and access parts location

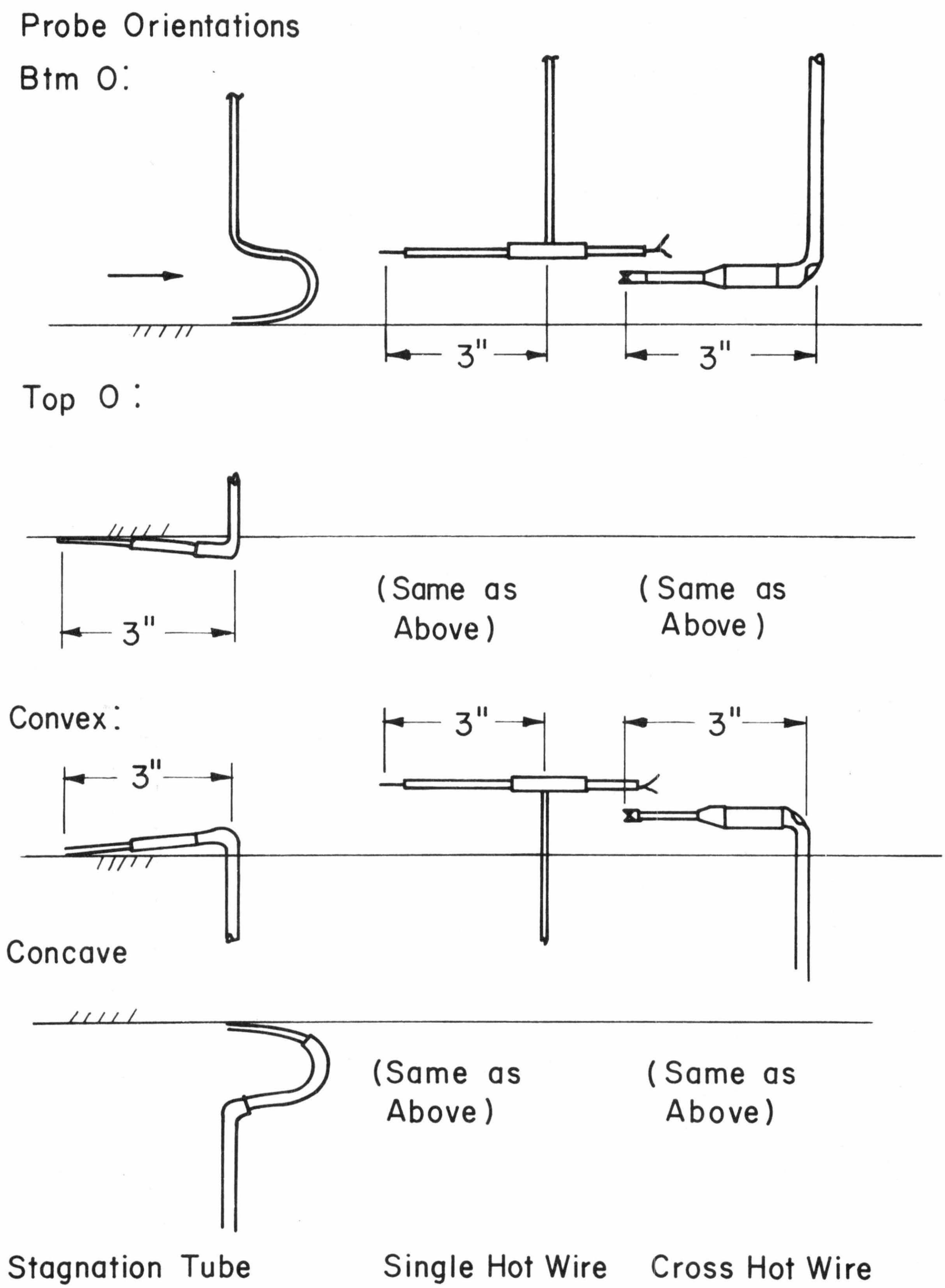

Figure 4: Instrumentation dimensions for vertical surreys

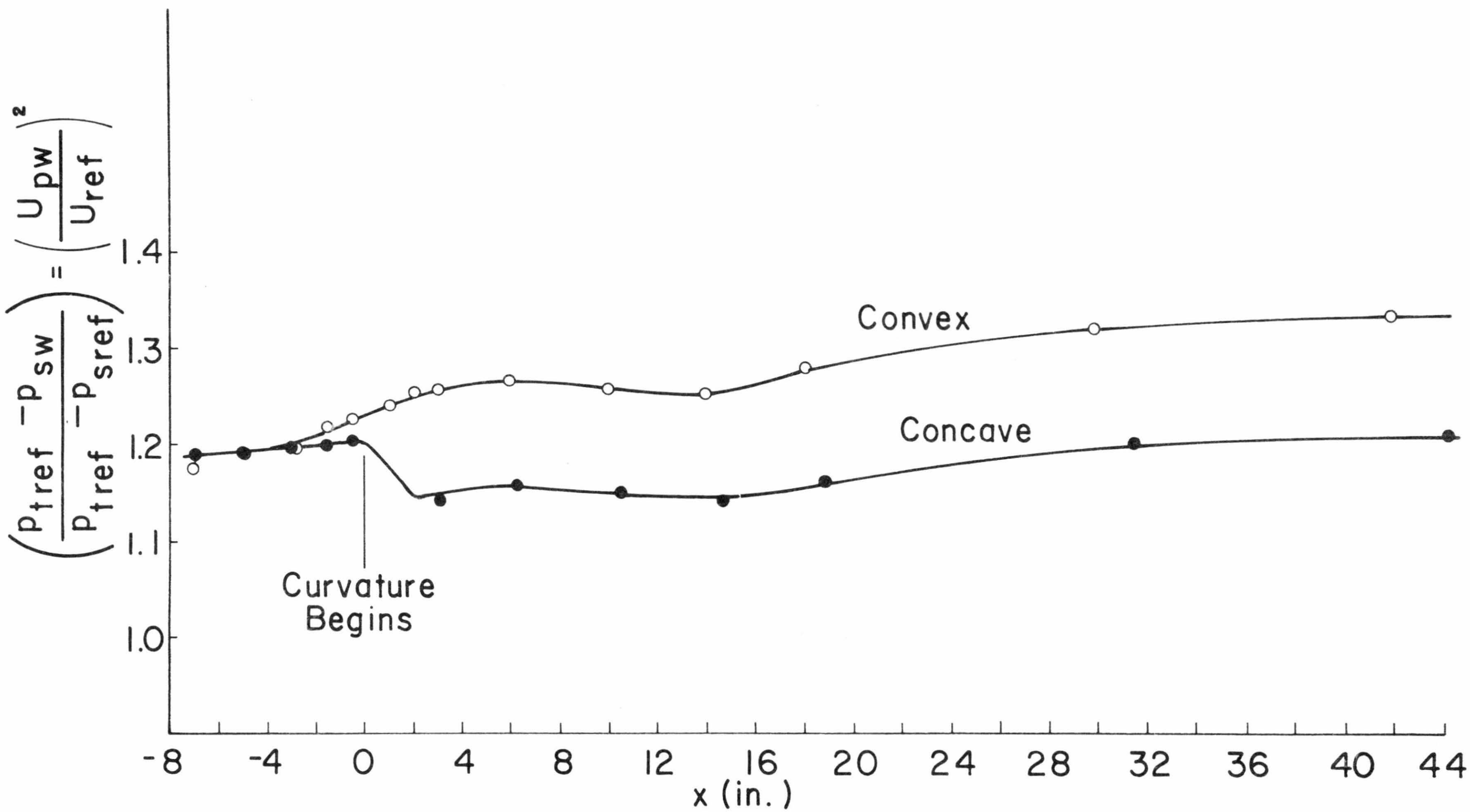

Figure 5: Wall static pressure distribution

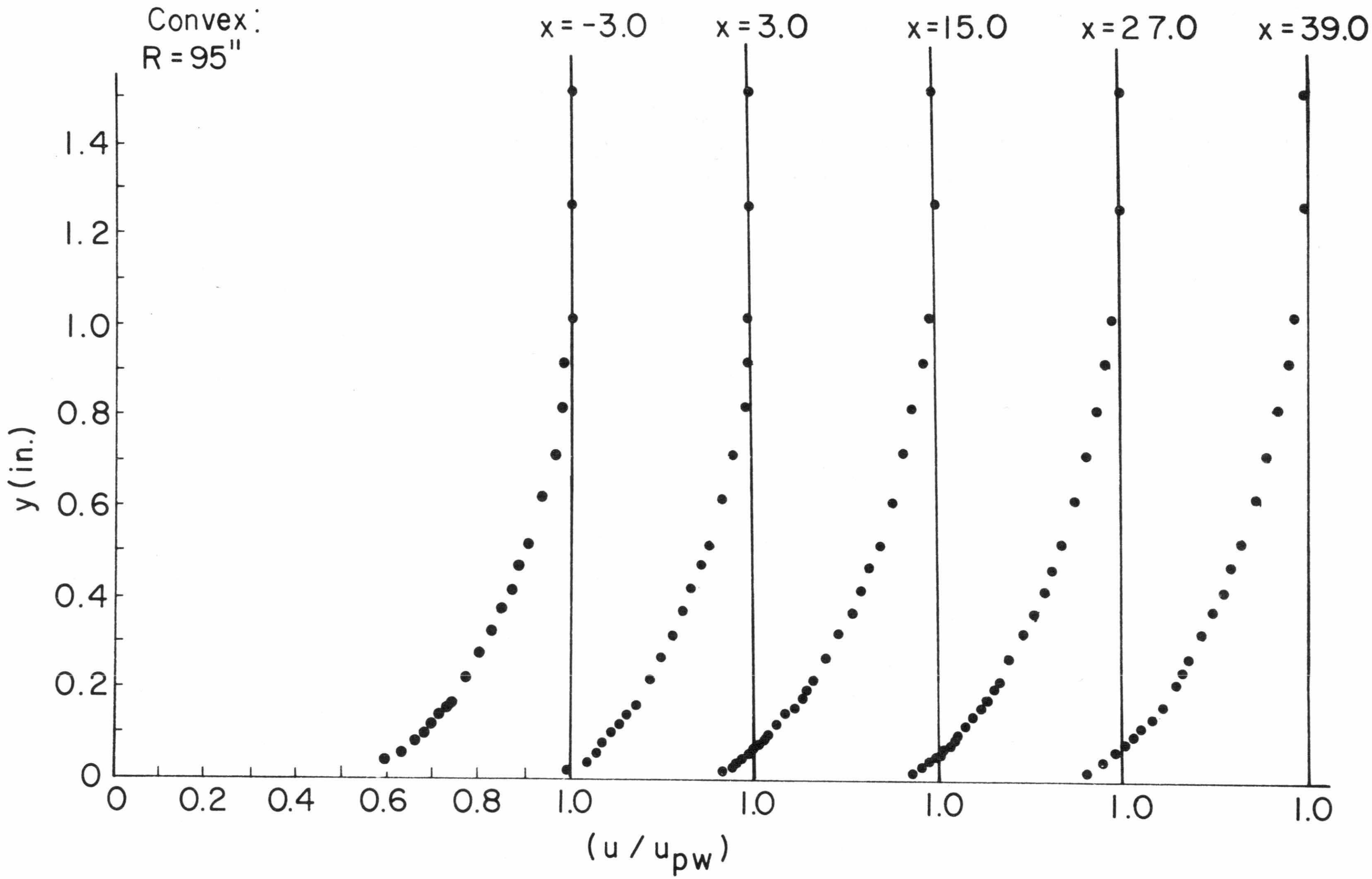

Figure 6: Velocity profiles over convex wall

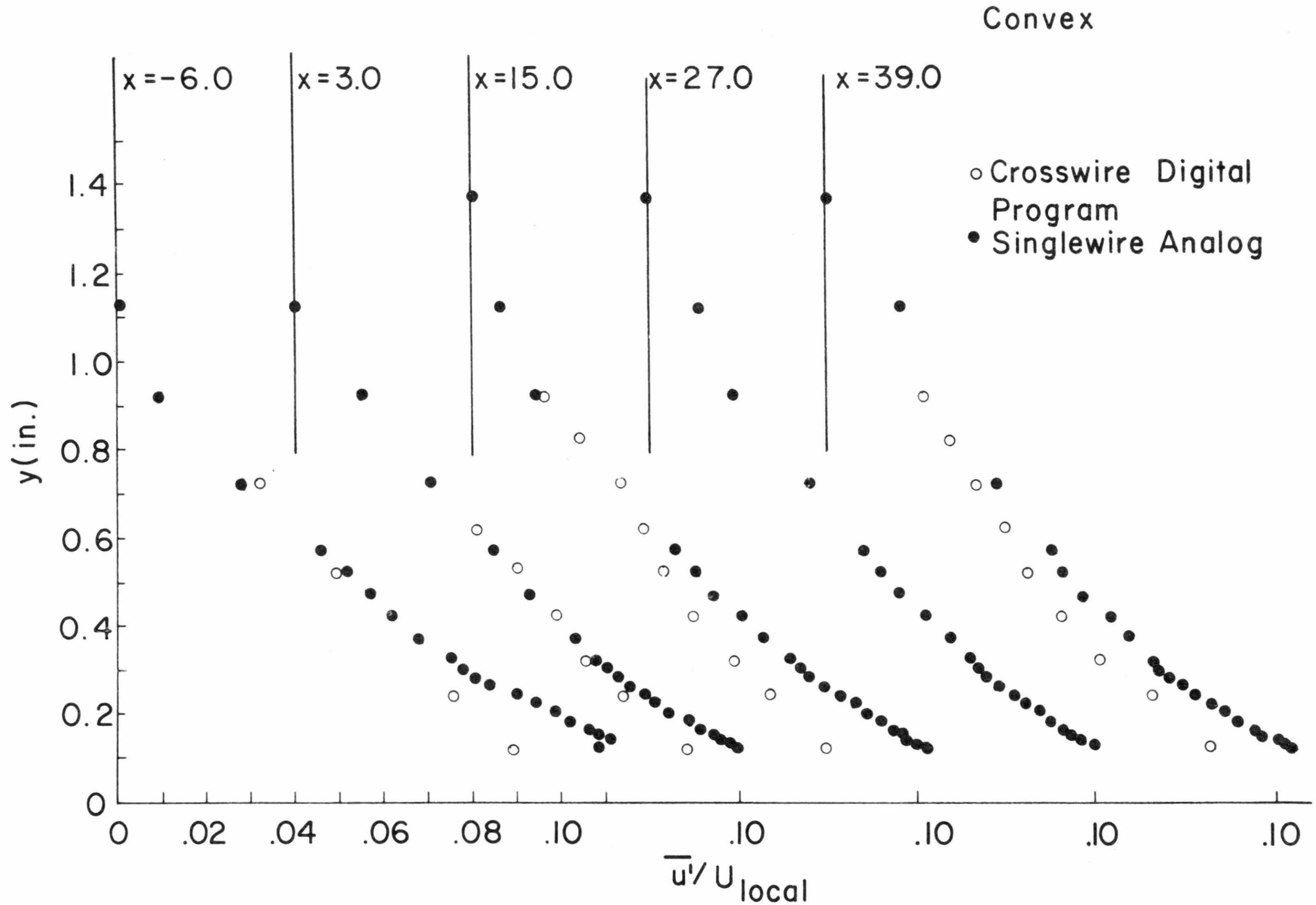

Figure 7: Longitudinal turbulence intensity over convex wall

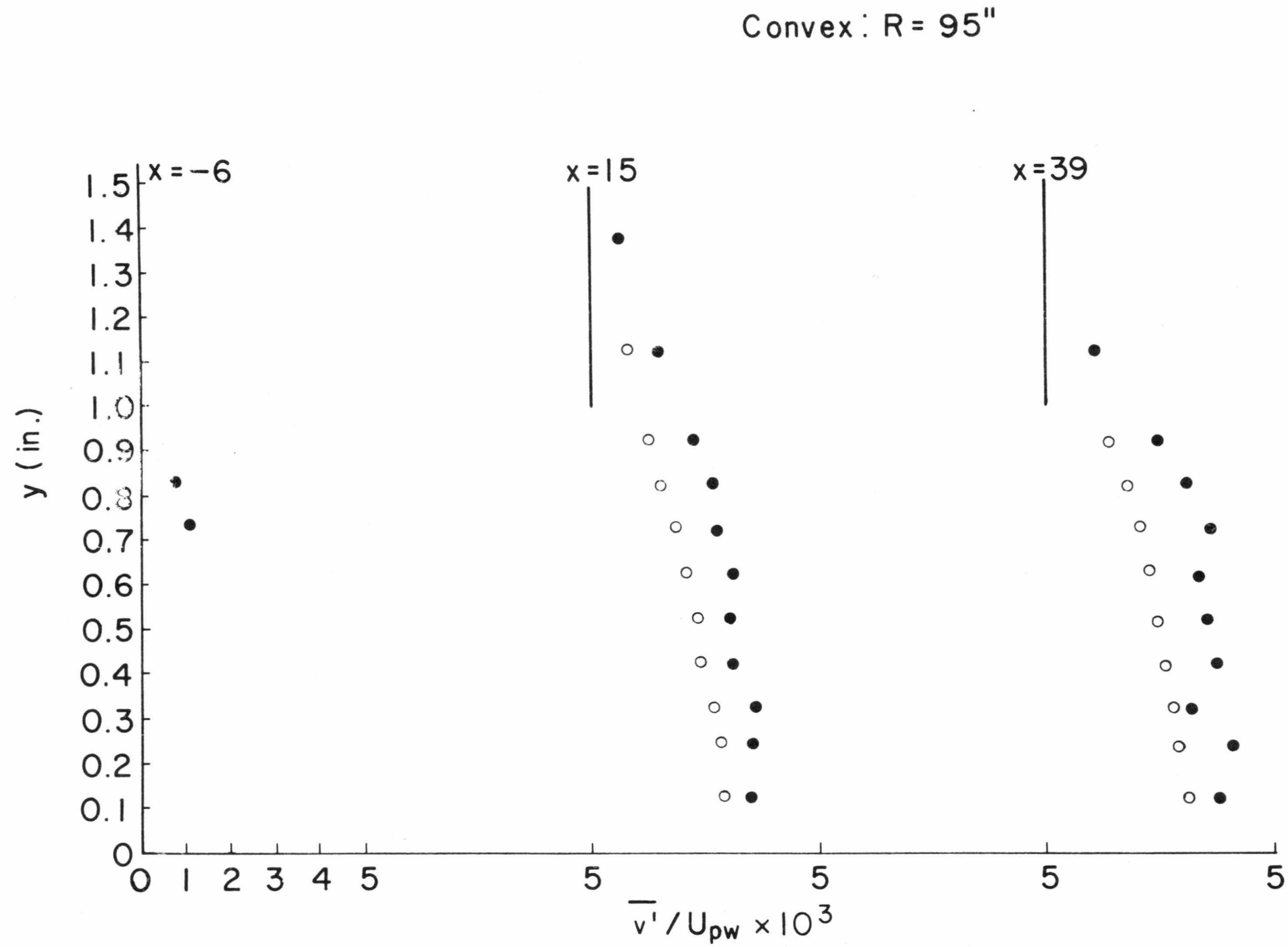

Figure 8: Vertical turbulent intensity over convex wall

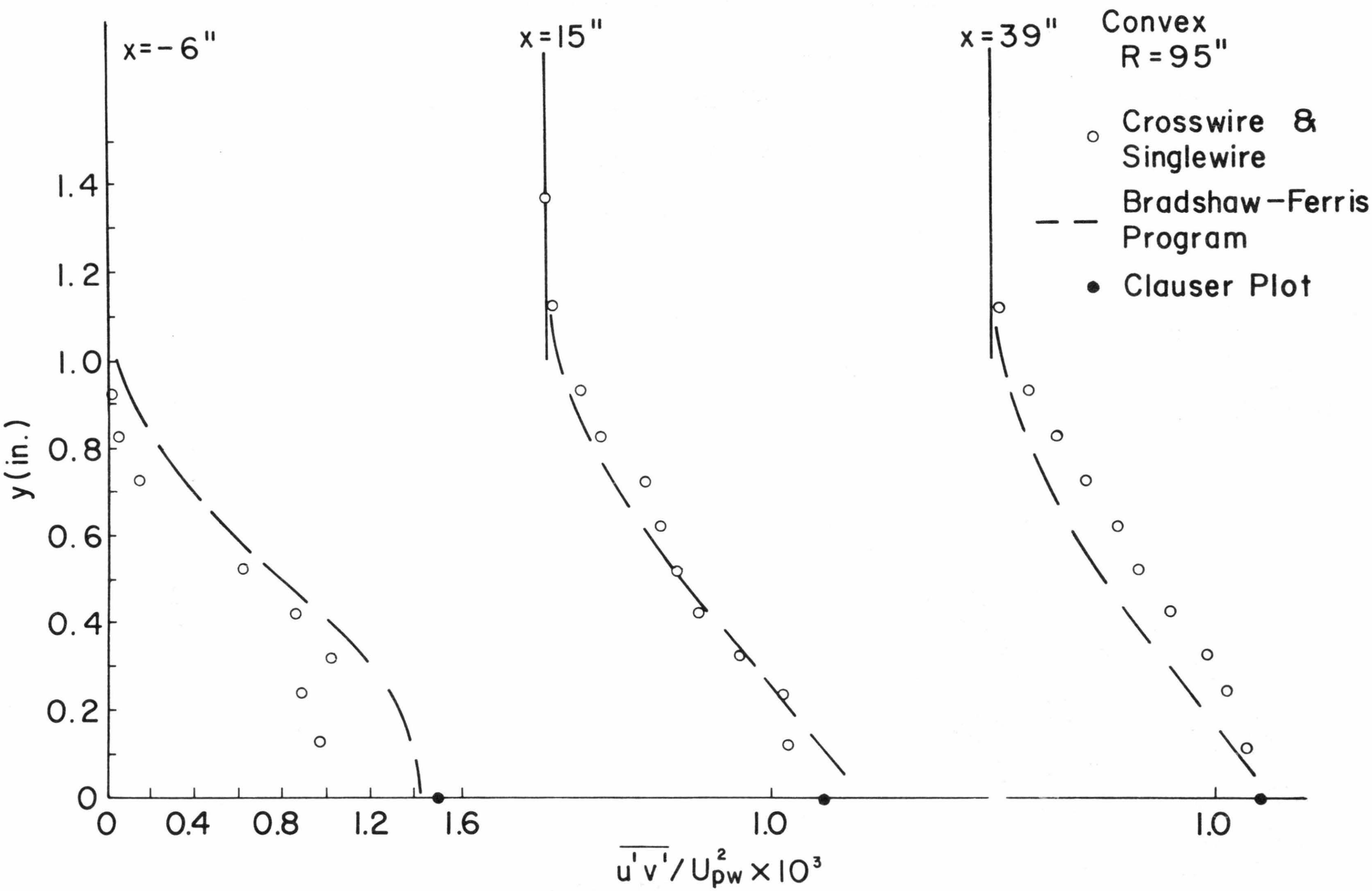

Figure 9: Shear stress profile over convex wall

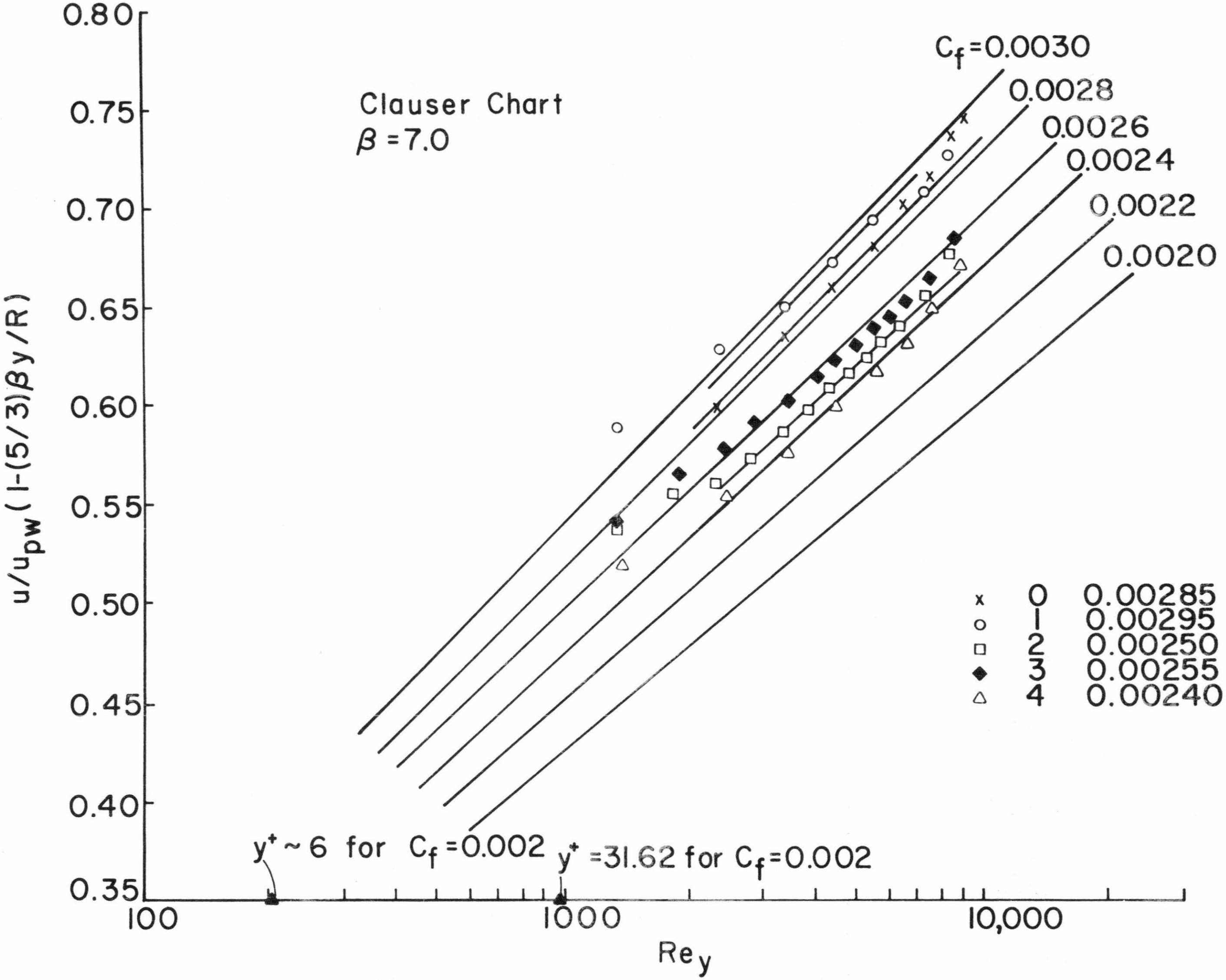

Figure 10: Modified Clauser chart: convex wall

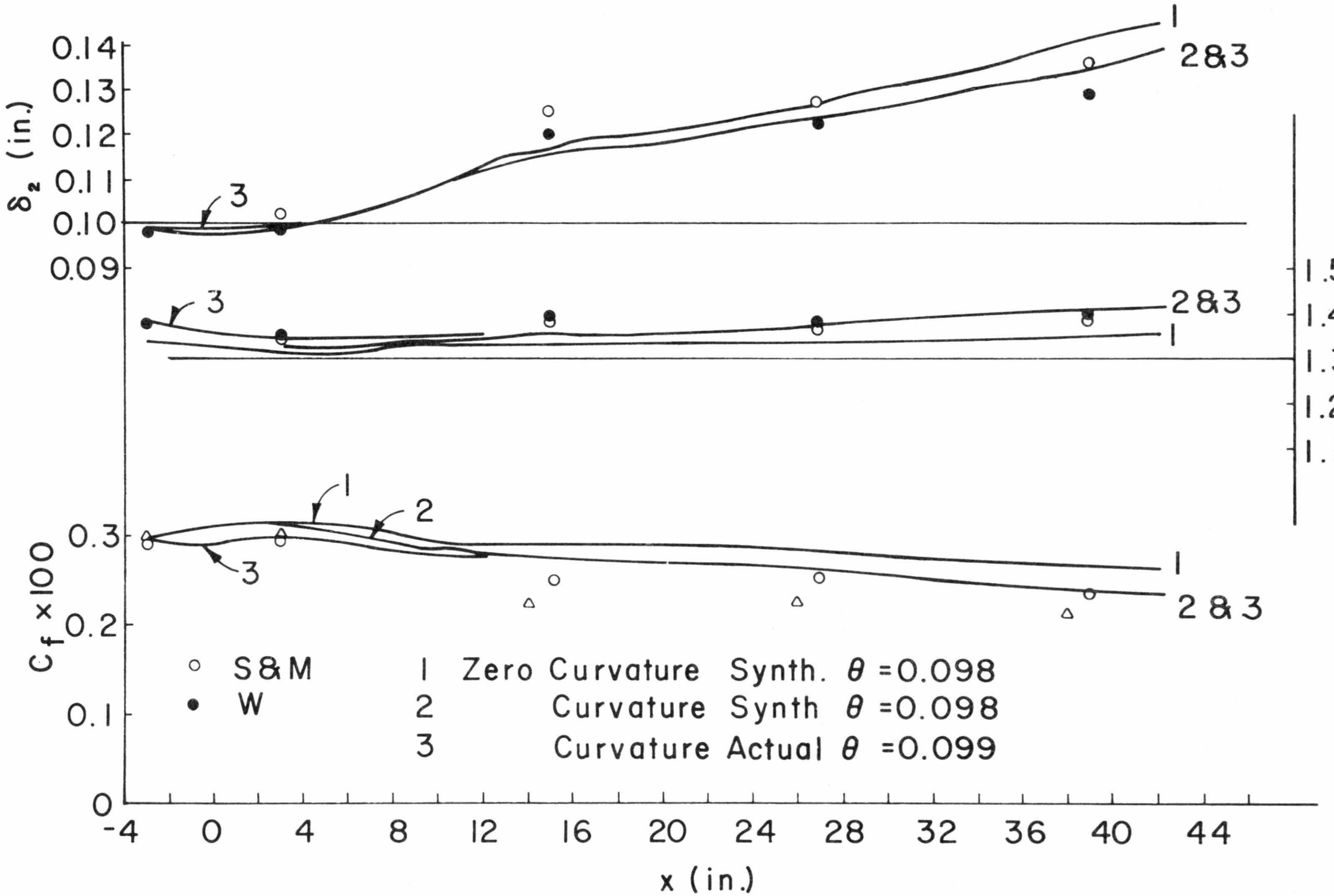

Figure 11a: Variation of integral boundary layer characteristics over convex wall

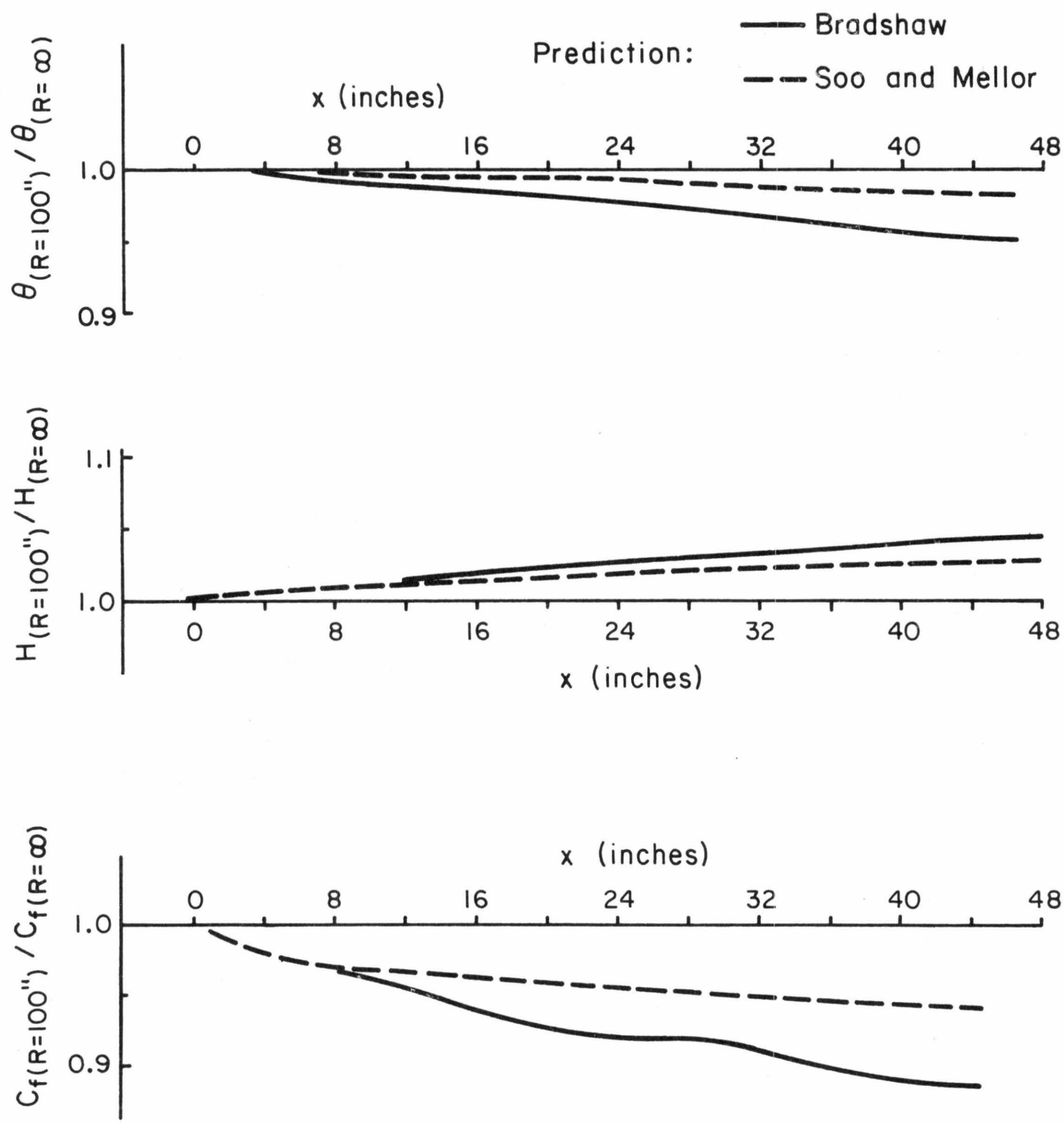

Figure 11b: Variation of integral boundary layer characteristics over convex wall: Soo and Mellor Prediction vs Bradshaw Prediction

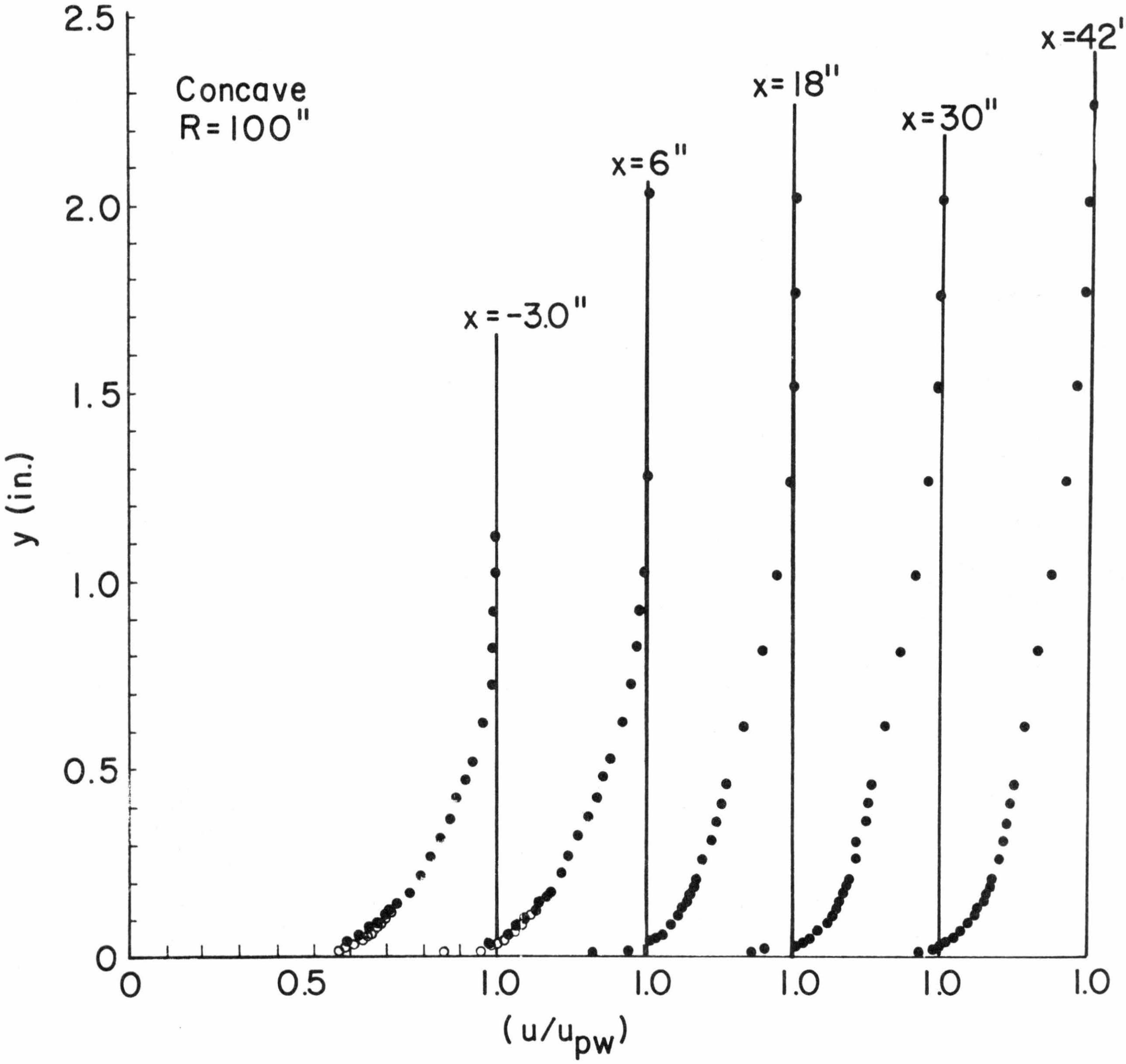

Figure 12: Velocity profiles over concave wall

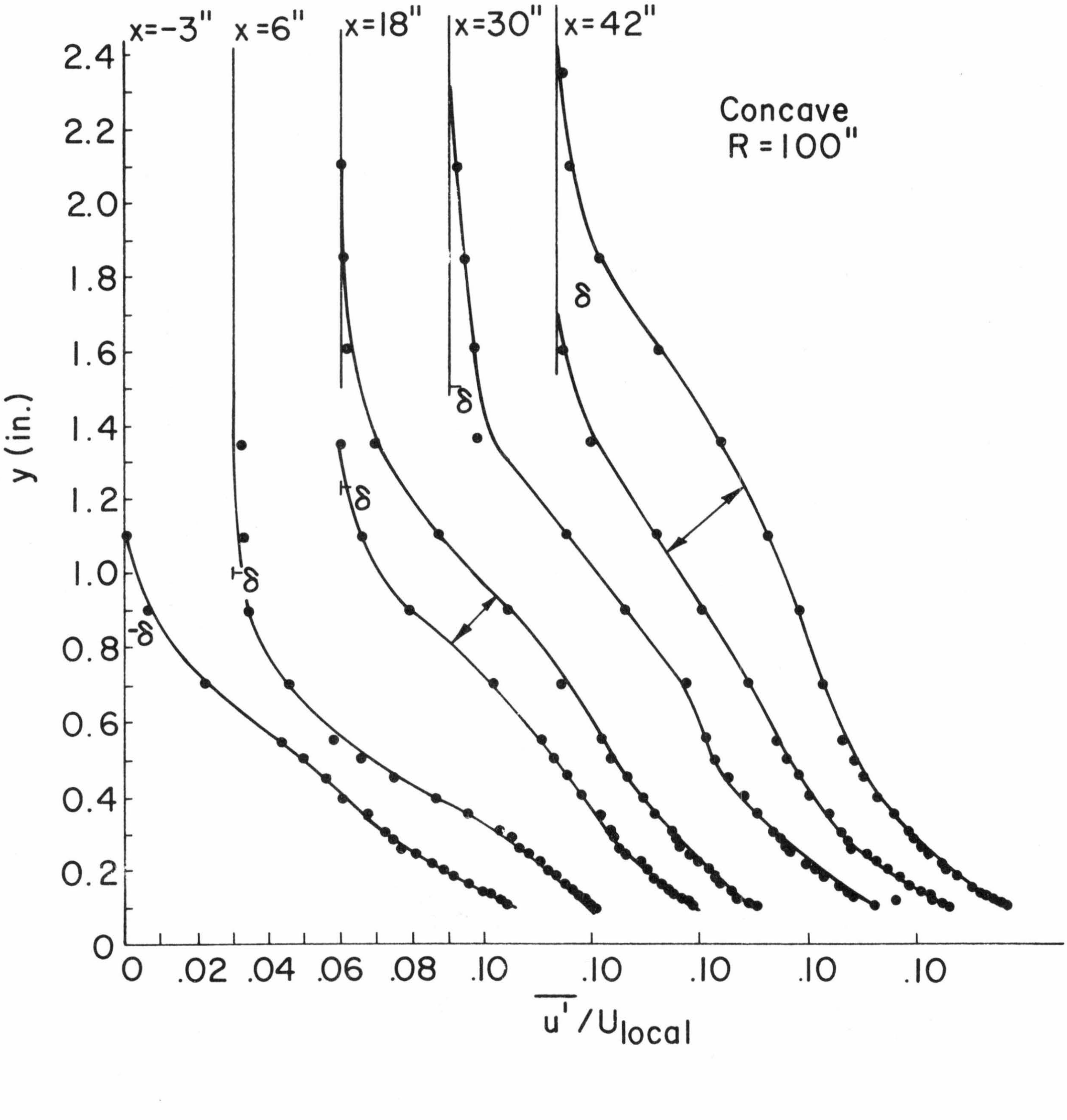

Figure 13: Longitudinal turbulent intensity over concave wall

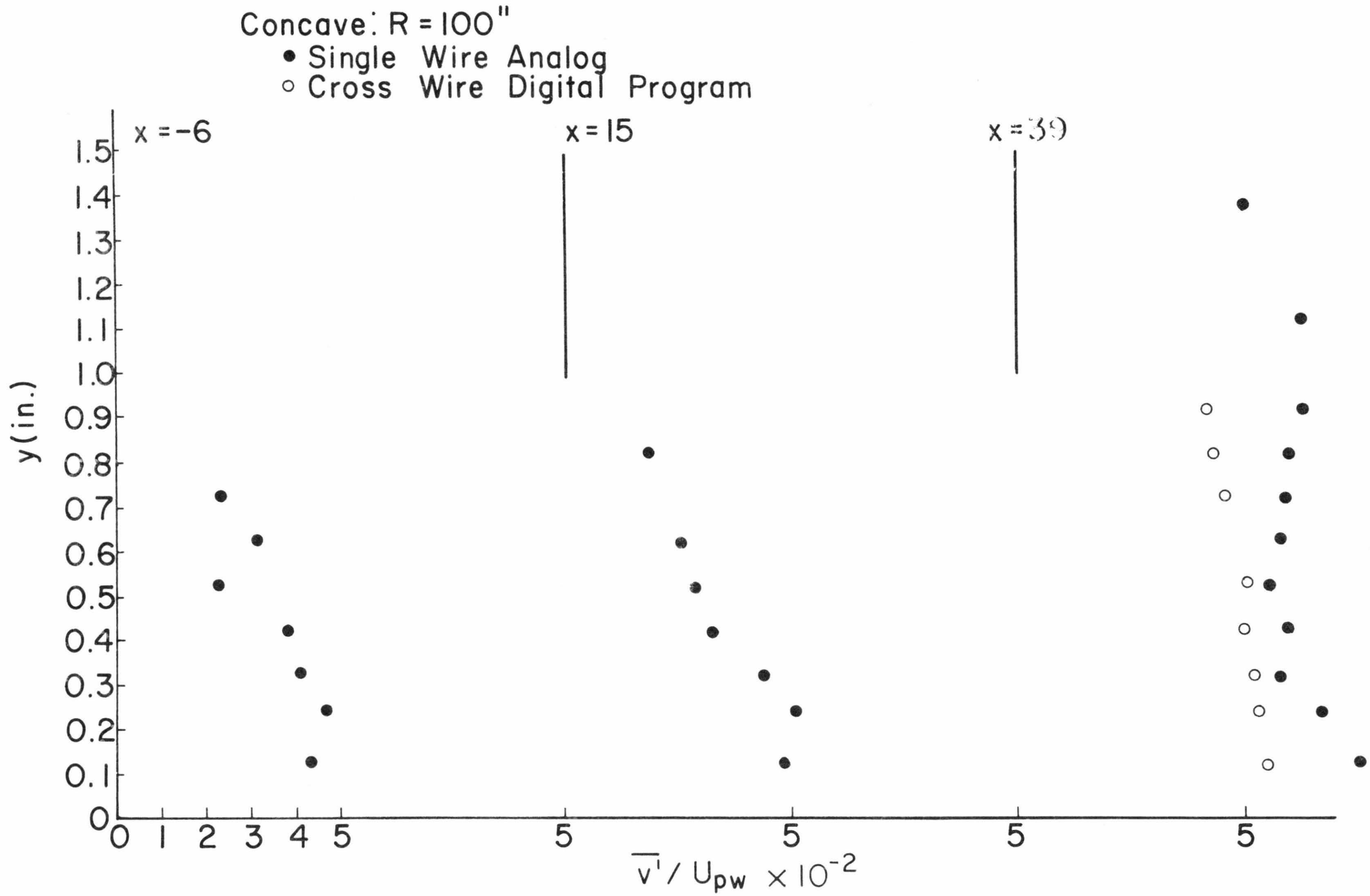

Figure 14: Vertical turbulent intensity over concave wall

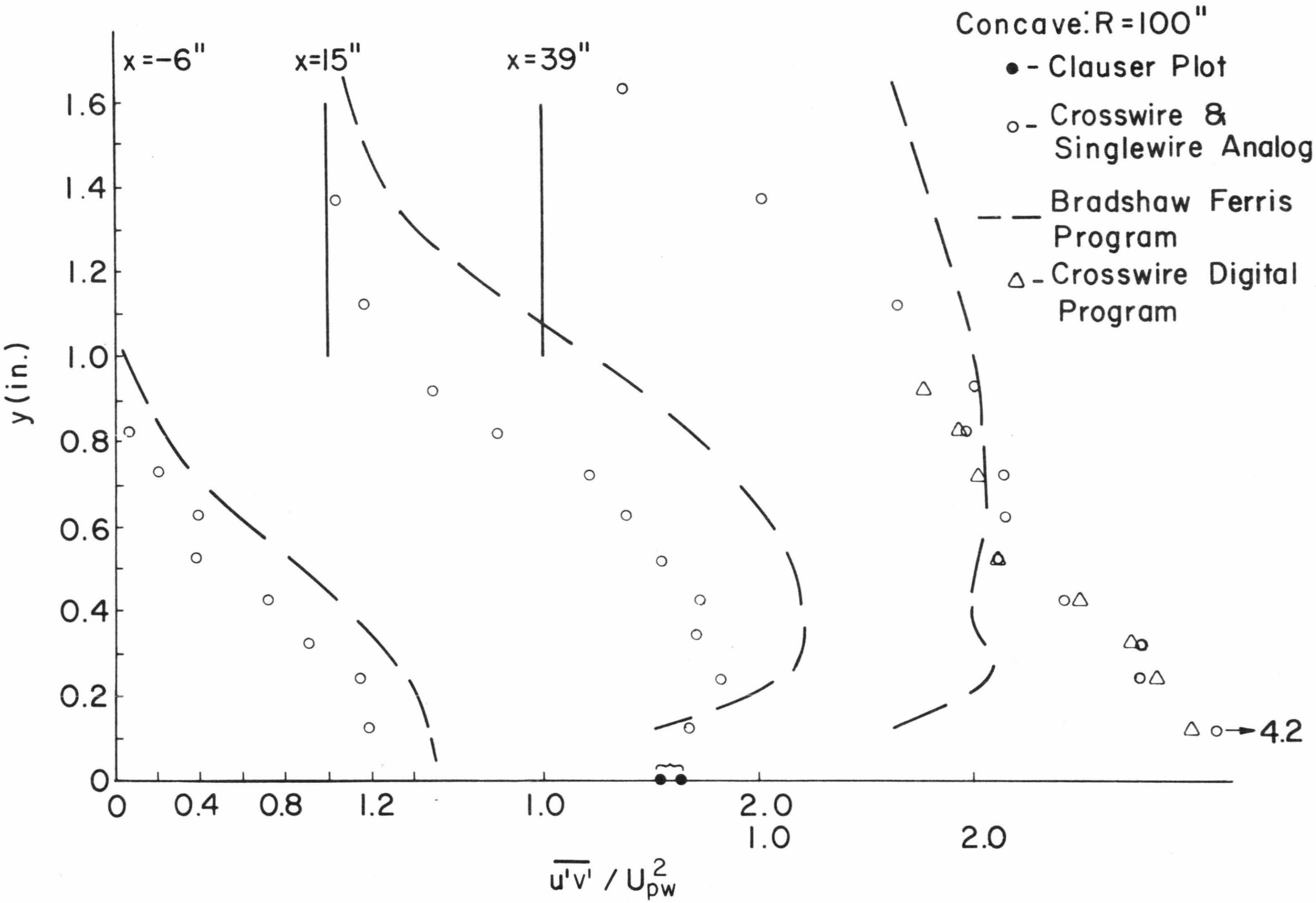

Figure 15: Turbulent shear stress profile over concave wall

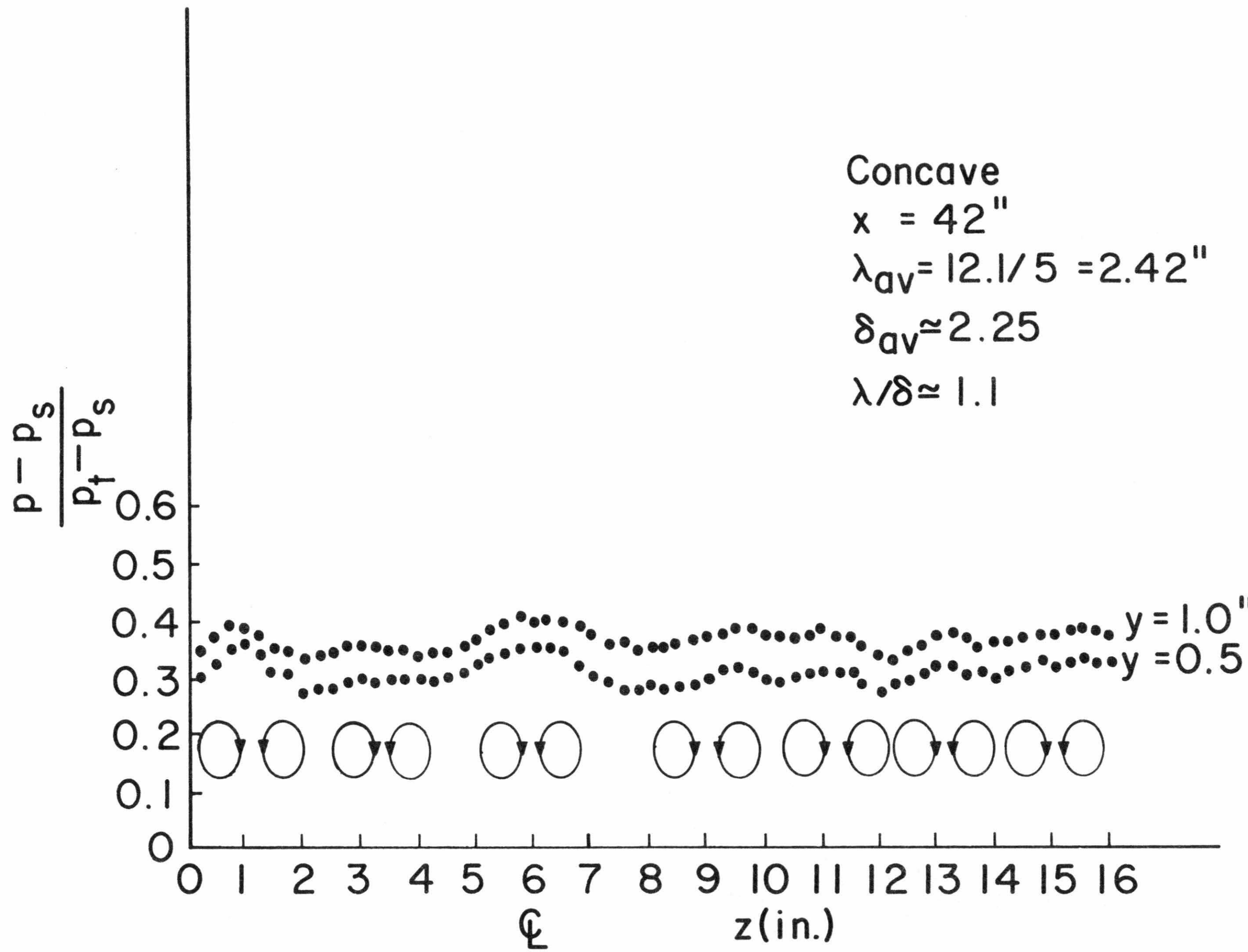

Figure 16: Lateral stagnation pressure traverse at duct exit over concave wall

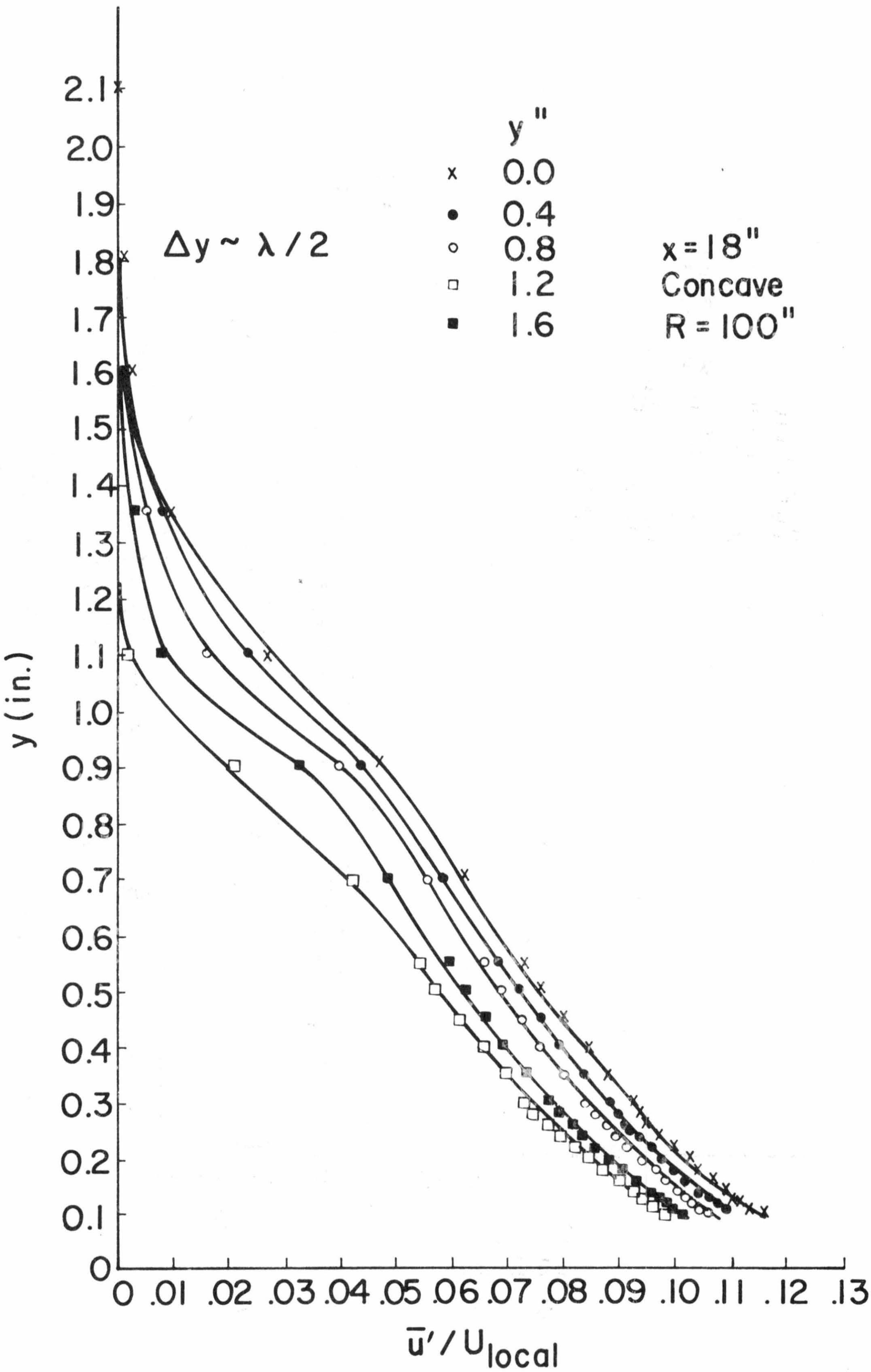

Figure 17: Lateral variation of longitudinal turbulent intensity over concave wall

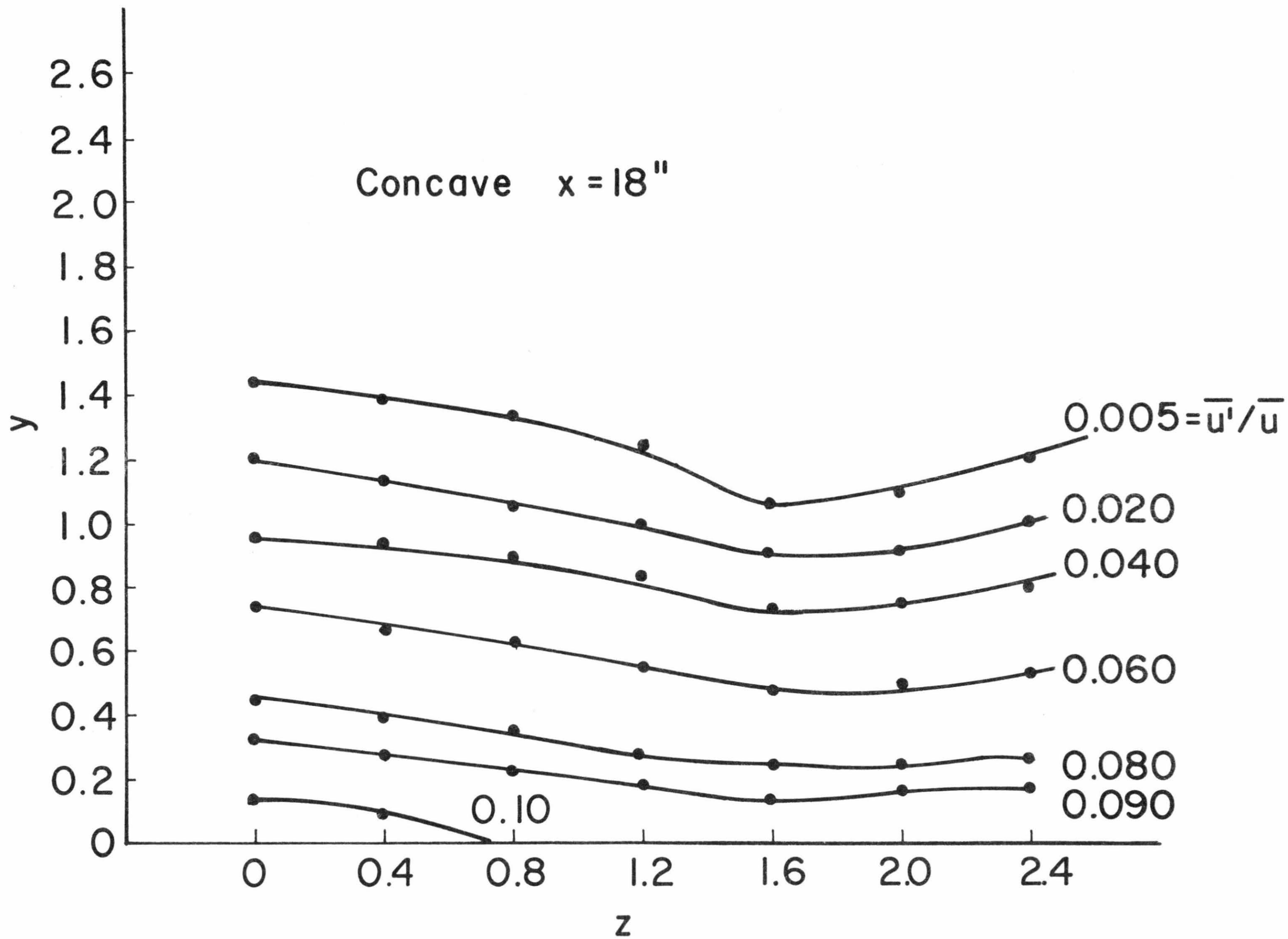

Figure 18: Lateral longitudinal turbulence intensity surrey concave wall: x = 18"

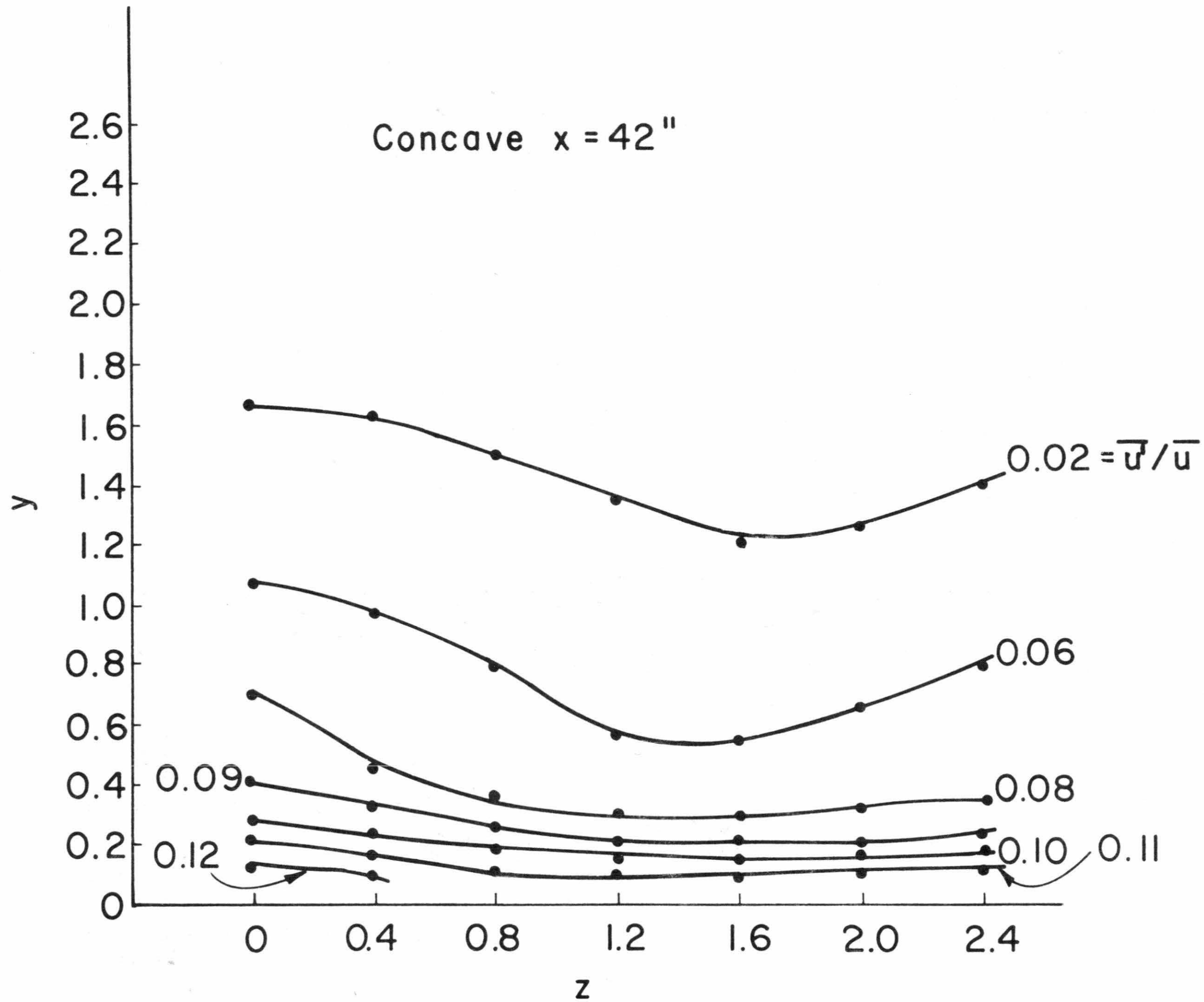

Figure 19: Lateral longitudinal turbulence intensity surrey concave wall: x = 42"

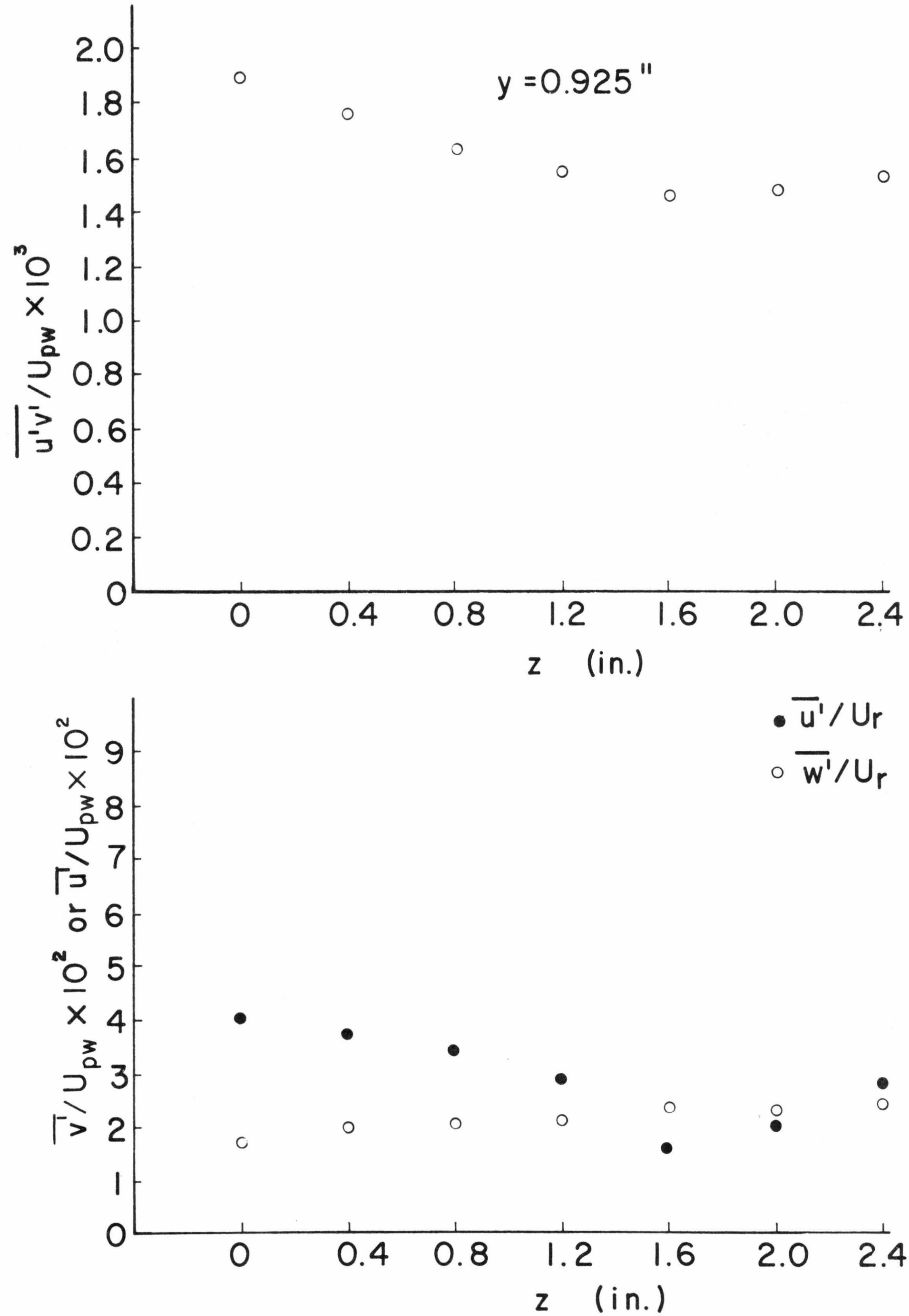

Figure 20: Lateral surreys of vertical turbulence intensity and shear stress: x = 42"

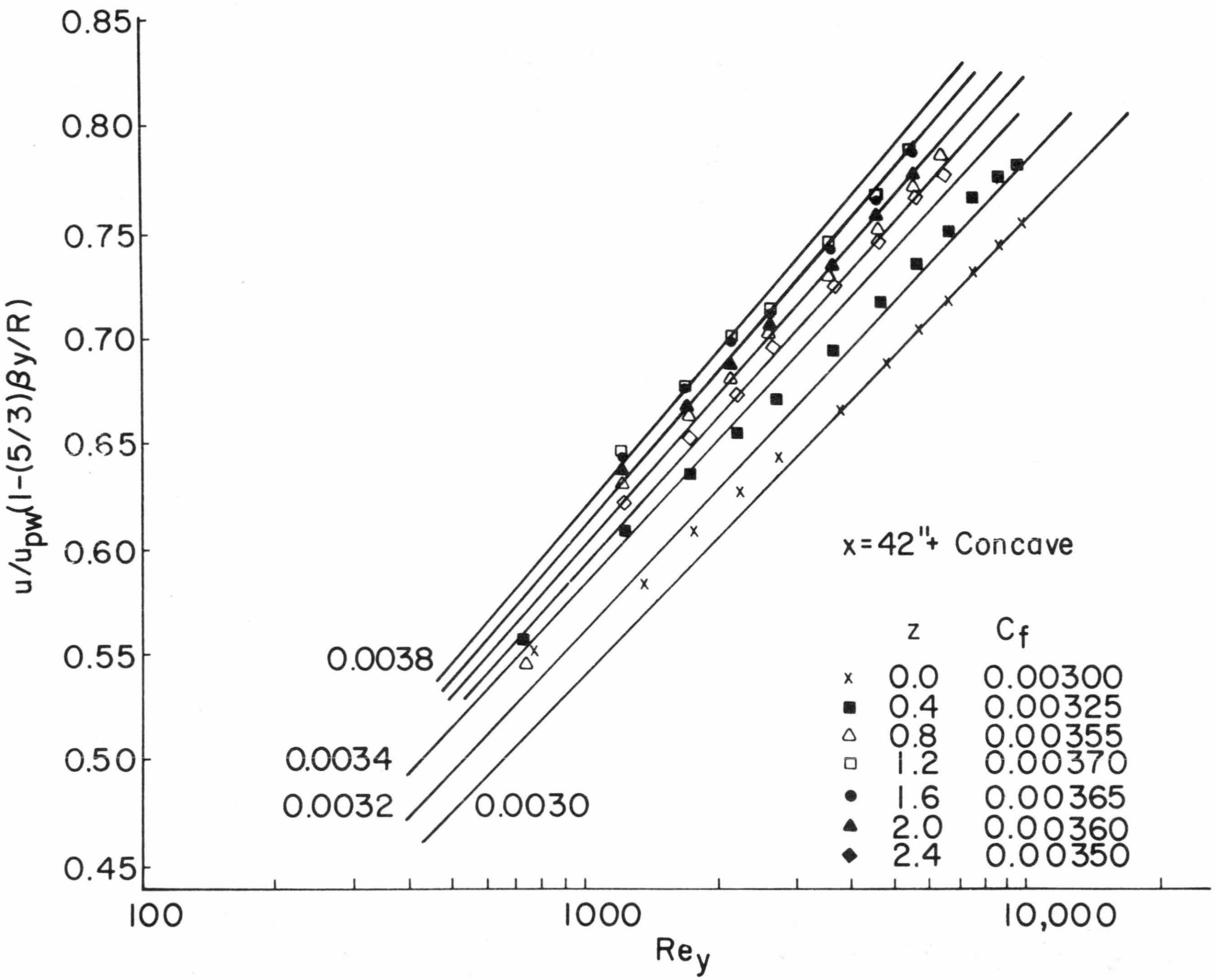

Figure 21: Modified Clauser chart: concave wall

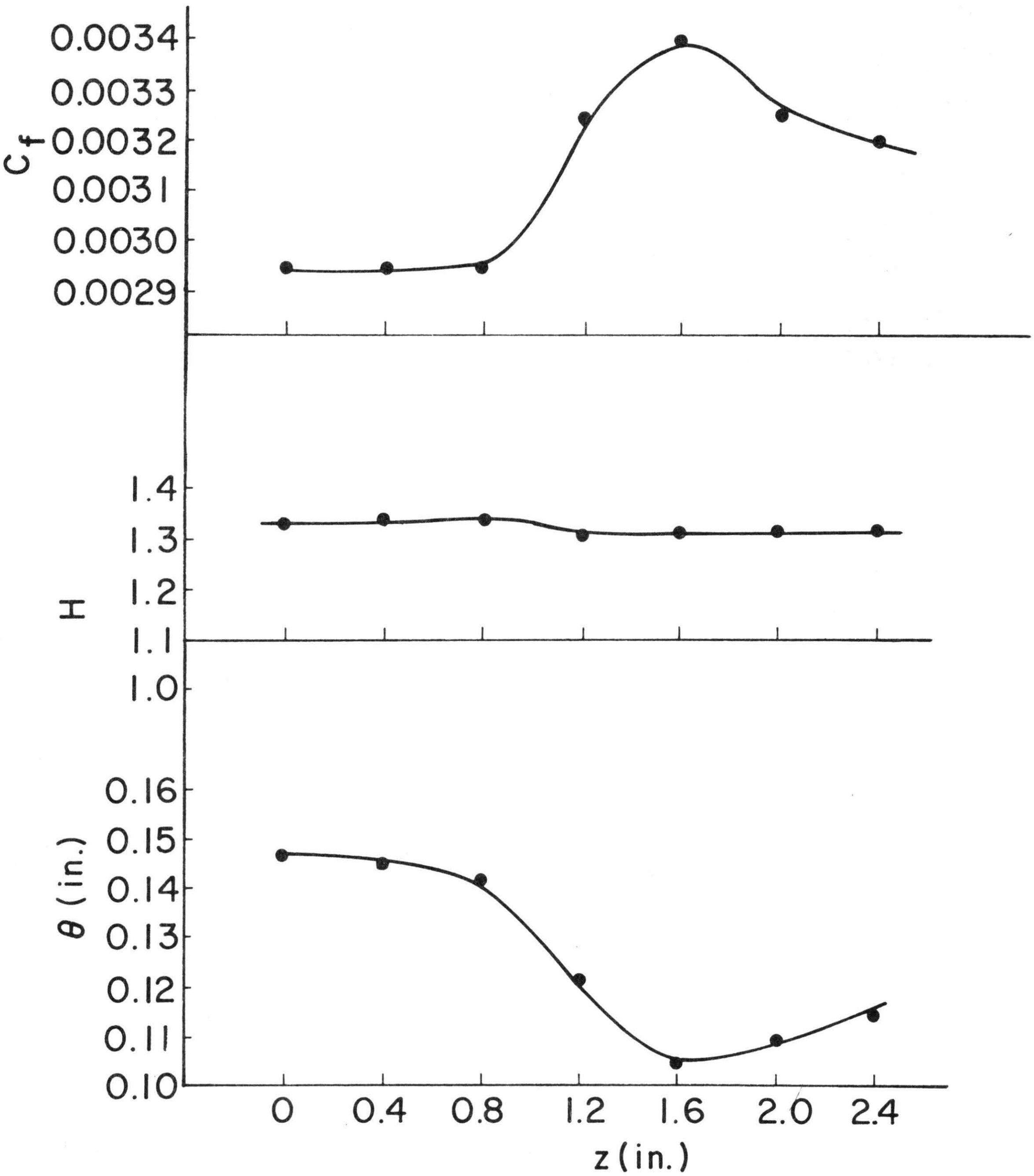

Figure 22: Lateral variation of integral boundary layer characteristics: x = 18"

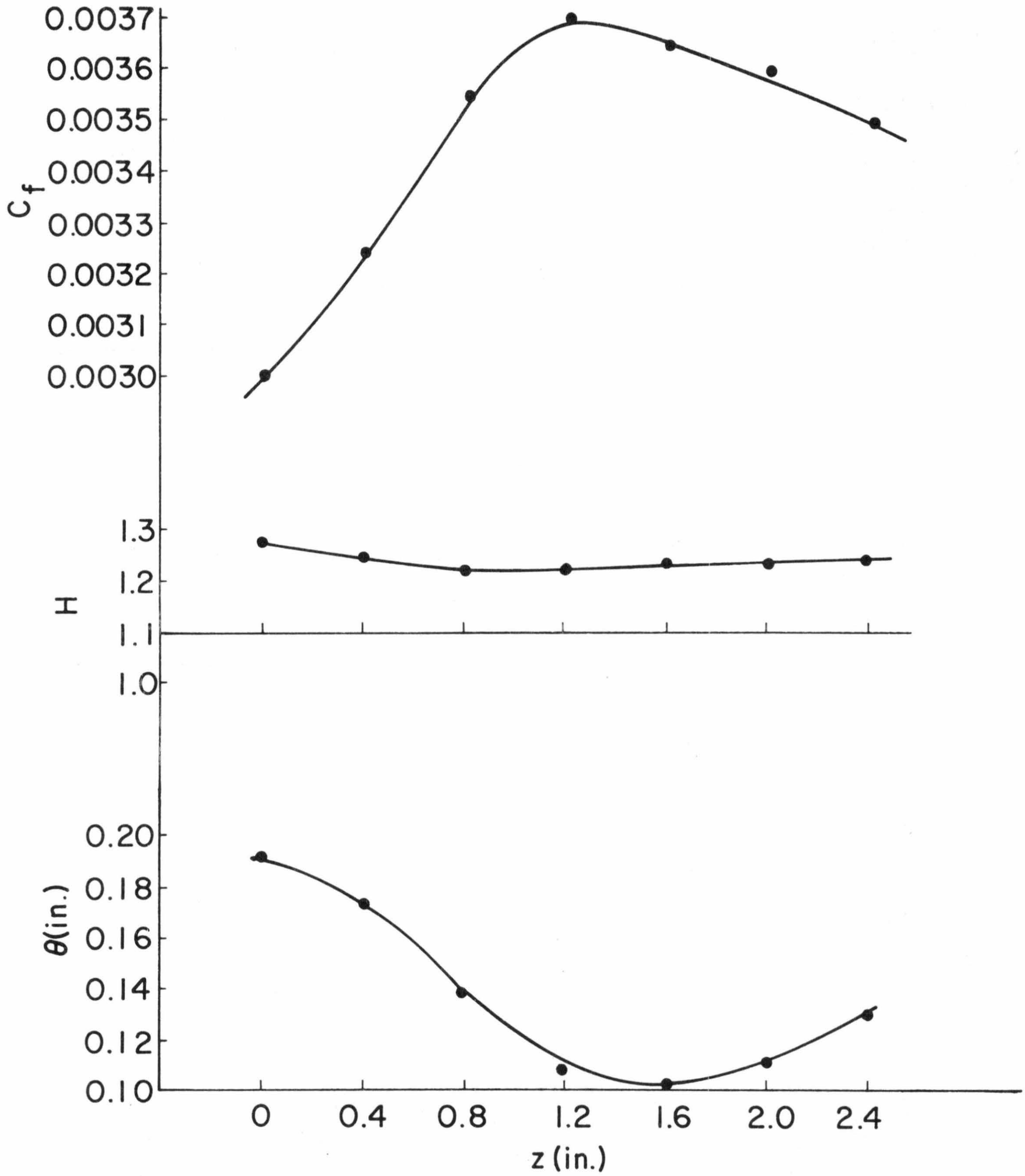

Figure 23: Lateral variation of integral boundary layer characteristics: x = 18"

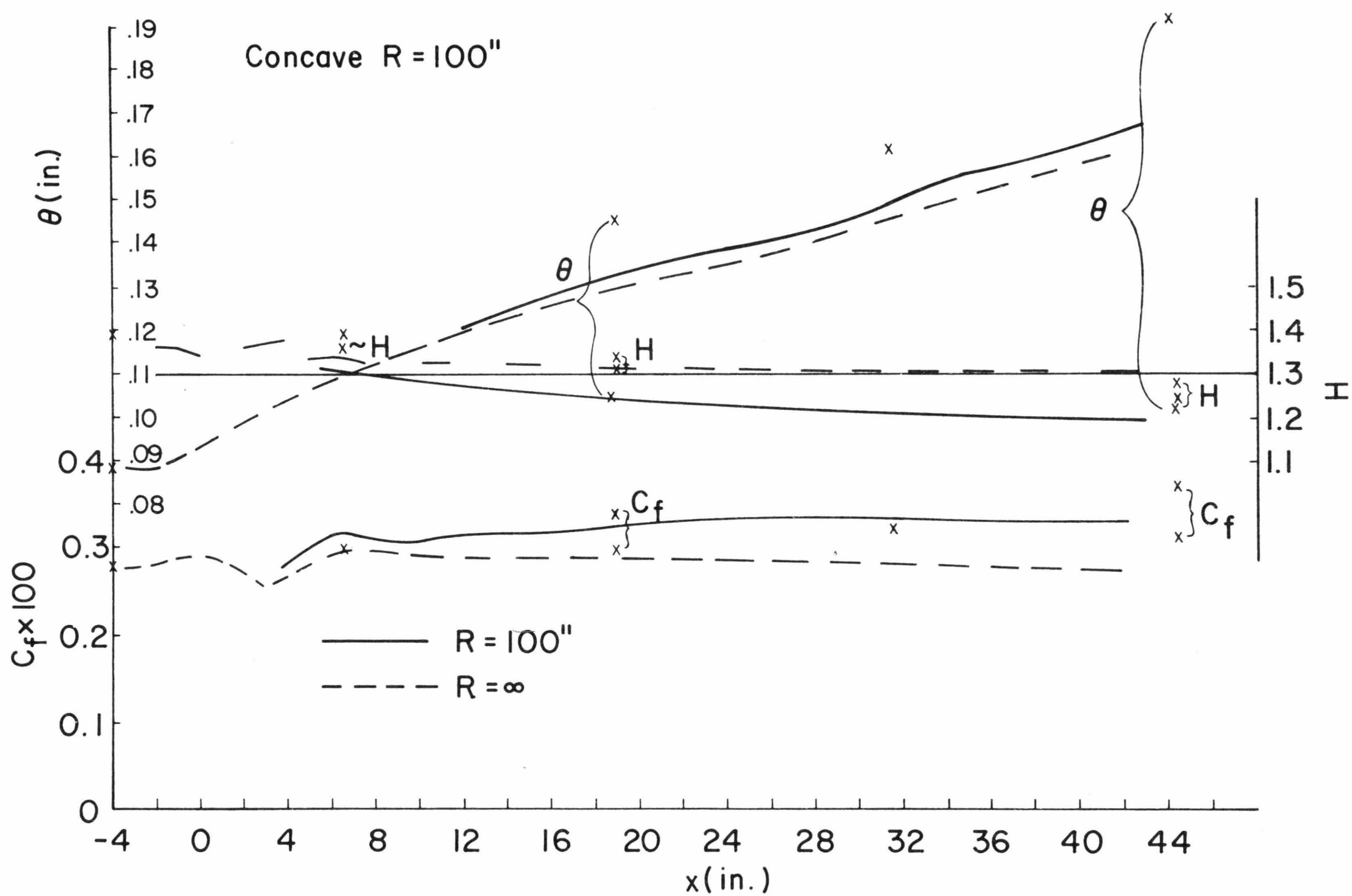

Figure 24: Variation of integral boundary layer characteristics over concave wall

unclassified
Security Classification

DOCUMENT CONTROL DATA - R & D		
(Security classification of title, body of abstract and indexing annotation must be entered when the overall report is classified)		
1. ORIGINATING ACTIVITY (Corporate author) Fluid Dynamics & Diffusion Laboratory College of Engineering, Colorado State University Fort Collins, Colorado 80521	2a. REPORT SECURITY CLASSIFICATION unclassified 2b. GROUP	
3. REPORT TITLE Measurements of Turbulent Boundary Layer Growth Over a Longitudinally Curved Surface		
4. DESCRIPTIVE NOTES (Type of report and inclusive dates) Technical Report		
5. AUTHOR(S) (First name, middle initial, last name) R. N. Meroney		
6. REPORT DATE January, 1974	7a. TOTAL NO. OF PAGES 76	7b. NO. OF REFS 32
8a. CONTRACT OR GRANT NO. N00014-68-A-0493-0001 b. PROJECT NO. c. d.	9a. ORIGINATOR'S REPORT NUMBER(S) CER73-74RNM26 9b. OTHER REPORT NO(S) (Any other numbers that may be assigned this report) THEMIS Tech. Rept. No. 25	
10. DISTRIBUTION STATEMENT Distribution of this report is unlimited		
11. SUPPLEMENTARY NOTES	12. SPONSORING MILITARY ACTIVITY U.S. Department of Defense Office of Naval Research	

13. ABSTRACT

The result of an "additional rate of Strain" on a turbulent parcel of fluid as it undergoes even mild streamline curvature can be very large. Yet until recently skin friction and heat transfer calculations have ignored this effect. Recent measurements over turbine cascades suggest curvature influences heat transfer by an order of magnitude. In addition there exists a strong analogy between the effects of centrifugal body forces and the buoyance body force arising in density stratified flow in a gravity field.

This note reports the results of a set of measurements of boundary layer development over convex and concave surfaces and compares the results with various turbulence models utilized in computational programs. A moderate curvature wind tunnel test section was constructed ($\delta/R \approx .01$ to $.02$) to examine the influence of curvature on boundary layer structure.

The boundary layer rate of growth, compared to that of a boundary layer in the same pressure gradient on a flat surface, was decreased on the convex surface and increased on the concave surface by ten to twelve percent as a result of only an apparent one to two percent perturbation on the size of the source terms in the Reynolds stress equations. Measurements are available of longitudinal static wall pressure, vertical stagnation pressure and single and cross-wire anemometer voltages at a sequence of five downstream stations. Lateral traverses at six heights for two downstream stations were completed over the concave side. Analog and digital interpretation of anemometer signals provided data of $\overline{u}$, $\overline{v}$, $\overline{u'^2}$, $\overline{v'^2}$, $\overline{u'v'}$, $\overline{u'v'^2}$, $\overline{u'^2v'}$, $\overline{u'^3}$ and $\overline{v'^3}$.

DD FORM 1 NOV 65 1473

unclassified
Security Classification

unclassified
Security Classification

14 KEY WORDS	LINK A		LINK B		LINK C	
	ROLE	WT	ROLE	WT	ROLE	WT
Turbulent Boundary Layer Turbine Blades Atmospheric Boundary Layer Longitudinal Rolls Vortex						

Security Classification

DISTRIBUTION LIST FOR UNCLASSIFIED TECHNICAL REPORTS ISSUED UNDER
CONTRACT N00014-68-A-0493-0001 TASK NR 062-414

All addressees receive one copy unless otherwise specified

Defense Documentation Center
Cameron Station
Alexandria, VA 22314 (12 copies)

Technical Library
Naval Ship Research & Dev. Center
Annapolis Laboratory
Annapolis, MD 21402

Professor Bruce Johnson
Engineering Department
Naval Academy
Annapolis, MD 21402

Library
Naval Academy
Annapolis, MD 21402

Professor C. S. Yih
Department of Engineering Mechanics
University of Michigan
Ann Arbor, MI 48108

Professor T. Francis Ogilvie
Department of Naval Architecture
and Marine Engineering
University of Michigan
Ann Arbor, MI 48108

Professor R. B. Couch
Department of Naval Architecture
and Marine Engineering
University of Michigan
Ann Arbor, MI 48108

Air Force Office of Scientific
Research (REM)
1400 Wilson Boulevard
Arlington, VA 22209

Dr. Coda Pan
Shaker Research Corporation
Northway 10 Executive Park
Ballston Lake, NY 12019

Professor S. Corrsin
Department of Mechanics and
Materials Sciences
The Johns Hopkins University
Charles and 34th Street
Baltimore, MD 21218

Professor O. M. Phillips
Department of Earth and Planetary
Sciences
The Johns Hopkins University
Charles and 34th Street
Baltimore, MD 21218

Professor M. Holt
Department of Mechanical Engineering
University of California
Berkeley, CA 94720

Professor E. V. Laitone
Department of Mechanical Engineering
University of California
Berkeley, CA 94720

Librarian
Department of Naval Architecture
University of California
Berkeley, CA 94720

Professor P. Lieber
Department of Mechanical Engineering
University of California
Berkeley, CA 94720

Professor J. R. Paulling
Department of Naval Architecture
University of California
Berkeley, CA 94720

Professor W. C. Webster
Department of Naval Architecture
University of California
Berkeley, CA 94720

Professor J. V. Wehausen
Department of Naval Architecture
University of California
Berkeley, CA 94720

Professor J. A. Schetz
Department of Aerospace Engineering
Virginia Polytechnic Institute
Blacksburg, VA 24061

Director
Office of Naval Research Branch Office
495 Summer Street
Boston, MA 02210

Commander
Boston Naval Shipyard
Boston, MA 02129

Commander
Puget Sound Naval Shipyard
Bremerton, WA 98314

Dr. Alfred Ritter
Calspan Corporation
P. O. Box 235
Buffalo, NY 14221

Professor G. Birkhoff
Department of Mathematics
Harvard University
Cambridge, MA 02138

Professor G. F. Carrier
Division of Engineering and
Applied Physics
Pierce Hall
Harvard University
Cambridge, MA 02138

Commanding Officer
NROTC Naval Administrative Unit
Massachusetts Institute of Technology
Cambridge, MA 02139

Professor M. A. Abkowitz
Department of Ocean Engineering
Massachusetts Institute of Technology
Cambridge, MA 02139

Professor C. C. Mei
Department of Civil Engineering
Massachusetts Institute of Technology
Cambridge, MA 02139

Professor Phillip Mandel
Department of Ocean Engineering
Massachusetts Institute of Technology
Cambridge, MA 02139

Professor L. N. Howard
Department of Mathematics
Massachusetts Institute of Technology
Cambridge, MA 02139

Professor R. F. Probstein
Department of Mechanical Engineering
Massachusetts Institute of Technology
Cambridge, MA 02139

Professor E. Mollo-Christensen
Department of Meteorology
Room 54-1722
Massachusetts Institute of Technology
Cambridge, MA 02139

Professor J. Nicholas Newman
Department of Ocean Engineering
Room 5-324A
Massachusetts Institute of Technology
Cambridge, MA 02139

Professor A. R. Kuhlthau, Director
Research Laboratories for the Engineering
Sciences
Thornton Hall
University of Virginia
Charlottesville, VA 22903

Director
Office of Naval Research Branch Office
536 South Clark Street
Chicago, IL 60605

Library
Naval Weapons Center
China Lake, CA 93555

Institute of Hydrodynamics and Hydraulic
Engineering
Technical University of Denmark
Building 115 dk-2800
Lyngby/Copenhagen, Denmark

Professor J. M. Burgers
Institute of Fluid Dynamics and
Applied Mathematics
University of Maryland
College Park, MD 20742

Professor Pai
Institute for Fluid Dynamics and
Applied Mathematics
University of Maryland
College Park, MD 20740

Acquisitions Branch (S-AK/DL)
NASA Scientific and Technical
Information Facility
P. O. Box 33
College Park, MD 20740

Technical Library
Naval Weapons Laboratory
Dahlgren, VA 22418

Computation & Analyses Laboratory
Naval Weapons Laboratory
Dahlgren, VA 22418

Dr. R. H. Kraichnan
Dublin, NH 03444

Army Research Office
Box CM, Duke Station
Durham, NC 27706

Dr. Martin H. Bloom
Polytechnic Institute of New York
Department of Aerospace Engineering
and Applied Mechanics
Farmingdale, NY 11735

Technical Documents Center
Army Mobility Equipment R&D Center
Fort Belvoir, VA 22060

Professor J. E. Cermak
Department of Civil Engineering
Fluid Mechanics Program
Colorado State University
Fort Collins, CO 80521

Professor O. H. Shemdin
Coastal and Oceanographic Engineering
Department
University of Florida
Gainesville, FL 32601

Technical Library
Webb Institute of Naval Architecture
Glen Cove, NY 11542

Professor E. V. Lewis
Webb Institute of Naval Architecture
Glen Cove, NY 11542

Dr. J. P. Breslin
Davidson Laboratory
Stevens Institute of Technology
Castle Point Station
Hoboken, NJ 07030

Mr. C. H. Henry
Stevens Institute of Technology
Davidson Laboratory
Castle Point Station
Hoboken, NJ 07030

Dr. D Savitsky
Davidson Laboratory
Stevens Institute of Technology
Castle Point Station
Hoboken, NJ 07030

Dr. A. Strumpf
Davidson Laboratory
Stevens Institute of Technology
Castle Point Station
Hoboken, NJ 07030

Dr. J. P. Craven
University of Hawaii
181 University Avenue
Honolulu, HI 96822

Professor F. Hussain
Department of Mechanical Engineering
Cullen College of Engineering
University of Houston
Houston, TX 77004

Professor J. F. Kennedy, Director
Institute of Hydraulic Research
University of Iowa
Iowa City, IA 52242

Professor L. Landweber
Institute of Hydraulic Research
University of Iowa
Iowa City, IA 52242

Professor E. L. Resler
Graduate School of Aerospace Engineering
Cornell University
Ithaca, NY 14850

Dr. D. E. Ordway
Sage Action, Incorporated
P. O. Box 416
Ithaca, NY 14850

Dr. S. A. Orszag
Flow Research, Inc.
1819 South Central Avenue
Suite 72
Kent, WA 98031

Professor J. W. Miles
Institute of Geophysics and
Planetary Physics
University of California, San Diego
La Jolla, CA 92037

Director
Scripps Institute of Oceanography
University of California
La Jolla, CA 92037

Dr. J. Young
Science Applications, Incorporated
1250 Prospect Street
La Jolla, CA 92037

Mr. Phillip Eisenberg, President
Hydronautics, Incorporated
7210 Pindell School Road
Laurel, MD 20810

Mr. M. P. Tulin
Hydronautics, Incorporated
7210 Pindell School Road
Laurel, MD 20810

Commander
Long Beach Naval Shipyard
Long Beach, CA 90801

Dr. C. W. Hirt
University of California
Los Alamos Scientific Laboratory
P. O. Box 1663
Los Alamos, NM 87544

Professor J. M. Killen
St. Anthony Falls Hydraulic Laboratory
University of Minnesota
Minneapolis, MN 55414

Lorenz G. Straub Library
St. Anthony Falls Hydraulic Laboratory
University of Minnesota
Minneapolis, MN 55414

Professor J. Ripkin
St. Anthony Falls Hydraulic Laboratory
University of Minnesota
Minneapolis, MN 55414

Dr. E. Silberman
St. Anthony Falls Hydraulic Laboratory
University of Minnesota
Minneapolis, MN 55414

Library
Naval Postgraduate School
Monterey, CA 93940

Technical Library
Naval Underwater Systems Center
Newport, RI 02840

Office of Naval Research
New York Area Office
207 W. 24th Street
New York, NY 10011

Professor V. Castelli
Department of Mechanical Engineering
Columbia University
New York, NY 10027

Professor H. G. Elrod
Department of Mechanical Engineering
Columbia University
New York, NY 10027

Engineering Societies Library
345 East 47th Street
New York, NY 10017

Professor J. J. Stoker
Courant Institute of Mathematical
Sciences
New York University
251 Mercer Street
New York, NY 10003

Society of Naval Architects and
Marine Engineers
74 Trinity Place
New York, NY 10006

Librarian, Aeronautical Laboratory
National Research Council
Montreal Road
Ottawa 7, Canada

Technical Library
Naval Coastal System Laboratory
Panama City, FL 32401

Dr. J. W. Hoyt
Naval Undersea Center
Pasadena Laboratory
3202 E. Foothill Boulevard
Pasadena, CA 91107

Technical Library
Naval Undersea Center
Pasadena Laboratory
3202 E. Foothill Blvd.
Pasadena, CA 91107

Professor A. J. Acosta
Department of Mechanical Engineering
California Institute of Technology
Pasadena, CA 91109

Professor H. W. Liepmann
Graduate Aeronautical Laboratories
California Institute of Technology
Pasadena, CA 91109

Professor M. S. Plesset
Engineering Science Department
California Institute of Technology
Pasadena, CA 91109

Professor A. Roshko
Graduate Aeronautical Laboratories
California Institute of Technology
Pasadena, CA 91109

Professor T. Y. Wu
Engineering Science Department
California Institute of Technology
Pasadena, CA 91109

Director
Office of Naval Research Branch Office
1030 E. Green Street
Pasadena, CA 91101

Professor K. M. Agrawal
Virginia State College
Department of Mathematics
Petersburg, VA 23803

Technical Library
Naval Ship Engineering Center
Philadelphia Division
Philadelphia, PA 19112

Technical Library
Philadelphia Naval Shipyard
Philadelphia, PA 19112

Professor R. C. MacCamy
Department of Mathematics
Carnegie Institute of Technology
Pittsburgh, PA 15213

Dr. Paul Kaplan
Oceanics, Inc.
Technical Industrial Park
Plainview, NY 11803

Technical Library
Naval Missile Center
Point Mugu, CA 93041

Commander
Portsmouth Naval Shipyard
Portsmouth, NH 03801

Commander
Norfolk Naval Shipyard
Portsmouth, VA 23709

Dr. H. Norman Abramson
Southwest Research Institute
8500 Culebra Road
San Antonio, TX 78228

Editor
Applied Mechanics Review
Southwest Research Institute
8500 Culebra Road
San Antonio, TX 78206

Dr. Andrew Fabula
Code 5002
Naval Undersea Center
San Diego, CA 92132

Office of Naval Research
San Fransisco Area Office
760 Market Street, Room 447
San Francisco, CA 94102

Library
Pearl Harbor Naval Shipyard
Box 400
FPO San Francisco 96610

Technical Library
Hunters Point Naval Shipyard
San Francisco, CA 94135

Professor Bruce H. Adee
Department of Mechanical Engineering
University of Washington
Seattle, WA 98195

Professor A. Hertzberg
Director, Aerospace Research Laboratory
University of Washington
Seattle, WA 98105

Fenton Kennedy Document Library
The Johns Hopkins University
Applied Physics Laboratory
8621 Georgia Avenue
Silver Spring, MD 20910

Professor E. Y. Hsu
Department of Civil Engineering
Stanford University
Stanford, CA 94305

Dr. Byrne Perry
Department of Civil Engineering
Stanford University
Stanford, CA 94305

Dr. R. L. Street
Department of Civil Engineering
Stanford University
Stanford, CA 94305

Professor R. C. DiPrima
Department of Mathematics
Rensselaer Polytechnic Institute
Troy, NY 12181

Professor J. L. Lumley
Department of Aerospace Engineering
Pennsylvania State University
University Park, PA 16802

Dr. J. M. Robertson
Department of Theoretical and
Applied Mechanics
University of Illinois
Urbana, IL 61803

Technical Library
Mare Island Naval Shipyard
Vallejo, CA 94592

Mr. Norman Nilsen
General Education Department
California Maritime Academy
P. O. Box 1392
Vallejo, CA 94590

Office of Naval Research
Code 438
800 N. Quincy Street
Arlington, VA 22217 (3 copies)

Office of Naval Research
Code 411-7
800 N. Quincy Street
Arlington, VA 22217

Office of Naval Research
Code 411-6
800 N. Quincy Street
Arlington, VA 22217

Office of Naval Research
Code 412-8
800 N. Quincy Street
Arlington, VA 22217

Office of Naval Research
Code 412-3
800 N. Quincy Street
Arlington, VA 22217

Office of Naval Research
Code 473
800 N. Quincy Street
Arlington, VA 22217

Office of Naval Research
Code 481
800 N. Quincy Street
Arlington, VA 22217

Naval Research Laboratory
Code 2627
Washington, DC 20375 (6 copies)

Naval Research Laboratory
Code 2629 (ONRL)
Washington, DC 20375 (6 copies)

Naval Research Laboratory
Code 6170
Washington, DC 20375

Naval Research Laboratory
Code 4000
Washington, DC 20375

Naval Research Laboratory
Code 8030
Washington, DC 20375

Naval Research Laboratory
Code 8040
Washington, DC 20375

Naval Ship Systems Command
Code 031
Washington, DC 20362

Naval Ship Systems Command
Code 0341
Washington, DC 20362

Naval Ship Systems Command
Code 03Z2 (L. Benen)
Washington, DC 20362

Naval Ship Systems Command
Code 03Z2 (J. Schuler)
Washington, DC 20362

Naval Ship Systems Command
Code 2052
Washington, DC 20362

Naval Ship Engineering Center
Code 6034
Center Building
Prince George's Center
Hyattsville, MD 20782

Naval Ship Engineering Center
Code 6101E
Center Building
Prince George's Center
Hyattsville, MD 20782

Naval Ship Engineering Center
Code 6110
Center Building
Prince George's Center
Hyattsville, MD 20782

Naval Ship Engineering Center
Code 6114
Center Building
Prince George's Center
Hyattsville, MD 20782

Naval Ship Engineering Center
Code 6136
Center Building
Prince George's Center
Hyattsville, MD 20782

Dr. A. Powell (Code 01)
Naval Ship Research & Dev. Center
Bethesda, MD 20034

Dr. W. M. Ellsworth (Code 11)
Naval Ship Research & Dev. Center
Bethesda, MD 20034

Dr. W. E. Cummins (Code 15)
Naval Ship Research & Dev. Center
Bethesda, MD 20034

Mr. G. H. Gleissner (Code 18)
Naval Ship Research & Dev. Center
Bethesda, MD 20034

Mr. R. Wermter (Code 152)
Naval Ship Research & Dev. Center
Bethesda, MD 20034

Dr. W. B. Morgan (Code 154)
Naval Ship Research & Dev. Center
Bethesda, MD 20034

Mr. J. B. Hadler (Code 156)
Naval Ship Research & Dev. Center
Bethesda, MD 20034

Library (Code 5641)
Naval Ship Research & Dev. Center
Bethesda, MD 20034

Dr. P. Pien (Code 1521)
Naval Ship Research & Dev. Center
Bethesda, MD 20034

Mr. Paul S. Granville (Code 1541)
Naval Ship Research & Dev. Center
Bethesda, MD 20034

Mr. J. McCarthy (Code 1552)
Naval Ship Research & Dev. Center
Bethesda, MD 20034

Dr. Nils Salvesen (Code 1552)
Naval Ship Research & Dev. Center
Bethesda, MD 20034

Ms. Joanna Schot (Code 1843)
Naval Ship Research & Dev. Center
Bethesda, MD 20034

Dr. M. Strasberg (Code 1901)
Naval Ship Research & Dev. Center
Bethesda, MD 20034

Naval Air Systems Command
AIR 03
Washington, DC 20361

Naval Air Systems Command
AIR 5301
Washington, DC 20361

Naval Air Systems Command
AIR 50174
Washington, DC 20361

Naval Ordnance Systems Command
ORD 03A
Washington, DC 20360

Naval Ordnance Systems Command
ORD 035
Washington, DC 20360

Naval Ordnance Systems Command
ORD 5413
Washington, DC 20360

Naval Ordnance Systems Command
ORD 0632
Washington, DC 20360

Strategic Systems Project Office
CNM (PM-1)
Washington, DC 20360

Oceanographer of the Navy
200 Stovall Street
Alexandria, VA 22332

Commander
Naval Oceanographic Office
Washington, DC 20373

Dr. A. L. Slafkosky
Scientific Advisor
Commandant of the Marine Corps
(Code AX)
Washington, DC 20380

Librarian Station 5-2
Coast Guard Headquarters
NASSIF Building
400 Seventh Street, S.W.
Washington, DC 20591

Office of Research and Development
Maritime Administration
441 G Street, N.W.
Washington, DC 20235

Division of Ship Design
Maritime Administration
441 G Street, N.W.
Washington, DC 20235

National Science Foundation
Engineering Division
1800 G Street, N.W.
Washington, DC 20550

Dr. G. Kulin
Fluid Mechanics Section
National Bureau of Standards
Washington, DC 20234

Science & Technology Division
Library of Congress
Washington, DC 20540

Chief of Research and Development
Office of Chief of Staff
Department of the Army
Washington, DC 20310

Professor A. Thiruvengadam
Department of Mechanical Engineering
Catholic University of America
Washington, DC 20017

Librarian
Naval Ordnance Laboratory
White Oak, MD 20910

Mr. J. Enig (Room 3-252)
Naval Ordnance Laboratory
White Oak, MD 20910

Dr. A. S. Iberall, President
General Technical Services, Inc.
451 Penn Street
Yeadon, PA 19050

Professor J. Clarke
Division of Engineering
Brown University
Providence, RI 02912

Commander and Director
Atmospheric Sciences Laboratory
U. S. Army Electronics Command
Attn.: AMSEL-BL-AS-M (Mr. Pries)
U. S. Army Missile Range
White Sands, NM 88002